UNIVERSITÀ DEGLI STUDI DI PADOVA

DIPARTIMENTO DI INGEGNERIA INDUSTRIALE

CORSO DI LAUREA MAGISTRALE IN INGEGNERIA CHIMICA E DEI PROCESSI INDUSTRIALI

Tesi di Laurea Magistrale in
Ingegneria Chimica e dei Processi Industriali

MEASUREMENTS AND CFD SIMULATIONS ON THE PT-CATALYZED HYDROGEN OXIDATION IN A STAGNATION-POINT FLOW GEOMETRY

Relatore: Prof. Paolo Canu

Correlatore: Dott. Nicola Michelon

Laureando: **FRANCESCO MONTECCHIO**

ANNO ACCADEMICO 2013-2014

Abstract

The present work is focused on the Pt-catalyzed hydrogen oxidation and its reaction mechanism. Indeed, it has been deeply studied in literature but, so far, it has not been defined a mechanism with a general validity. This is because several variables (like the activity of the catalyst, the reactor geometry and the fluid dynamics) may influence the reaction.

Following this idea, the first research topic is an evaluation of the variation of the platinum activity because of different surface treatments. Oxidations, reductions and high temperature treatments were performed to measure how the activity of a bulk platinum disk with a diameter of 10 mm may change. These tests were carried out in a stagnation-point flow geometry to ensure a homogeneous reagents-catalyst contact time. Especially oxidation treatments produced a great activity change (from ~ 20% up to ~ 85%) so it is possible to conclude that the thermochemical history of the catalyst influences significantly its activity.

The importance of the reactor geometry and of the mass transfer phenomena was deeply studied in the next research topic. It was experimentally proved that the maximum conversion changes significantly because of *gap* and inlet flow rate variations. A CFD simulation validates these experimental data and it shown that, at low flow rates, the reagents tend to bypass the catalyst while, at high flow rates, they are forced towards the catalyst but the reagents-catalyst contact time is reduced. The CFD simulation also deals with the different importance of convection and diffusion in the hydrogen mass transfer towards the catalyst.

The ignition temperature was evaluated during the following research topic and experiments shown a general increase of the temperature with the hydrogen composition. These data were compared with literature but a scarce reproducibility was found because of a different reactor geometry and configuration and a different fluid dynamics inside the reactor.

This work is concluded by an evaluation of the heat produced during the reaction ignition that shown how the way of measuring the temperature is crucial in the studied system.

Riassunto

Questa Tesi tratta della reazione di ossidazione dell'idrogeno catalizzata dal platino. Al contrario di altri lavori di catalisi che si focalizzano sulla produzione di un particolare prodotto o sull'abbattimento di un reagente, il presente lavoro è principalmente basato sulla reazione in sé e sul suo meccanismo. Infatti, se si analizza la letteratura, è possibile trovare una grande varietà di meccanismi ma ognuno è consistente solo nel sistema in cui è stato sviluppato mentre, se lo si cerca di implementare in configurazioni geometriche diverse, si assiste ad una scarsa riproducibilità sperimentale. Risulta evidente che uno studio approfondito è necessario anche perché il meccanismo dei reazione dell'idrogeno è un sotto-meccanismo delle reazioni di ossidazione di tutti gli idrocarburi.

Questa reazione viene condotta su di un catalizzatore di platino bulk di forma circolare con un diametro di 10 mm che viene testato in un particolare tipo di geometria, detta a flusso stagnante perché tutti i reagenti investono ortogonalmente il catalizzatore.

La prima variabile che può influenzare la reazione portando ad una scarsa riproducibilità della letteratura è l'attività del platino che può subire delle variazioni indotte da particolari trattamenti termochimici. Di conseguenza, la prima parte dell'attività sperimentale di questa Tesi riguarda lo studio delle variazioni dell'attività del platino. Sono stati realizzati trattamenti termici e riduttivi che hanno dimostrato di aumentare moderatamente l'attività catalitica ma i risultati migliori si sono ottenuti in seguito a trattamenti ossidativi che consentono, oltre ad una pulizia della superficie precedentemente osservata, anche un adsorbimento facilitato dell'ossigeno.

Siccome si è dimostrato come, in condizioni stechiometriche, l'attività catalitica dipende fortemente dalla storia termochimica del catalizzatore, si è scelto di operare, per le prove successive, con un'atmosfera reagente in forte eccesso di ossigeno che ha prodotto dei risultati più consistenti.

L'attenzione sperimentale si è successivamente spostata su come le variabili geometriche e la fluidodinamica del sistema possano influenzare la reazione. In particolare, si è analizzata la conversione massima al variare del *gap* e della portata totale in ingresso. Si è visto come la reazione non sia mai completa e raggiunge il suo valore massimo per il valore minimo di *gap* e per portate < 100 mL/min. Un aumento del *gap* fa calare significativamente la conversione (fino al 10% in meno) mentre un aumento di portata ha un effetto decrescente più moderato ($\Delta X \approx$ 2-4%). Si è ipotizzato che, a portate basse, l'idrogeno non reagisca completamente perché tenda a bypassare il catalizzatore transitando al di sopra della superficie. Al contrario, per portate maggiori, il reagente è forzato verso il catalizzatore ma il tempo di contatto è ridotto quindi la

conversione cala nuovamente. Per *gap* più elevati, il fenomeno di bypass del catalizzatore è più accentuato quindi la conversione è ragionevolmente minore.
Si è realizzata una simulazione CFD che ha validato le ipotesi basate sui dati sperimentali e ha evidenziato l'effetto della diffusione e della convezione circa il trasporto di idrogeno verso la superficie catalitica. Si nota come, per basse portate, il trasporto è legato principalmente alla diffusione che ha un effetto moderato ma opera già dall'ingresso dei reagenti nella zona reattiva mentre la convezione non ha un effetto determinante. Al contrario, a portate maggiori si possono osservare due zone distinte per quanto riguarda il mass transfer. L'idrogeno è trasportato per convezione fino a 0.5 mm dal catalizzatore e, successivamente, la velocità del flusso cala notevolmente. Di conseguenza diventa più significativa l'attività della diffusione che è spinta dal maggior gradiente di concentrazione rispetto al caso a bassa portata.
Inoltre, si è analizzata la temperatura di innesco della reazione in modo da fare un paragone con la letteratura visto è questo il parametro più studiato. I risultati sperimentali hanno mostrato un aumento della temperatura di innesco all'aumentare della concentrazione di idrogeno in aria, in accordo con la letteratura. Tuttavia, le temperature registrate sono considerevolmente superiori rispetto a quelle di altri autori. Quindi, si può affermare come una differente configurazione geometrica influenzi anche i parametri cinetici della reazione e, conseguentemente, tutti i meccanismi di reazione che sono sviluppati a partire dai dati sperimentali.
Questa tematica sperimentale ha sollevato il dubbio che, in corrispondenza dell'innesco della reazione, ci siano dei fenomeni termici non correttamente misurati con la configurazione utilizzata. Di conseguenza, l'ultima tematica sperimentale ha valutato la temperatura della superficie reattiva e il calore prodotto dall'innesco della reazione e ha confermato come vi sia un aumento della temperatura non precedentemente rilevato.
Questa Tesi è il risultato di una collaborazione accademica tra due Dipartimenti dell'Università degli Studi di Padova: il Dipartimento di Scienze Chimiche e il Dipartimento di Ingegneria Industriale. Il primo ha fornito il catalizzatore usato in questo lavoro e ha realizzato analisi superficiali quali SEM e XRD mentre il secondo ha realizzato le prove sperimentali testando il catalizzatore. La maggior parte del lavoro presentato è stato svolto presso il Dipartimento di Ingegneria Industriale sotto la supervisione del Prof. Paolo Canu.

Table of contents

Introduction

The Pt-catalyzed hydrogen oxidation is one of the most studied reactions in the catalysis world. Indeed, it has a simple but important reaction mechanism because it is part of all others oxidation mechanisms. However, a wide range of mechanisms has been proposed so far but none of them has a general validity because they are based on experimental data that are affected by several variables (like the activity of the catalyst, the reactor geometry and the fluid dynamics) that vary in each literature paper. So, the core of this Thesis is an evaluation of the most important variables that influence the kinetic parameters.

The first topic of this Thesis is the evaluation of the variations of the catalytic activity due to thermochemical surface treatments. The experimental tests are performed by treating a bulk platinum disk (model catalyst) with thermal, reductive and oxidative treatments. The stagnation-point flow geometry is the best reactor configuration to study this particular disk because it allows a homogeneous contact time between the reagents and the catalyst.

Another important topic of this Thesis is the evaluation of the influence of the reactor geometry and fluid dynamics in the kinetic features. To do that, the variations of maximum conversion were observed at different values of these key geometry variables:

- the *gap* that is the distance between the reagents nozzle and the catalyst;
- the total inlet flow rate.

To have a deeper comprehension of all mass transfer phenomena, a CFD simulation is performed and its results are compared with the experimental data.

Since the ignition temperature is the most studied kinetic parameter in literature, its evaluation at different hydrogen compositions is performed in the third research topic. In this way, it is possible to compare the results with literature and to underline how the geometry of the reactor and its fluid dynamics affect the reaction.

The last idea that leads the experimental work is the estimation of the heat produced during the ignition of the reaction because the reactive surface is expected to be composed by a large number of local hot spots so the proper measurement of reaction temperature is crucial.

This Thesis is divided into 5 Chapters and it begins with and overview about platinum in heterogeneous catalyst.

The second Chapter introduces the state of art of all reaction features considered in this Thesis. At first the most important kinetic properties are introduced, then the variation of platinum activity through the restructuring of its surface is presented and, at the end, there is a critical analysis of all literature stagnation-point flow geometries and their fluid dynamics.

The third Chapter describes the experimental equipment used to carry out the experimental work. The main attention is focused on the used reactors and on the analysis equipment (gas chromatograph and/or mass spectrometer).
The results of the CFD simulation are described in Chapter 4 with a particular attention on the hydrogen mass flux and on the phenomena involved to transport hydrogen towards the catalyst.
The experimental work is presented in Chapter 5 and it is divided into 4 research areas involving the evaluation of:

- the catalyst activity variations through surface treatments;
- the maximum conversion at different *gaps* and inlet flow rates;
- the ignition temperature at different hydrogen compositions;
- the reaction heat produced during the ignition.

This Thesis is the result of an academic collaboration between two Departments of the Università degli Studi di Padova: the Dipartimento di Scienze Chimiche and the Dipartimento di Ingegneria Industriale. The first one provides the catalyst used in this work and it is involved in surface analyses like the SEM or the XRD analysis while the second performs the kinetic experiments on the catalyst. Most of the work presented in this Thesis is carried out at the Dipartimento di Ingegneria Industriale under the supervision of Prof. Paolo Canu.

Chapter 1

An overview on platinum in heterogeneous catalysis

The aim of this work is the fundamental understanding of the catalytic properties of platinum and their enhancing at ambient pressure and high temperature, in a well defined geometry amenable to detailed flow modelling.
The choice of using bulk platinum as catalyst follows the idea of having a well characterized, ideal surface. This Thesis disregards any economic evaluation.
The aim of the first Chapter is the introduction of the main features and uses of platinum in heterogeneous catalysis.

1.1 Platinum in heterogeneous catalysis

Platinum is a rare and precious metal but it is also a well-known catalyst and it is used in many industrial applications for its great catalytic properties. Table 1.1 shows a comparison between the current prices of metals used in heterogeneous catalysis while Figure 1.1 represents the platinum global distribution.

Table 1. 1. *A comparision between the price of metals used in heterogeneous catalysis. (http://www.infomine.com/investment/metal-prices/ 26/10/2013)*

Metal	Price (€/g)
Palladium	17.3
Rhodium	22.8
Gold	31.5
Platinum	33.9

In nature, platinum is found in many different forms and usually mixed with other metals as well as sand. To obtain pure platinum we need many stages to purify it from all metals and waste materials. At first, a water cleaning is needed to separate metals from sand, then different acids are used to separate and dissolve platinum. Citric acid is used to separate iron and copper, then platinum is dissolved in hot *aqua regia* (a concentrated mixture of nitric and hydrochloric acid) and it is precipitated by using ammonium chloride. The final purification steps involve the melting of the previous compound and other final precipitations.

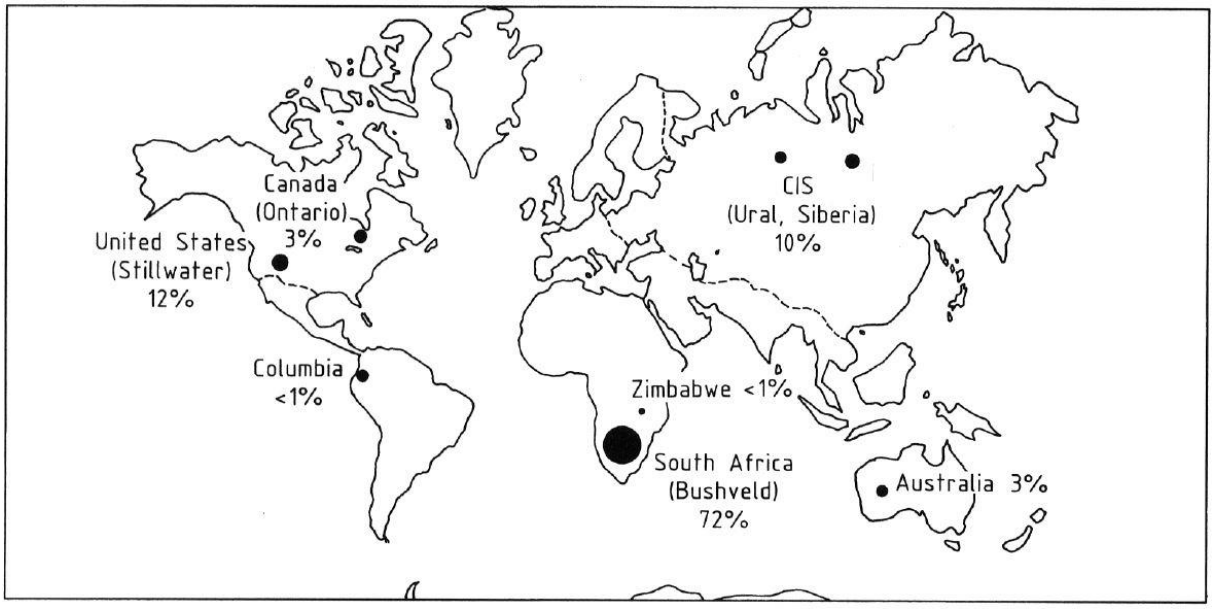

***Figure 1. 1**. World platinum group metal reserves (total 70 000 t) (Renner, 2003).*

Platinum is used as a catalyst in a wide range of industrial processes and it is often dispersed on a silica or silica-allumina support. The catalytic properties are due to the easy intermolecular exchange of π- and πσ electrons (Panster, 2003) and the main catalyzed reactions are oxidation reactions (ammonia oxidation to nitric oxide (NO) or oxidation of residual hydrocarbons after combustion in automotive engines) as well as reduction and isomeration reactions (hydrogen addition, reforming of crude oil or reduction of ketones to alcohols).

1.1.1 Automotive platinum catalytic converter

The most famous application of platinum in industry is the automotive catalytic converter daily used in all cars. Indeed, cars engine produces a wide range of air pollutant so a catalytic conversion is needed to decrease their concentration. The first of the three main components used in all modern catalytic converters is a cheap support called substrate. It is usually a ceramic monolith with a honeycomb structure and the cordierite is the most used compound. The second compound of the converter is the washcoat that provides a fine dispersion of catalytic powder on its surface. Ceramic materials (e.g. aluminum oxide or titanium dioxide) are typically used for the washcoat because their rough surface and chemical nature allow a fine dispersion of the catalysts. The last and most precious compound is the catalyst itself that is made by platinum and rhodium that are dispersed on the washcoat to catalyze reduction and oxidation reactions to decrease pollutants emission. With this kind of converter, we can achieve a significant reduction of pollutants as well as low pressure drops.

Modern converters are called “three-way” because they catalyze the reaction of the three main pollutants: carbon monoxide, unburned hydrocarbon and oxides of nitrogen. Platinum is mainly

used for oxidation reactions while the main use of rhodium is the catalysis of reduction reactions. The global reactions involved are the following:

$$2CO + O_2 \rightarrow 2CO_2; \quad (1.1)$$

$$2NO_x \rightarrow xO_2 + N_2; \quad (1.2)$$

$$C_xH_{2x+2} + [(3x01)/2]O_2 \rightarrow xCO_2 + (x+1)H_2O. \quad (1.3)$$

Nowadays some new catalytic converters are being developed based on non-precious group metals, nor on rare earths (Iovino, 2013) but all these solutions are still in the research stage so platinum is still largely used in all cars.

1.1.2 An example of hydrogen electrochemical oxidation with platinum: fuel cells

Another interesting application of platinum as catalyst are fuel cells that directly convert the chemical energy of the fuel (e.g. hydrogen) into electricity through a mechanism based on an electrochemical hydrogen oxidation reaction. A wide range of different types of fuel cells can be found in literature but all of them are made by a negative side (anode), a positive side (cathode) and an electrolyte. At the negative side, we have a production of electrons that move to an external electric circuit producing electricity, while the electrolyte is placed between the anode and the cathode and it allows charges to transfer between the two sides. The mechanism of all fuel cells is similar but they differ on the type of electrolyte used because a different electrolyte can allow the movement of different charges. Figure 1.2 shows the scheme of a proton-conducting fuel cell where we have the electrochemical reaction of hydrogen split into ions at the negative side:

$$H_2 \rightarrow 2H^+ + 2e^-; \quad (1.4)$$

protons can pass through the electrolyte to the cathode where we have the combination of oxygen, ions and electrons to produce water.

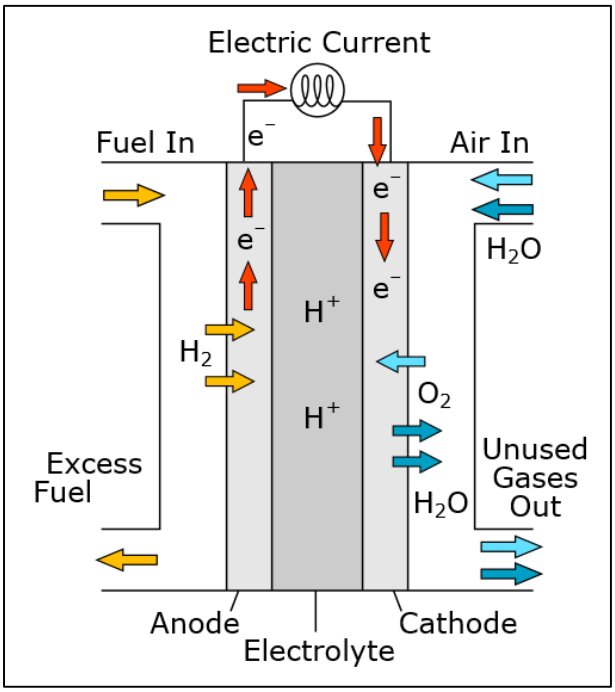

Figure 1. 2. *Scheme of a proton-conducting fuel cell.*

This technology is very interesting because it allows a direct production of electricity from fuels and it has an energy efficiency usually between 40–60%, or up to 85% if waste heat is captured. This device uses platinum as anode or cathode: for the negative side, a platinum/ruthenium catalyst is preferred while, for the positive side, platinum is dispersed on a carbon support. (Diehl, 2003)

Chapter 2

The state of art of the main reaction and catalyst features

The second Chapter presents a critical analysis of the literature on this subject. The first part deals with the surface reaction mechanism and with the Pt surface restructuring during chemical treatments. The second part deals with all kinds of stagnation-point flow geometries and it makes a critical analysis and a comparison between literature geometries. At the end of the Chapter, there is an introduction to the main geometry features of the reactor used in this Thesis.

2.1 Surface reaction mechanism and kinetic properties in the stagnation-point flow geometry

For the catalytic hydrogen oxidation, different reaction mechanisms have been proposed but 6 are the most widespread (Table 2.1 and 2.2). All of them propose a Langmuir-Hinshelwood model to describe chemical adsorption and all reactions have the generic form to express *K*, the kinetic constant [cm, mol, s – reaction depending]:

$$k(T) = \mathrm{A}e^{-\mathrm{Ea}/\mathrm{R}T} \tag{2.1}$$

where A is the pre-exponential factor [cm, mol, s – reaction depending] Ea is the activation energy [kJ/mol] and R is the ideal gas constant.
However, there are significant differences between the mechanisms and they can be divided into 3 groups according to the similarities they have:

1. Group of Först (2002), Deutschmann *et al.* (1996) and Rinnemo *et al.* (1997);

The involved reactions and the value of kinetic parameters in these mechanisms are very similar between themselves and they are taken from literature references. Earlier models do not take into account reactions of atomic adsorption and desorption while Först (2002)'s mechanism considers them. However, the influence in the global mechanism of atomic adsorption/desorption is not relevant (low pre-exponential factors and high activation energy).

2. Group of Bui *et al.* (1997), Vlachos and Bui (1996) and Fernandes *et al.* (1999)

Table 2. 1. *A comparison between the pre-exponential factor or the sticking coefficient of the main reaction mechanisms.*

Reaction	**A [cm, mol, s] or sticking coefficient [-]**					
	Först (2002)	**Deutschmann *et al.* (1996)**	**Rinnemo *et al.* (1997)**	**Warnatz *et al.* (1994)**	**Bui *et al.* (1997) / Valchos Bui(1996)**	**Fernandes *et al(1999)***
$H_2 \rightarrow 2H^*$	0.046	0.046	0.046	**N/A**	1	1
$H \rightarrow H^*$	1	1	**N/A**	1	**N/A**	**N/A**
$2H^* \rightarrow H_2$	$3.70 \cdot 10^{21}$	$3.70 \cdot 10^{21}$	$3.70 \cdot 10^{21}$	**N/A**	$1.66 \cdot 10^{4}$	$1 \cdot 10^{13}$
$H^* \rightarrow H$	$1 \cdot 10^{13}$	**N/A**	**N/A**	**N/A**	**N/A**	**N/A**
$H_2 \rightarrow H_2^*$	**N/A**	**N/A**	**N/A**	0.05	**N/A**	**N/A**
$H_2^* \rightarrow 2H^*$	**N/A**	**N/A**	**N/A**	$7.5 \cdot 10^{22}$	**N/A**	**N/A**
$O_2 \rightarrow 2O^*$	0.023	0.07	0.07	**N/A**	0.279/0.04	0.279
$O \rightarrow O^*$	1	1	**N/A**	1	**N/A**	**N/A**
$2O^* \rightarrow O_2$	$3.70 \cdot 10^{21}$	$3.70 \cdot 10^{21}$	$3.70 \cdot 10^{21}$	**N/A**	$1.66 \cdot 10^{4}$	$1 \cdot 10^{13}$
$O^* \rightarrow O$	$1 \cdot 10^{13}$	**N/A**	**N/A**		**N/A**	**N/A**
$O_2 \rightarrow O_2^*$	**N/A**	**N/A**	**N/A**	0.023	**N/A**	**N/A**
$O_2^* \rightarrow 2O^*$	**N/A**	**N/A**	**N/A**	$2.5 \cdot 10^{24}$	**N/A**	**N/A**
$OH \rightarrow OH^*$	1	1	1	1	**N/A**	**N/A**
$H^* + O^* \rightarrow OH^*$	$3.70 \cdot 10^{21}$	$3.70 \cdot 10^{21}$	$3.70 \cdot 10^{21}$	$3.7 \cdot 10^{21}$	$1.66 \cdot 10^{6}$	$1 \cdot 10^{15}$
$OH^* \rightarrow OH$	$1 \cdot 10^{14}$	$1 \cdot 10^{13}$	$1 \cdot 10^{13}$	**N/A**	$2.49 \cdot 10^{4}$	$1.5 \cdot 10^{13}$
$OH^* \rightarrow H^* + O^*$	**N/A**	**N/A**	**N/A**	**N/A**	$1.66 \cdot 10^{-1}$	$1 \cdot 10^{8}$
$H^* + OH^* \rightarrow H_2O^*$	$3.70 \cdot 10^{21}$	$3.70 \cdot 10^{21}$	$3.70 \cdot 10^{21}$	$3.7 \cdot 10^{21}$	$1.49 \cdot 10^{8}$	$9 \cdot 10^{16}$
$OH^* + OH^* \rightarrow H_2O^* + O^*$	$3.70 \cdot 10^{21}$	$3.70 \cdot 10^{21}$	$3.70 \cdot 10^{21}$	$3.7 \cdot 10^{24}$	$1.66 \cdot 10^{6}$	$1 \cdot 10^{15}$
$H_2O \rightarrow H_2O^*$	0.7	0.75	0.75	0.75	0.1	0.1
$H_2O^* \rightarrow H_2O$	$1 \cdot 10^{13}$	$1 \cdot 10^{13}$	$1 \cdot 10^{13}$	**N/A**	$1.66 \cdot 10^{4}$	$1 \cdot 10^{13}$
$H_2O^* \rightarrow H^* + OH^*$	**N/A**	**N/A**	**N/A**	**N/A**	$2.99 \cdot 10^{4}$	$1.8 \cdot 10^{13}$
$H_2O^* + O^* \rightarrow 2OH^*$	**N/A**	**N/A**	**N/A**	**N/A**	0	0

The considered reactions are different from the previous group: they do not take into account the atomic adsorption and desorption but they include the reverse reactions of catalytic production of products and intermediates:

$$OH^* \rightarrow H^* + O^*; \quad (2.2)$$
$$H_2O^* \rightarrow H^* + OH^*; \quad (2.3)$$
$$H_2O^* + O^* \rightarrow 2OH^*; \quad (2.4)$$

where "*" indicates an adsorbed species. However, the contribution of these reactions to the global mechanism seems not to be relevant (low pre-exponential factors and high activation energy, as argued by Försth *et al.* (1999)).

All these mechanism are based on Williams *et al.* (1992)'s mechanism.

3. Group of Warnatz et al. (1994)

The mechanism of this group is very different from previous ones. His main differences regard the adsorption of hydrogen and oxygen because it is divided into 2 steps ("dissociative adsorption"):

$$H_2 / O_2 \rightarrow H_2^* / O_2^*; \quad (2.5)$$

$$H_2^* / O_2^* \rightarrow 2H^* / 2O^*. \quad (2.6)$$

All considered reactions are reversible so the total amount of reactions are higher than the previous mechanisms.

Table 2.2. *A comparison between the activation energy of the main reaction mechanisms.*

Reaction	**E_a [KJ/mol]**					
	Först (2002)	**Deutschmann *et al.*(1996)**	**Rinnemo *et al.* (1997) [eV]**	**Warnatz *et al.* (1994)**	**Bui *et al.* (1997) / Valchos Bui (1996)**	**Fernandes *et al. (1999)***
$H_2 \rightarrow 2H^*$	0	0	0	**N/A**	0	0
$H \rightarrow H^*$	0	0	**N/A**	0	**N/A**	**N/A**
$2H^* \rightarrow H_2$	67	$67 - 6 \cdot \Theta_{H2}$	$0.7 - B \cdot \Theta$	**N/A**	75	$75 - A \cdot \Theta_{H2}$
$H^* \rightarrow H$	249	**N/A**	**N/A**	**N/A**	**N/A**	**N/A**
$H_2 \rightarrow H_2^*$	**N/A**	**N/A**	**N/A**	0	**N/A**	**N/A**
$H_2^* \rightarrow 2H^*$	**N/A**	**N/A**	**N/A**	16	**N/A**	**N/A**
$O_2 \rightarrow 2O^*$	0	0	0	**N/A**	0	0
$O \rightarrow O^*$	0	0	**N/A**	0	**N/A**	**N/A**
$2O^* \rightarrow O_2$	213	$213–60 \cdot \Theta_{O2}$	$2.2-0.42 \cdot \Theta$	**N/A**	218	$218 – A$
$O^* \rightarrow O$	356	**N/A**	**N/A**	**N/A**	**N/A**	**N/A**
$O_2 \rightarrow O_2^*$	**N/A**	**N/A**	**N/A**	0	**N/A**	**N/A**
$O_2^* \rightarrow 2O^*$	**N/A**	**N/A**	**N/A**	0	**N/A**	**N/A**
$OH \rightarrow OH^*$	0	0	0	0	**N/A**	**N/A**
$H^* + O^* \rightarrow OH^*$	54	11	0.12	19.3	10	$10-A \cdot \Theta_{O2}$
$OH^* \rightarrow OH$	245	193	2	**N/A**	201	201
$OH^* \rightarrow H^* + O^*$	**N/A**	**N/A**	**N/A**	**N/A**	21	21
$H^* + OH^* \rightarrow H_2O^*$	65	17	0.18	0	63	63
$OH^* + OH^* \rightarrow H_2O^* + O^*$	74	48	0.5	101	51	51
$H_2O \rightarrow H_2O^*$	0	0	0	0	0	0
$H_2O^* \rightarrow H_2O$	65	40	0.42	**N/A**	45	45
$H_2O^* \rightarrow H^* + OH^*$	**N/A**	**N/A**	**N/A**	**N/A**	155	155
$H_2O^* + O^* \rightarrow 2OH^*$	**N/A**	**N/A**	**N/A**	**N/A**	133	133

Most of authors propose an activation energy for the desorption of oxygen and hydrogen that is related to the surface coverage (Θ) and to experimental parameters (A and B). While the

adsorption is not influence by the situation on the catalyst surface, the desorption of a species is favored (lower activation energy) when the surface is already occupied by the same species. All these mechanisms find good agreement with experimental data; however, the kinetic parameters need to be further fitted to correspond to the data.

One of the most important parameters in this Thesis is the ignition temperature and only Vlanchos and Bui (1996) compare the experimental ignition temperature with the simulation. After performing a sensitivity analysis, they observed that the temperature ignition is very affected by the activation energy needed for the hydrogen desorption so they fitted the activation energy with the experimental data. Since they performed 2 experiments and they obtained two different activation energies, it is questionable whether there is a lack of reproducibility.

Another issue regarding literature papers is that they performed either a simulation work (Bui *et al.*, 1997 etc.) or an experimental investigation (Brady *et al.*, 2010 etc.) without validating the obtained data.

It is important to notice that the energy barrier for the desorption of hydrogen is much lower than the one for oxygen in all considered mechanisms. The result is that hydrogen may react to form water or may desorbed while oxygen more likely reacts. Horch *et al.* (1999) confirm this assumption because they observed that hydrogen can easily adsorb on platinum also at room temperature while oxygen needs a higher temperature.

Bui *et al.*, (1997)'s model is in accord with this suggestion and it proposes two different reaction paths according to the dominant compound adsorbed on the surface. When hydrogen is the dominant compound, there is a hydrogenation reaction of OH^* following the path:

$$\frac{1}{2}H_2 \overset{ads}{\leftrightarrow} H^* \overset{O^*}{\rightarrow} OH^* \overset{H^*}{\rightarrow} H_2O^*. \tag{2.7}$$

On the other hand, when oxygen is dominant on the surface, there is a disproportion reaction of OH^* according to the path (Bui *et al.*, 1997):

$$O_2 \overset{ads}{\longrightarrow} 2O^* \overset{2H^*}{\longrightarrow} 2OH^* \rightarrow H_2O^* + O^*. \tag{2.8}$$

Figure 2.1 illustrates a schematic representation of the comparison between the two paths.

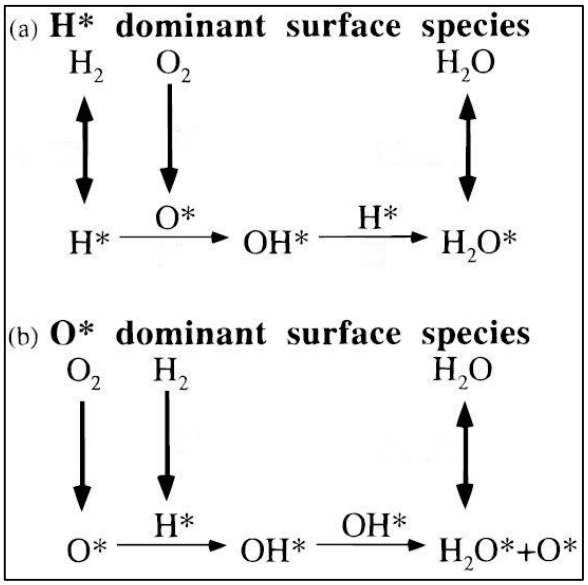

Figure 2.1. *A schematic representation of the two reaction paths (Bui et al., 1997).*

The number of platinum sites is analyzed in a wide range of modelling and experimental papers. Different authors propose different numerical values; however, their estimation is always comprised between 0.92*1015 site/cm^2 and 1.6*1016 site/cm^2 (Försth *et al.*, 1999; Bui *et al.*, 1997 and Minca *et al.*, 2007).

2.1.1 The coverage of the platinum surface

Bui *et al.* (1997) also carried out several calculations to predict the surface concentration varying the inlet composition of reagents. In particular, they divided the situation before and after the catalytic ignition. The modelled system is a mixture of hydrogen in air where Y_{H2} is the molar fraction of hydrogen in the inlet gas phase.

Before the ignition, oxygen is the dominant surface component if $Y_{H2} < 0.15$ while hydrogen is the dominant component if $Y_{H2} > 0.15$. The situation is slightly different after the ignition because the dividing molar fraction is $Y_{H2} = 0.03$ instead of 0.15. The system exhibit an interesting behavior when $0.03 < Y_{H2} < 0.15$ because the dominant surface component swiftly changes from hydrogen to oxygen right after the ignition. For this composition range, most of hydrogen reacts with the ignition so, during the course of the reaction, the oxygen partial pressure increases and the surface composition changes.

Fernandes *et al.* (1999) performed similar calculations to predict the surface concentration. They vary the inlet reagents volume ratio (H_2/O_2) in a 88% N_2 dilution and they observed two completely different situations before and after the ratio: $H_2/O_2 = 0.9$. When $0 < H_2/O_2 < 0.9$, oxygen is the dominant surface component while, when $H_2/O_2 > 0.9$ hydrogen is dominant. It is important to notice that the ratio: $H_2/O_2 = 0.9$ corresponds to the stoichiometric surface composition.

Figure 2.2 shows Fernandes *et al.* (1999)'s results that are in agreement with Bui *et al.* (1997)'s argumentations.

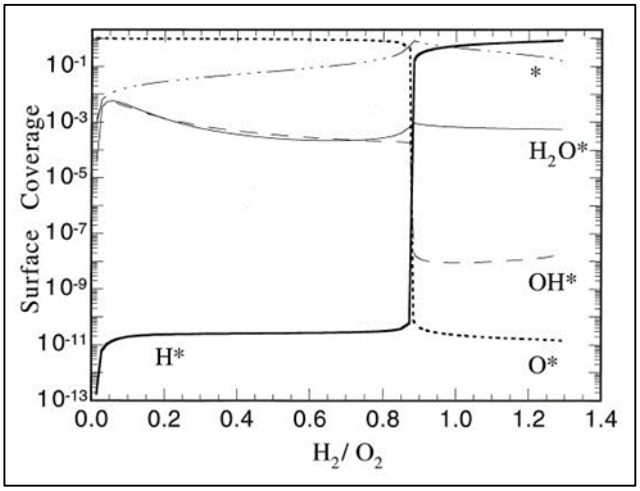

Figure 2. 21. *Fernandes et al. (1999)'s estimation of the surface coverage varying the inlet reagents volume ratio (H_2/O_2) in a 88% N2 dilution. The "strain rate" is 5 s^{-1} (parameter described in §2.4), the pressure is atmospheric and the temperature is the autothermal temperature (Fernandes et al., 1999).*

Similar considerations are argued by Försth *et al.* (2000) because they observed a similar swift variation of the surface coverage, according to Bui *et al.* (1997)'s and Fernandes *et al.* (1999)'s papers. They analyzed the surface composition varying the parameter:

$$\alpha = \frac{p_{H2}}{p_{H2}+p_{O2}} \tag{2.4}$$

where p_{H2} is the hydrogen partial pressure and p_{O2} is the oxygen partial pressure. Their result is shown in Figure 2.3.

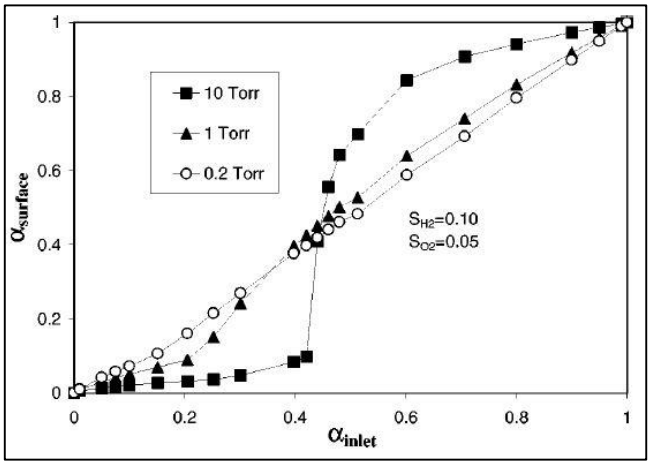

Figure 2.3. *CHEMKIN simulation of the surface coverage according to the variation of the reagents inlet partial pressure at 700 K (Försth et al., 2000).*

2.1.2 Minor effects on the ignition of the reaction

The ignition of the reaction has been deeply studied since it is a very important kinetic feature. The presence of the catalyst inhibits the ignition in the gas phase because the catalyst adsorbs reagents and desorbs water. The global result of this phenomenon is the raise of the temperature needed for the gas-phase ignition of about 150 K (Bui *et al.,* 1996; Vlachos, 1996 and Försth *et al.,* 1999). However, the catalytic reaction happens at lower temperature than the gas-phase reaction so it can provide the increase of temperature needed for the gas-phase reaction. In conclusion, it is still not clear if the catalyst promotes or inhibits the reaction in the gas phase. Figure 2.4 a prediction of the variation of the compounds molar fraction near the catalyst surface.

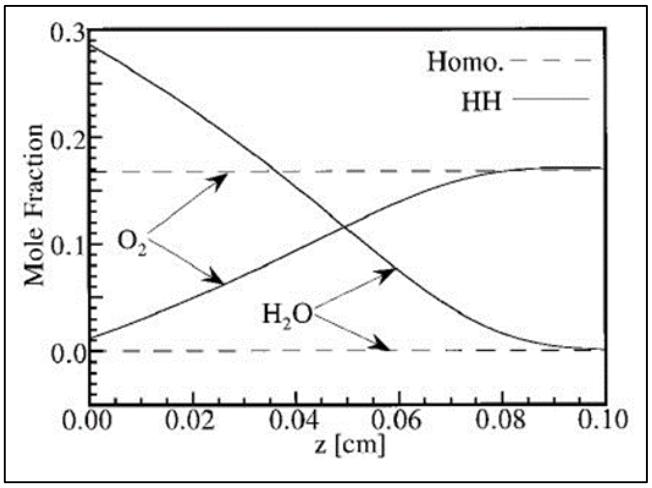

Figure 2.4. *Mole fractions of H_2O and O_2 close to the catalyst surface for the homogeneous (dashed line) and homogeneous-heterogeneous (solid line) processes for 20% H_2-air. In the homogeneous-heterogeneous process, a significant fraction of H_2O is formed catalytically before gas-phase ignition (Bui et al., 1996).*

The kinetic model performed by Bui *et al.* (1997) shows also the auto-inhibition effect of hydrogen that can raise the ignition temperature. Since the hydrogen adsorption is preferred over the oxygen adsorption, the platinum surface can be easily saturated (‘poisoned’) by hydrogen if the inlet hydrogen composition is sufficient. Oxygen adsorption is inhibited because the surface is already saturated and the global effect is the raise of the ignition temperature. Indeed, a higher temperature is needed to desorb hydrogen from the surface so it can be accessed by oxygen.

Figure 2.5 shows the auto-inhibition and temperature effect observed by Bui *et al.* (1997).

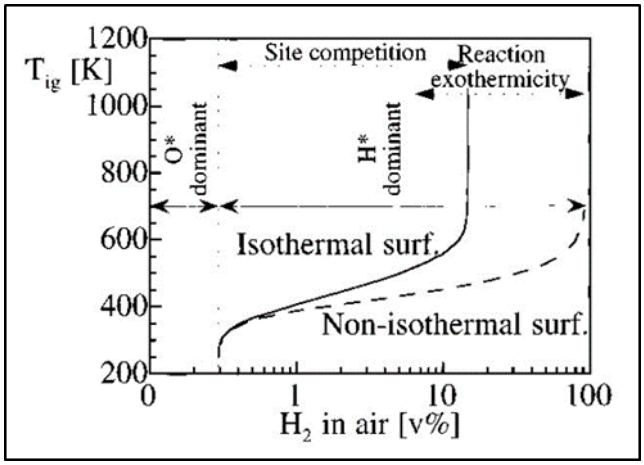

Figure 2.5. *(Solid and dashed lines) Catalytic ignition temperature as a function of H_2 composition in air with an isothermal surface and a nonisothermal surface respectively. H_2 self-inhibits its catalytic ignition. Very fuel-lean mixtures ignite upon contact with platinum. The parameters are pressure of 1 atm and strain rate of 500 s^{-1} (parameter described in §2.4) (Bui et al., 1997).*

Pressure is also influencing the ignition temperature because the auto-inhibition phenomenon is proportional to pressure Bui *et al.* (1997) and reagents dilution has a similar effect because a variation in dilution corresponds to a variation in the reagents partial pressure Park *et al.* (1999).

2.2 The restructuring of the platinum surface

The surface reaction may also be influenced by the restructuring of the Pt surface because these changes affect the activity of the catalyst.

Previous studies on a platinum catalyst at the Chemical Reaction Engineering Laboratory of the University of Padua show that thermal and chemical treatments on the platinum surface can create a completely different surface made by micro-facets locally oriented without a global direction of orientation (Figure 2.6).

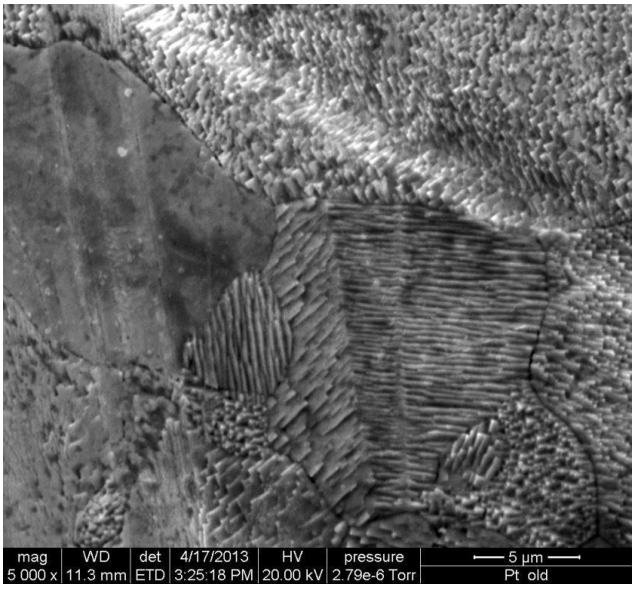

Figure 2. 6. *A scanning electron microscope (SEM) image of the Pt catalyst previously tested at the Chemical Reaction Engineering Laboratory of the University of Padua. The original flat surface is deeply modified and the final structure has a wide range of micro-facets with a local orientation.*

Many authors observed similar effects on platinum foils and they confirmed that thermal and chemical treatments (e.g. adsorption of molecules or surface reactions) can modify the platinum surface creating many "*roofs*" connected by sharply defined edges (Kraehnert and Baerns, 2007; Fernandes *et al.*, 1999). The driving force of this phenomenon is the reaching of an equilibrium state because, with the reformed surface, the minimum of the total surface free energy is approached (Cabié *et al.*, 2010) (Iddir *et al.*, 2007).

Kraehnert and Baerns (2007) suggest that a thermal treatment on the catalytic surface does not induce any structural change; they performed a thermal treatment of 30 h at 374 °C and a sequence of treatments up to 700 °C for a total of 240 h without observing any change.

Some surface changes can be obtained during the course of catalytic reactions (e.g. hydrogen oxidation (Fernandes *et al.*, 1999, Figure 2.7) and ammonia oxidation (Kraehnert and Baerns, 2007, Figure 2.8)) and by treating the catalytic surface with hydrogen and oxygen at high temperature (Imbihl *et al.*, 2007, Figure 2.9).

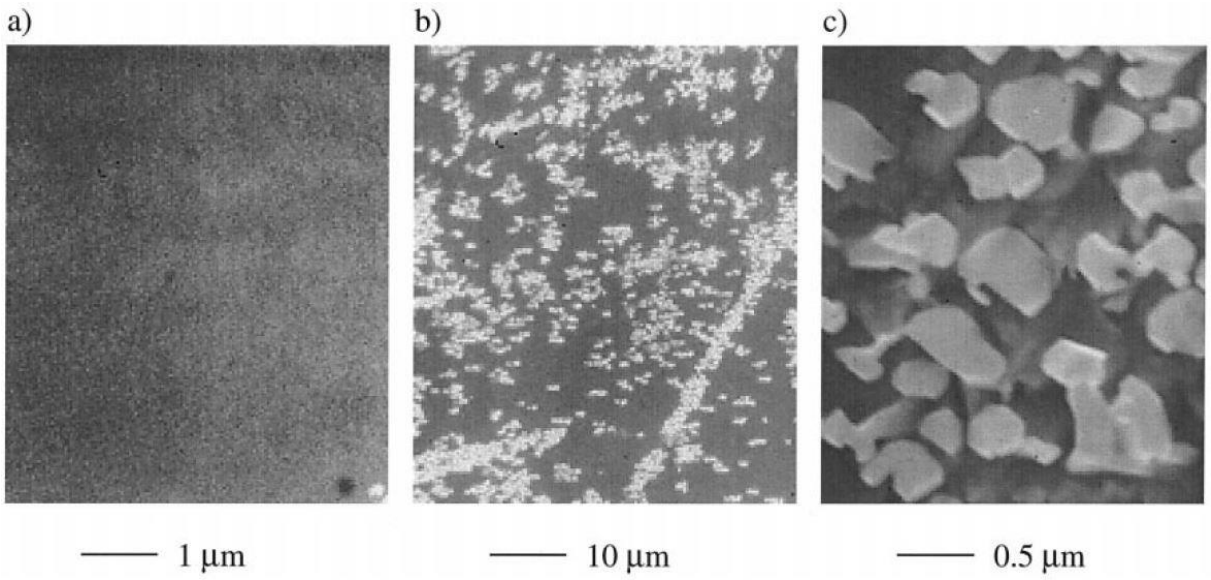

Figure 2. 7. *Scanning electron micrographs of a fresh platinum foil (a) and a platinum foil after 10 hr of catalytic oxidation at 873K, H_2/O_2 = 0.5, and 88% N_2 dilution at two different magnifications (b, c). Chemical oxidation causes morphological evolution of the catalyst (Fernandes et al., 1999).*

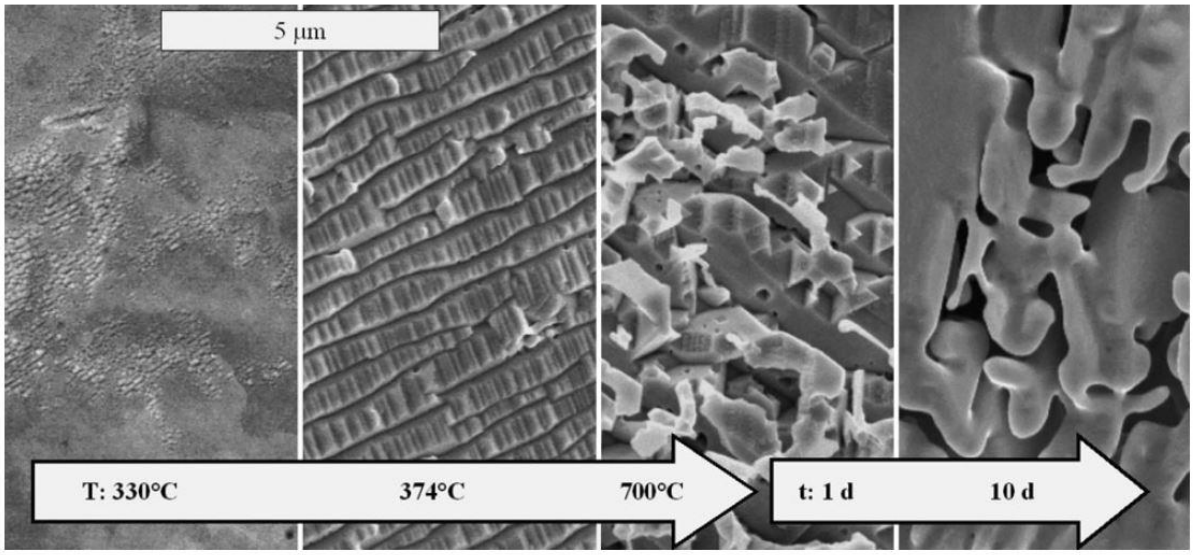

Figure 2. 8. *SEM images of the surface of Pt foil, indicating the progressing roughening of the surface of Pt foil induced by ammonia oxidation at different temperatures and times-on-stream (same scale in all images) (Kraehnert and Baerns, 2007).*

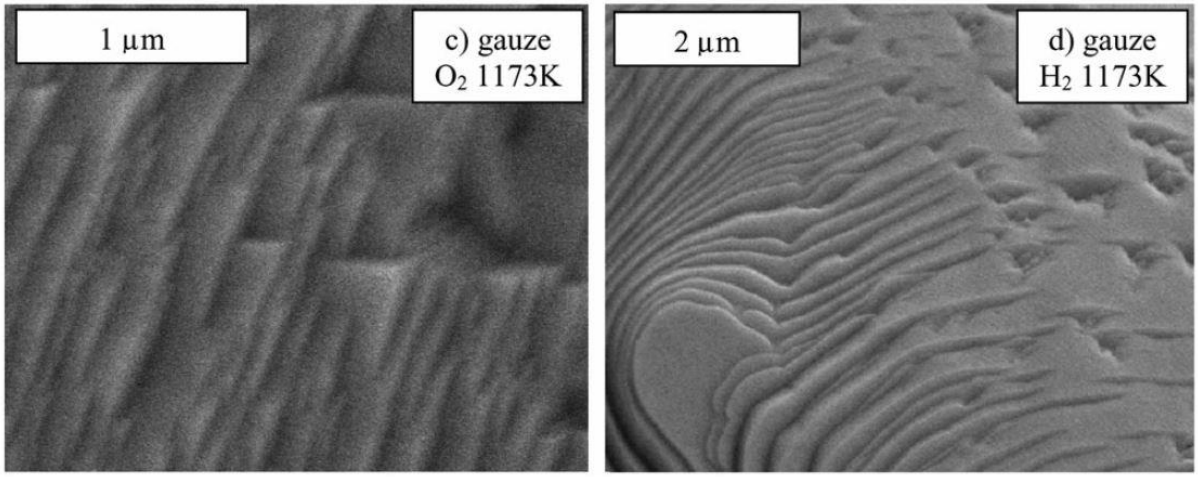

Figure 2. 9. *SEM of platinum gauze: (a) Pt gauze treated in O2 at 1173 K. (d) Pt gauze regenerated in H2 at 1173 K (Imbihl et al., 2007).*

As shown in Figure 2.8, the restructuring mechanism and the configuration of the surface may vary also because of pressure, temperature and time of treatment. Since adsorbed compounds promote the restructuring mechanism, increasing the pressure can increase the entity of adsorption and the restructuring mechanism as well (Baerns *et al.*, 2005; Horch *et al.*, 1999). However, temperature differences are extremely important in the reformed structure: when the temperature is above 500 °C, the obtained surface is tri-dimensional while, under 500 °C, we have a flat structure, as further discussed in §2.2.1 and §2.2.2

2.2.1 High temperature restructuring (500-700 °C)

When the temperature reaches about 700 °C, the reformed structure becomes tri-dimensional with many protuberances outside the original surface.

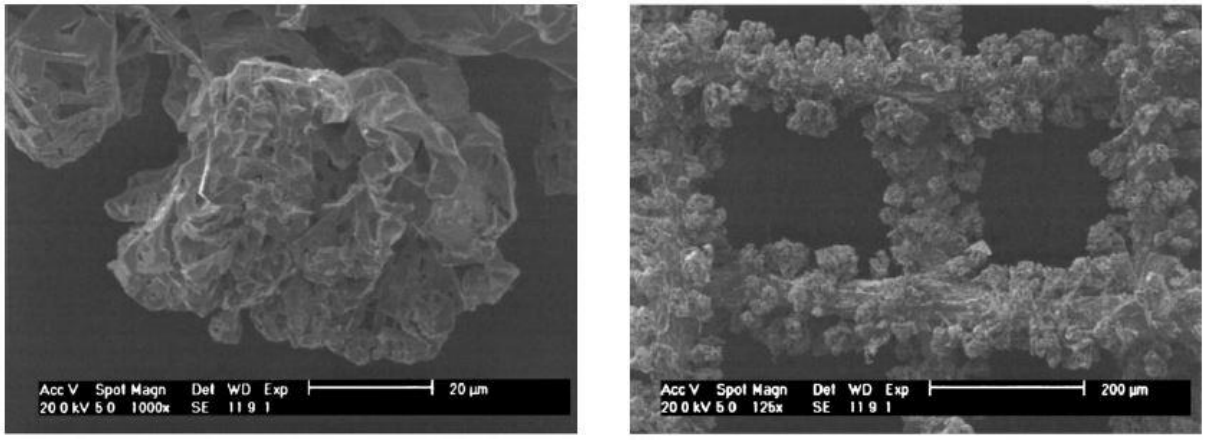

Figure 2. 10. *A typical protuberance of platinum (a) developed during ammonia oxidation on a platinum catalyst net (b) (Nielsen et al. 2001).*

Imbihl *et al.* (2007) suggest that the main mechanism for the surface restructuring is the great mobility of the Pt-adsorbed compounds. An increase of temperature can enhanced the mobility

of Pt atoms as well as the adsorption of gases so the surface restructuring is increased by the adsorbed compounds.
Apart from the surface structure, the main difference between the restructuring mechanism at high and low temperature is the adsorbed compound. Indeed, oxygen can significantly adsorb and enhance the surface diffusion only at high temperature while hydrogen adsorption is significant only at temperatures lower than 500 °C. There is a correspondence between the final surface structure and the adsorbed species: oxygen adsorption produces tri-dimensional structures while bi-dimensional facets are obtained with hydrogen adsorption.
Since the aim of this Thesis is the study of hydrogen oxidation at low temperature, the adsorption and restructuring mechanism at high temperature will not be described in detail.

2.2.2 Low temperature restructuring (300-500 °C)

At lower temperature, the reformed structure is completely different because it has a planar shape with many facets made by flat planes connected by sharply defined edges (Kraehnert and Baerns, 2007).
Horch *et al.* (1999) analyze the effect of hydrogen adsorption on platinum and they underline how the displacement of Pt-H compounds at room temperature is up to 500 times higher the displacement of Pt atoms. Indeed, Pt-H compounds have a lower energy barrier needed for the displacement.
Water has a significant role in this complex mechanism because a steam treatment modifies the reformed structure reducing the sharp edges of facets. The structure becomes curved and smooth (Nielsen *et al.*, 2001) because water reduces the total surface free energy so the driving force of the faceting mechanism is reduced.
Nielsen *et al.* (2001) also observed that water desorption is enhanced by the new platinum structure because water is much closer to a sharp edge where it can easily desorb. The catalytic activity is globally enhanced because of this phenomenon and because there is an increase of the total platinum surface area during the faceting process.
The paper by Cabié *et al.* (2010) deeply studies the platinum crystals during the faceting process: at first, it underlines, according to Imbihl *et al.* (2007), that hydrogen and oxygen treatments induce surface changes with a different orientation that can be reversibly modified with a treatment of the other gas. Then, the authors observed that the most stable thermodynamic form of the platinum crystal, after an oxygen treatment, is a cubic structure limited by (100) faces and truncated at corners by (111) faces. However, during a hydrogen treatment, this stability configuration is modified since (100) faces shift to (111) faces and the ratio between surfaces free energies ($\sigma_{100}/\sigma_{111}$) is 1.12. The final structure due to a hydrogen treatment has a cuboctahedric shape still limited by 8 (111) faces and truncated by (001) faces

(Cabié *et al.*, 2010). At the end, the authors performed an oxygen treatment and they were able to restore the original cubic shape.

Iddir *et al.* (2007) performed a thermodynamic calculation on free Pt particles in order to estimate the most stable structure and they observed a truncated octahedric particle shape with a very thin (110) face between the other faces.

One of the research topics of this Thesis is the evaluation of the catalytic activity after a hydrogen or oxygen pre-treatment. Earlier experiments reported dramatic increases/decreases of activity after exposure to H_2 or O_2 reach mixtures, but no rationale was identified. The first authors who tried to "activate" the catalyst in this way are Fernandes *et al.* (1999). In particular, they underline how the catalyst activity is closely related to the history of the catalyst and they observed a much higher activity after a thermochemical treatment. They performed a treatment at 873 K for 20 h in a hydrogen and oxygen atmosphere with a ratio $H_2/O_2 = 0.5$ in 88% N_2 dilution and, in this way, they could "activate" the catalyst by restructuring its surface. This result is confirmed also by Brady *et al.* (2010) because they noticed that the ignition temperature decreases by 40 K when the catalyst is restructured.

2.3 Generalities about the stagnation-point flow geometry

The stagnation-point flow geometry is a particular reactor configuration where the catalyst is placed orthogonally to the inlet flow. In this way, there is a stagnation zone where reagents velocity is reduced and it reaches values close to 0 at the center of the surface. After reaching the catalytic surface, the fluid flow is forced to deflect and it reaches the outlet usually placed alongside the catalyst (Figure 2.11).

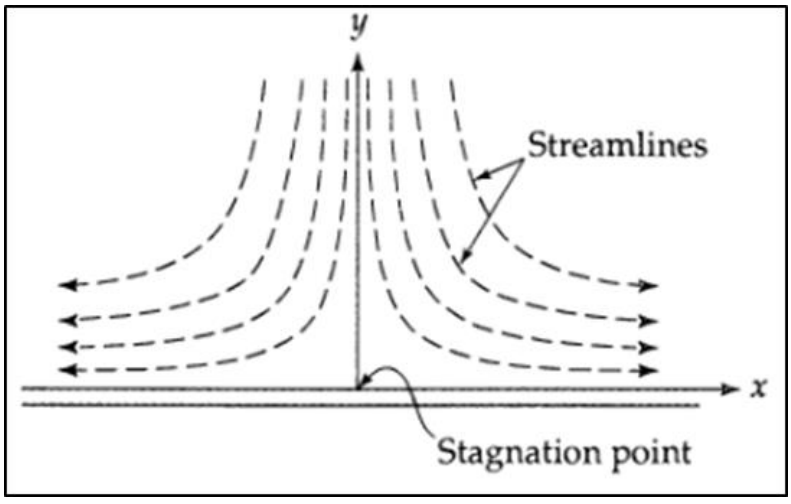

Figure 2.11. *A general scheme of the stagnation-point flow geometry.*

The use of this geometry is important to achieve a homogeneous contact time of reagents on the catalytic surface: indeed, if the inlet channel is much smaller than the catalytic surface,

reagents reach the center of the catalyst then they deflect and flow on the catalytic surface with an homogeneous contact time. However, this is only a theoretical configuration because the fluid flow may be affected by turbolent phenomena. The ideal flow can be achieved with a high degree of aproximation in particular geometries that reduce the by-pass of catalyst and all turbolent phenomena, as discuss in §2.4 and §2.5.
The use of this geometry is particularly important when the catalyst has a circular shape because it is the only geometry that allows a uniform contact time in any radial direction. On the contrary, a tangential fluid flow would create a highly inhomogeneous contact time with the catalyst in the shape of a disk, so the study of kinetic properties would be affected by this behaviour.

2.4 Different types of stagnation-point flow geometries

The definition of stagnation-point flow geometry can be adapted to many different geometries and the earliest literature configuration involves only a 1D thin wire of platinum. This flow arrangement reduces the computational complexity of the reactor modelling because only one dimension needs to be modelled.
However, this configuration is quite old-fashioned because, nowadays, computers performance allows the modelling of the actual 2D flow geometry. The most used configuration is a supported thin platinum foil but, even in this case, we can underline some differences. Indeed, if the inlet channel is much smaller than the catalyst and its support, all reagents are forced to reach the surface and the reaction conversion is globally increased. On the other hand, if the inlet channel is larger than the catalyst, reagents can flow around it without interacting with the catalyst.
Another minor difference concerns the measurement of the surface temperature: some research groups use a resistance measurement while others use an arrangement of thermocouples.
The catalyst used in this Thesis has a circular shape while all catalysts found in literature are foil or 1D wires. Because of that, the reactor configuration in this Thesis is different from any other configuration but it still has many similarities.
Literature configurations can be divided according to the involved research group and the main groups are:

1. Group of Warnatz, Allendorf, Lee and Coltrin at **Universität Stuttgart** (modelling part) and group of Ljungström, Kasemo, Rosen, Wahnström and Fridell at the **University of Göteborg** (experimental part).

They both used a 1D thin platinum wire as shown in Figure 2.12.

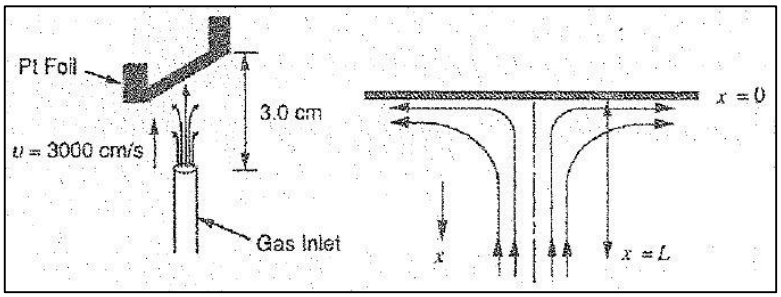

Figure 2.12. *Schematic representation of the experimental configuration used by Ljungström et al. (1989)*

2. Group of Rinnemo, Deutschmann, Behrendt and Kasemo at **Chalmers University of Technology** and **University of Göteborg**.
   Their geometry is similar to the previous one but they used a curved Pt wire (Figure 2.13).

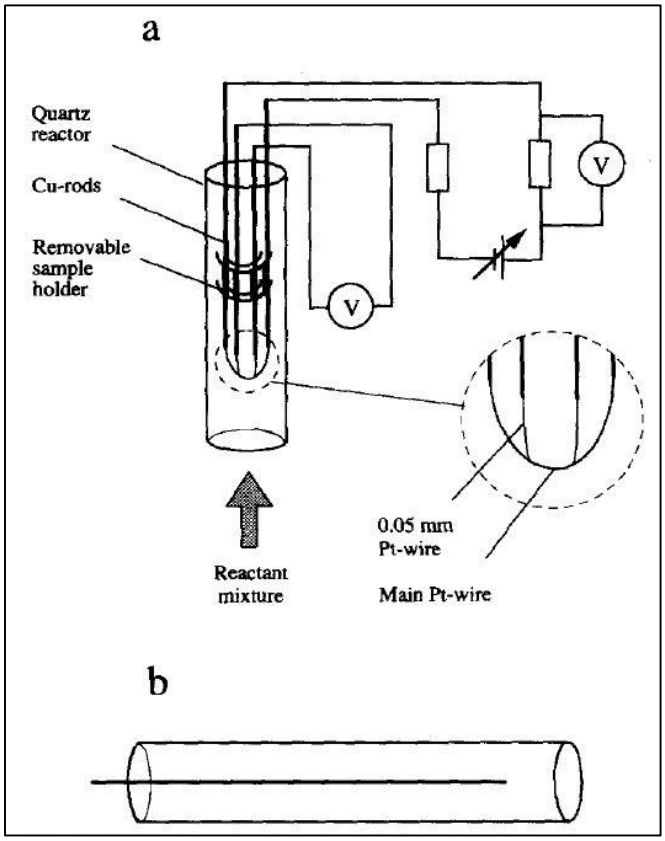

Figure 2.13. *Schematic representation of the experimental configuration used by Rinnemo et al. (1997)*

These 1D configurations cannot be considered proper stagnation-point geometries because most of reactants flow around the Pt wire without reaching its surface and reacting. In particular, the second configuration has only one point (the lower point of the Pt wire) where the inlet flow is orthogonal to the catalyst. Another inaccuracy of these geometries is the different contact

time between reagents and catalyst on the Pt surface. These geometries are the most easily modelled but they are also quite inaccurate.

3. Group of Behrendt, Deutschmann, Schmidt and Warnatz at **Universität Heidelberg**
   They use a Pt foil placed on a vertical support with a larger inlet channel (Figure 2.14).

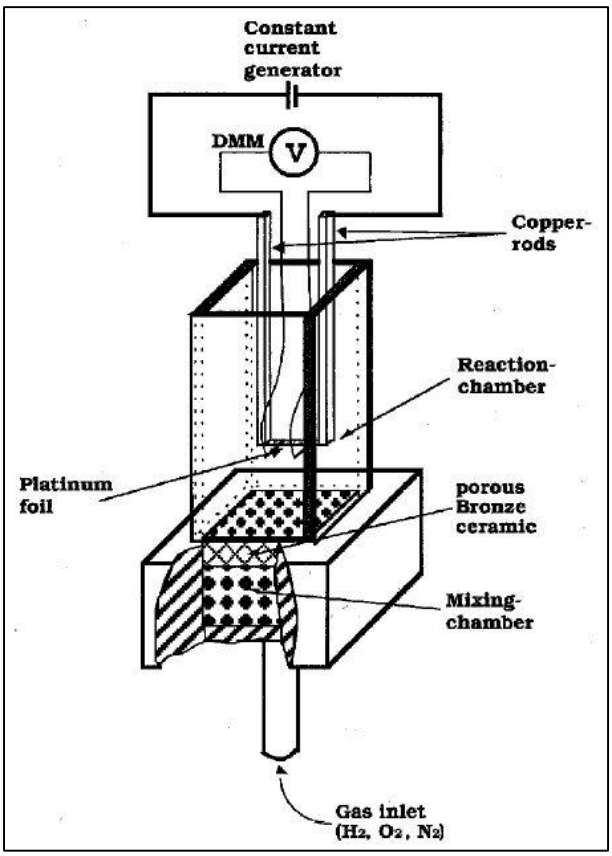

Figure 2.14. *Schematic representation of the experimental configuration used by Behrendt et al. (1996).*

4. Group of Fernandes, Park, Bui and Vlachos at **University of Massachusetts Amherst**. (Figure 2.15).
   They used a geometry similar to the third group (Figure 2.14).

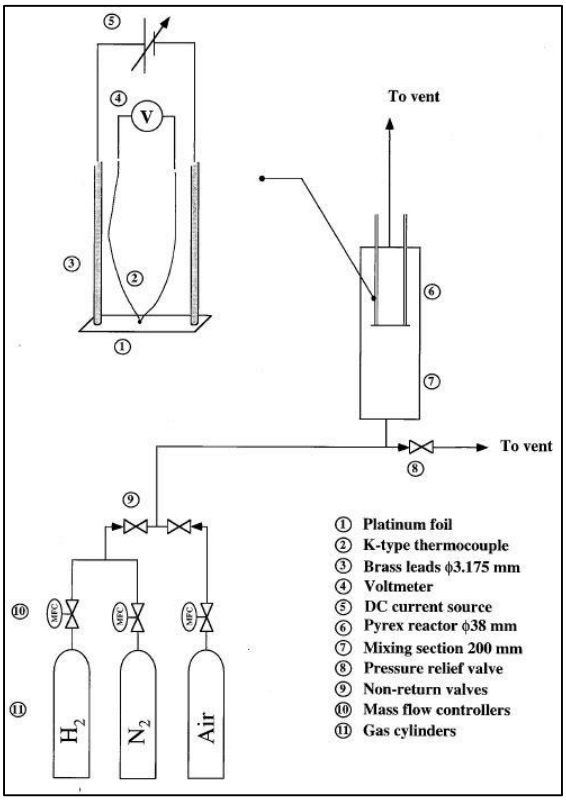

Figure 2. 15. *Schematic representation of the experimental configuration used by Fernandes et al. (1999).*

Behrendt *et al.*'s and Fernandes *et al.*'s geometries are quite similar: they both have a rectangular Pt foil for the catalyst and the inner channel is larger than the Pt support. These configurations improves the 1D geometry because most of the inlet flow is forced to reach orthogonally the Pt surface and to deflect. However, a significant amount of streamlines can still bypass laterally the catalyst. These reactors also have a inhomogeneous reactants-catalyst contact time, so several improvements are still needed.

5. Group of Försth, Gudmundson, Persson and Rosén at **Chalmers University of Technology and Göteborg University**. (Figure 2.16)

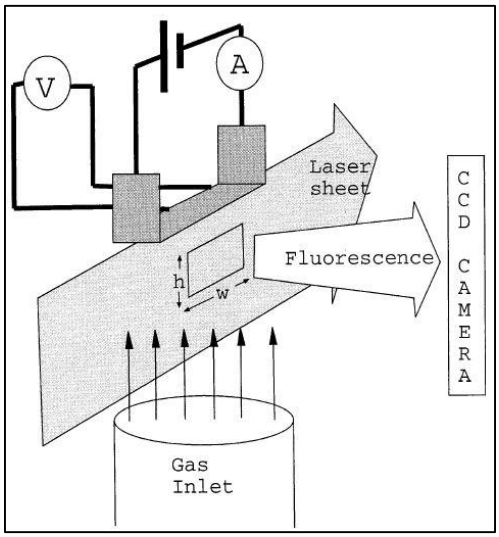

Figure 2. 26. *Schematic representation of the experimental configuration used by Försth et al. (1999)*

They use a configuration similar to the Warnatz *et al*.'s group. However, they perform a detailed kinetic modelling through the software tool "CHEMKIN" unlike the Universität Stuttgart's group. Even if the modelling of the system is refined, there still are the issues of the previous geometries (catalyst bypass, different contact time etc…).

6. Group of Brady, Sung and T'ien at **University of Connecticut**. (Figure 2.17)

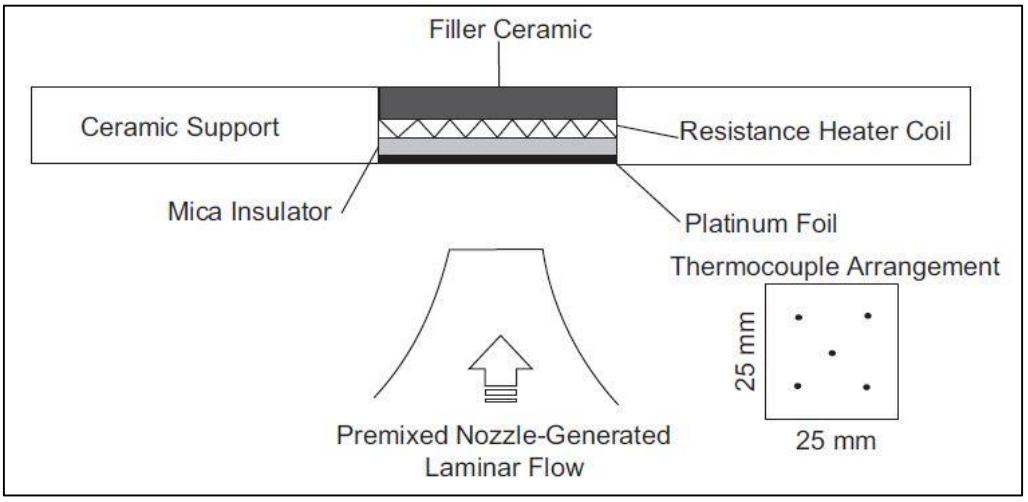

Figure 2. 37. *Schematic representation of the experimental configuration used by Brady et al. (2010).*

This group uses a different configuration from all others because it is the first that proposes a reactor configuration where the catalyst and its support are larger than the inlet channel (Figure 2.17). This is the first step toward an optimized configuration and the reactor configuration proposed in this Thesis has some similarities with this configuration. With Brady *et al.* (2010)'s reactor, all inlet streamlines deflect orthogonally when they reach the catalyst. In this way, all

streamlines can reach the catalyst and no streamlines bypass it laterally. However, there still are fluid dynamics issues like the inhomogeneous contact time of reagents (Figure 2.18).

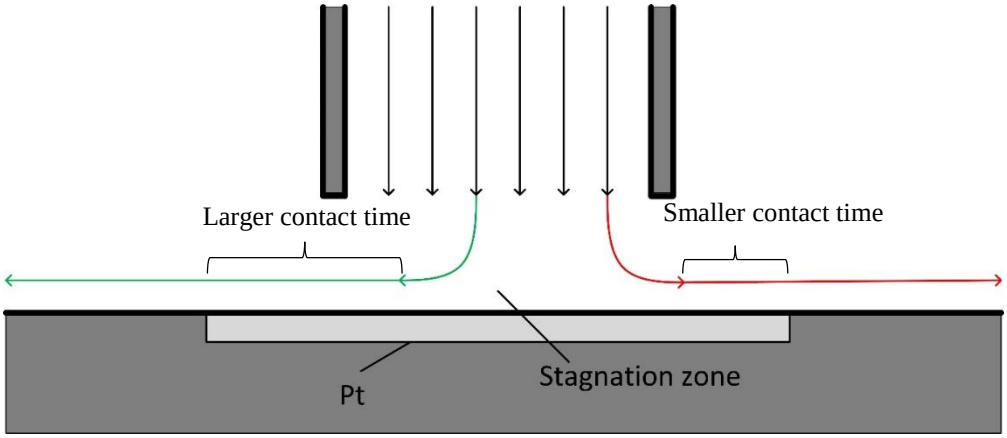

Figure 2.18. *A schematic representation of Brady et al. (2010)'s configuration that underlines the difference in terms of contact time with the catalyst of two different streamlines.*

Indeed, their platinum foil has a width of 25.4 mm and the nozzle has a diameter of 10.4 mm so reagents can reach the catalyst surface in the center as well as in other peripheral zones. This difference results in a different contact time like the green streamline on the left and the red streamline on the right of Figure 2.18.

Flow differences inside the reactor are related also the effect of the "*strain* (or *stretch*) *rate*". This parameter is defined as u/L where u is the average inlet fluid velocity and L is the distance between the reagents nozzle and the catalyst; Valchos and Bui (1996) underline that the *strain rate* is proportional to the reagents mass transfer toward the catalyst.

2.5 Critical analysis of literature configurations and the development of a new one

Since all configurations have significant geometry differences, the investigation of the kinetic features appears largely influenced by the fluid dynamics (e.g. conversion increases greatly from Warnatz *et al.* (1994)'s configuration to Brady *et al.* (2010)'s). It is clear that such different experimental equipment produces results scarcely reproducible. Ignition temperature is the most studied kinetic feature so it will be compared to evaluate the reproducibility of literature papers.

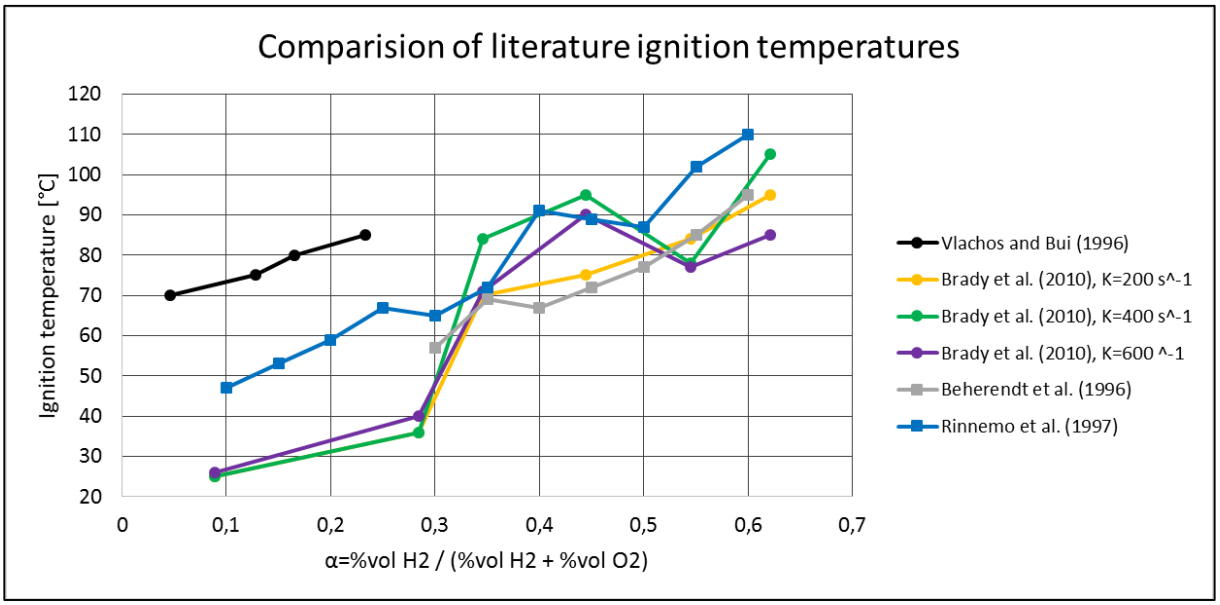

Figure 2.19. *A comparison between the literature ignition temperatures in a stagnation-point flow geometry. For all experiments, hydrogen / air mixture are used and the strain rate varies. Behrendt et al. (1996) does not give enough information to estimate the strain rate (K).*

Because of the differences in the reactor flow conficuration, the reproducibility of the ignition temperature is quite scarce: all works show an increase of the ignition temperature with the hydrogen amount in the mixture but it is not possible to define a unique behavior. Only Bui *et al.* (1997) analyze the Vlachos and Bui (1996)'s data and they relate their behavior to the auto-inhibition effect (Figure 2.5).

Furthermore, the *strain rate* (*K*) seems to be a very important parameter; however, no paper clarifies its influence on the system. Valchos and Bui (1996) and Bui *et al.* (1997) suggest that the ignition temperature is proportional to the *strain rate* while any other paper did not mention the issue.

The aim of the reactor configuration proposed in this Thesis is approaching more reproducible flow paths, hopefully overcoming the issues of previous geometries. Figure 2.20 shows a schematic representation of our geometry. The Pt catalyst is circular and the reactor is symmetrical around the central axis. The main features and improvements of this new configuration are:

- Absence of lateral bypass since the catalyst support is larger than the inlet channel;
- Homogeneous reagents-catalyst contact time because the catalyst is circular and the inlet channel is much smaller than the catalyst: the ratio Φ_{cat}/Φ_i =5 compares with Brady et al. (2010)'s ratio of only 2.4;
- Minimum distance between the reagents inlet and the catalyst (*gap* = *d*= 1 – 5 mm). The *strain rate* and the mass transfer toward the catalyst is increased without lowering the reactants-catalyst contact time.

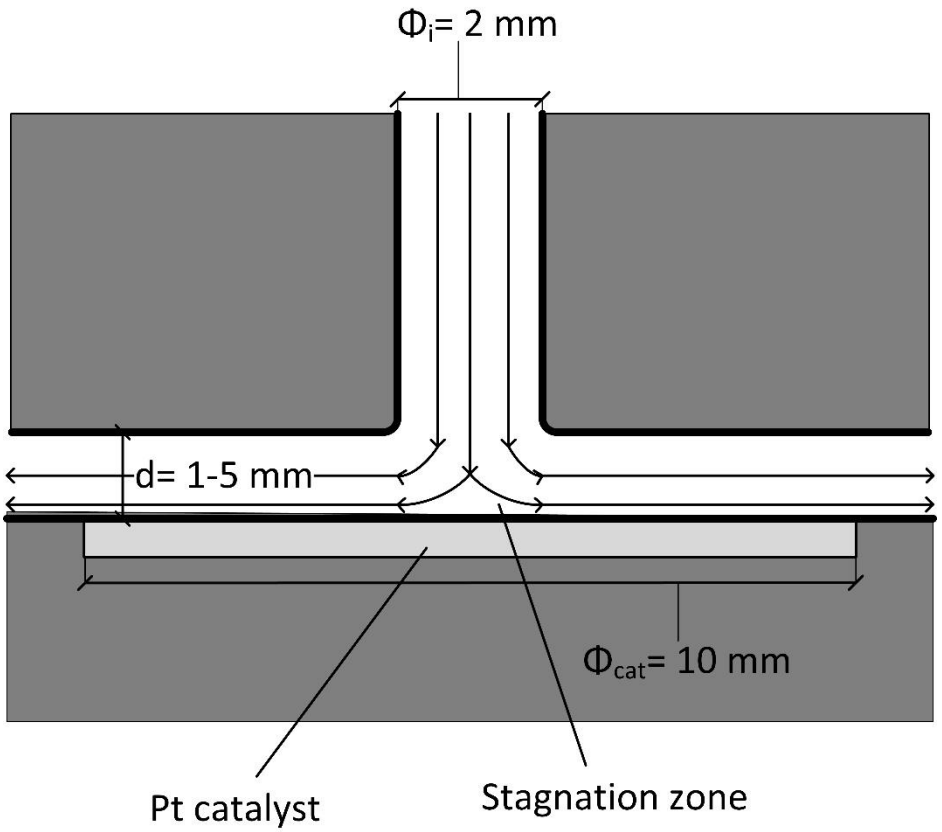

Figure 2.20. *A schematic representation of the reactor configuration used in this Thesis*

Note that the modelling of the reactor is affected by all fluid dynamics inaccuracies. Indeed, even if the fitted kinetic parameters are in accord with the literature experimental data, they may provide ambiguous results because mass transfer effects are confused with kinetic effects. The result is a scarce reproducibility of proposed models in different reactor configurations.
A new geometry is needed to evaluate the real value of kinetic parameters despite the mass transfer effects so they should apply also to different reactors.

Chapter 3

The experimental equipment and procedures

The third Chapter describes the experimental equipment and procedures. At first, the tested catalyst and the reactors are detailed presented, then the attention is shifted to the flow meters and the analysis equipment. The final paragraph describes the results elaboration.
The core of the whole experimental work has been developed with the FFC reactor but some characteristics were studied through the FF reactor even if it has not a proper stagnation-point flow geometry (§3.2.2).
The experimental system is made by several units connected together. They are:

1. flow meters;
2. reactors (either FFC reactor or FF reactor);
3. analysis equipment (gas chromatograph and/or mass spectrometer).

3.1 An overview about crystallography and the tested platinum catalyst

The structure of platinum is made either by only one crystal (monocrystalline structure) or by a wide range of crystals (polycrystalline structure). The atoms disposition in the crystal cell forms a face-centred cubic cell in which Pt atoms occupy the vertices of the cubic structure and the center of each face (Figure 3.1).

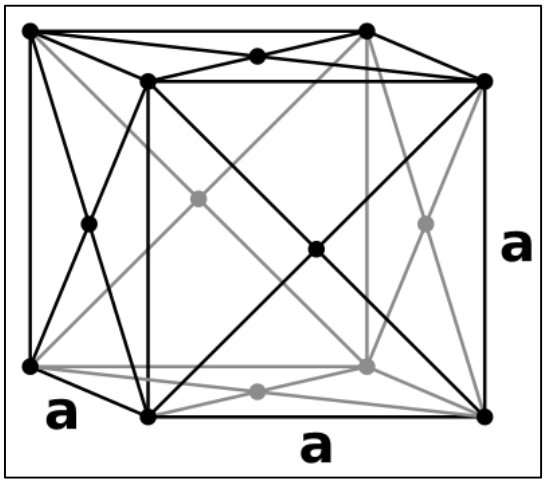

Figure 3. 1. *A schematic representation of a face-centred cubic cell. Platinum crystals have the same atoms distribution.*

To distinguish between different types of crystals, the Miller indices are used. They are formed by three integers (hkl) and each index denotes a plane orthogonal to a direction in the system of Cartesian axes (h, k, l): for instance, Miller index (100) represents a plane orthogonal to direction h, index (010) represents a plane orthogonal to direction k and so on.

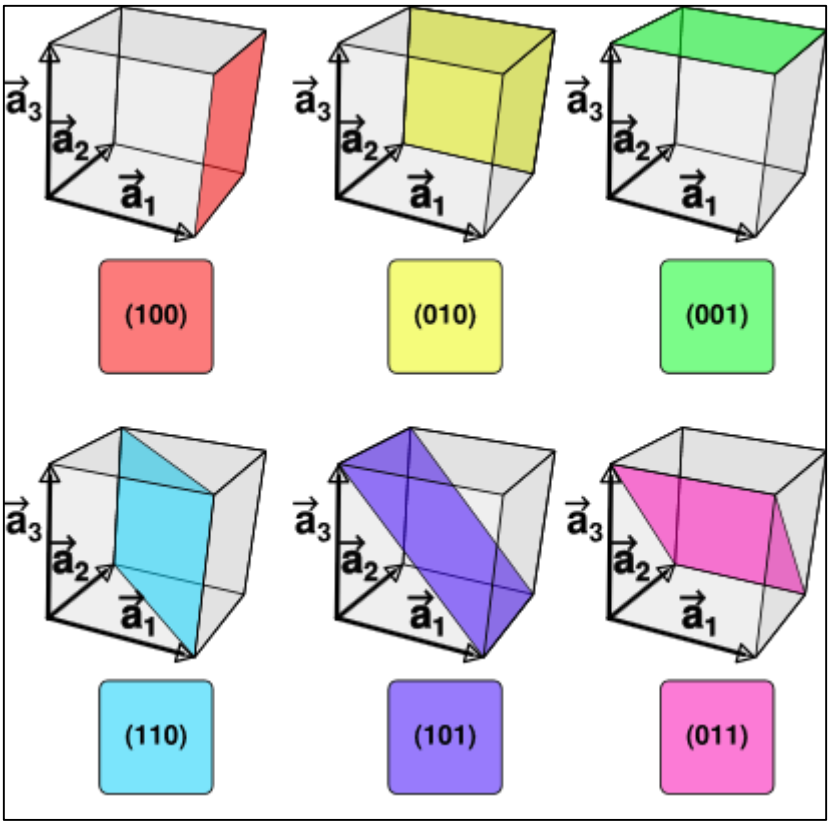

Figure 3. 2. *Planes with different Miller indices in cubic crystals*

The catalyst tested in this Thesis is a platinum polycrystal so its structure is strongly dominated by the presence of defects and it is not possible to identify a precise structural order. It has a circular shape with a diameter of 11 mm and a thickness of 1 mm (Figure 3.3). The catalyst is placed horizontally on the bottom of the reactor and reagents invest it orthogonally (§3.2).

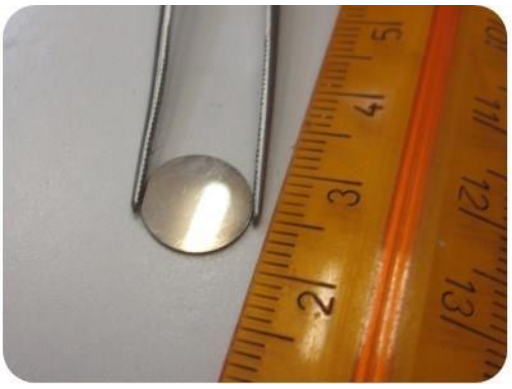

Figure 3. 3. *A picture of the tested platinum catalyst.*

This Thesis is the result of an academic collaboration between the Surface Science research Group and the Department of Industrial Engineering. In particular, the Chemical Reaction Engineering Laboratory (CRELab) evaluates the performance of the catalyst made by the Surface Science Group.

3.2 The reactors

Two different reactors were used for the experimental work: the first one ("*Flusso Frontale Centrato*" - FFC) was largely employed and it allows to properly test the catalyst in a stagnation-point flow geometry. However, its particular geometry leads to several analysis limitations (§3.2.1).
Because of the characteristic geometry of the second reactor ("*Flusso Frontale"* – FF), reagents can bypass the catalyst (§3.2.2) but, only through this reactor, it is possible to measure the temperature of the upper and reactive surface of the catalyst. This measurement and the difference between the temperature of upper and lower surface are key parameters of one topic of this Thesis (§5.4). Since the stagnation-point flow geometry cannot be properly achieved with this reactor, it is used only in experiments directed to test the upper surface temperature.

3.2.1 The FFC reactor

The reactor is made by stainless steel with a titanium nitride (TiN) coating and it is heated by an electric heater with a 40 W power. The coating improves the surface properties of the stainless steel because it is extremely hard and inert in the involved temperature range.
The reactor is made by two parts: the upper part is composed by a flange joint with a steel cylinder with a height of 30 mm and a diameter of 24 mm. In the center of the cylinder there is a 2 mm channel used for the inlet of reagents. The lower part is made by a hollow cylinder with a housing for the catalyst at the bottom of the cylinder. The inner diameter is 28 mm while the outer diameter is 40 mm. The housing of the catalyst has a diameter of 12 mm and a depth of 1 mm and it is placed on the center of the cylinder. A K-type thermocouple is placed inside the housing so it can touch the lower surface of the catalyst.
This way of measuring the reaction temperature assumes that there is not any difference between the upper and lower surface of the catalyst so the temperature monitored corresponds perfectly to the reaction temperature. However, this is not a precise assumption as it will be discussed in (§5.4).

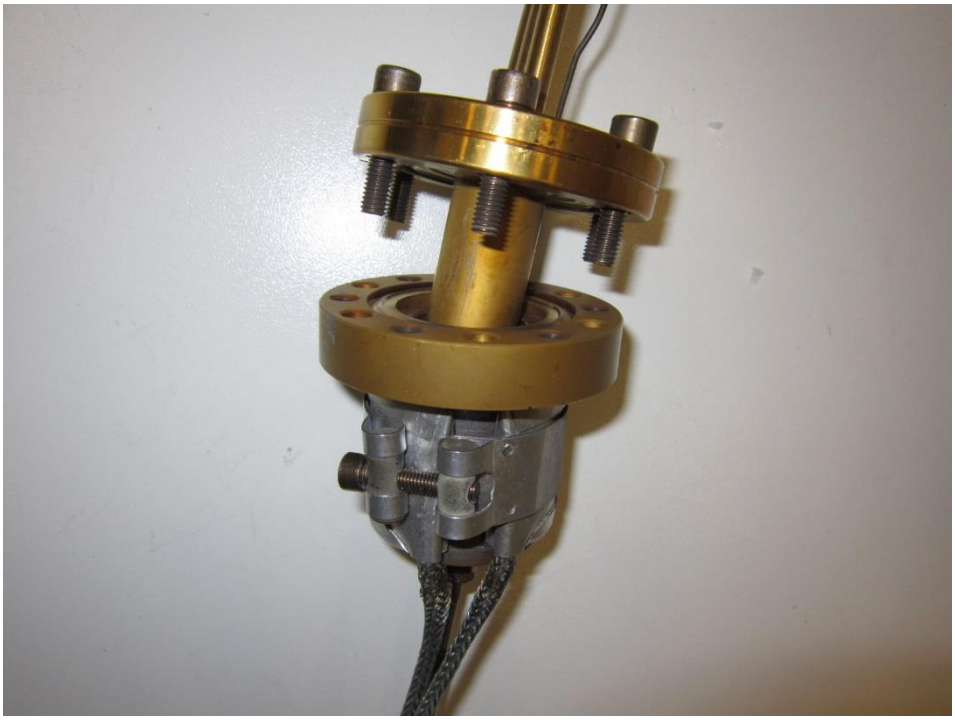

a.

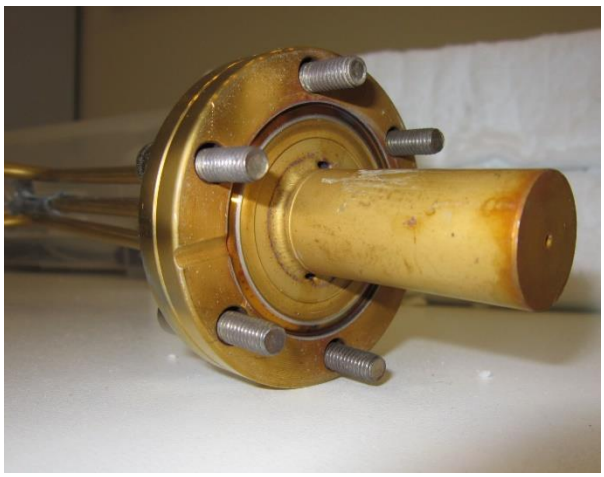

b.

c.

Figure 3. 4. *Pictures of the FFC reactor. (a) represents the disposition of the upper part (b) inside the lower part (c) around which there is the electric heater.*

Reagents enter from the central channel of the upper reactor part and they flow through the inner cylinder until they reach the catalyst surface, then they deflect radially through the gap between the two reactor parts. When the outlet gases reach the flange on the upper side, they exit through two channels placed on the top of the flange.

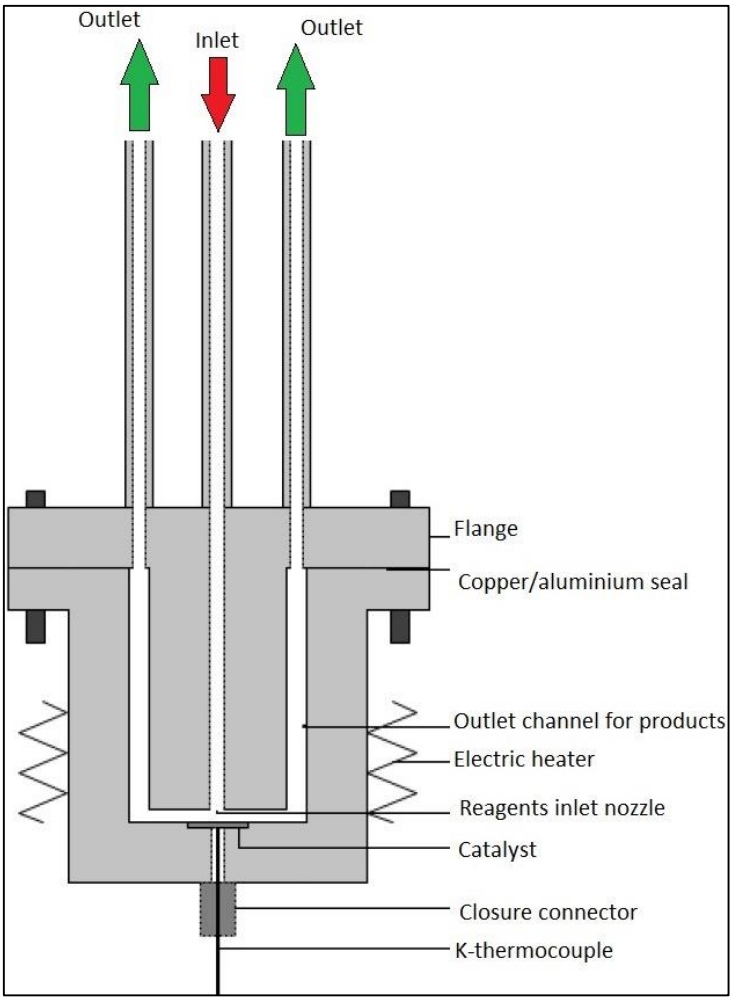

Figure 3. 5. *A schematic representation of the FFC reactor.*

3.2.2 The FF reactor

The other reactor used in this Thesis is the FF ("*Flusso Frontale*") reactor that has a bigger size than the FFC and also a different geometry. The FF reactor is composed by two main parts: the oven and the reaction volume: the first part is used to heat the gases and it includes the second part. The oven can reach a temperature of 1200 °C and it is composed by an electric heater with a 1 KW power and a quartz-wool insulation layer. This layer is used to homogenize the temperature profile inside the oven and for safety reasons due to the high temperatures. The electric heater is distributed around a ceramic tube with an inner diameter of 36 mm and an outer diameter of 46 mm. The oven has cylindrical shape and it is covered by a steel layer with a height of 310 mm and a diameter of 250 mm. Outside this structure, there is a metal grid with a height and a diameter of 290 mm that is used to connect the oven to its support.

A quartz tube placed coaxially inside the oven makes the reaction volume. It has an outer diameter of 18 mm, an inner diameter of 16 mm and the length may vary but it is usually 750 mm. The catalyst is placed inside the quartz tube on the top of an inert cordierite monolith and quartz wool is used to retain the monolith inside the tube. The temperature of the upper catalyst

surface is monitored by a thermocouple placed in contact with the catalyst. The catalyst is placed about 100 mm above the exit of the oven because that zone has the most homogeneous temperature.

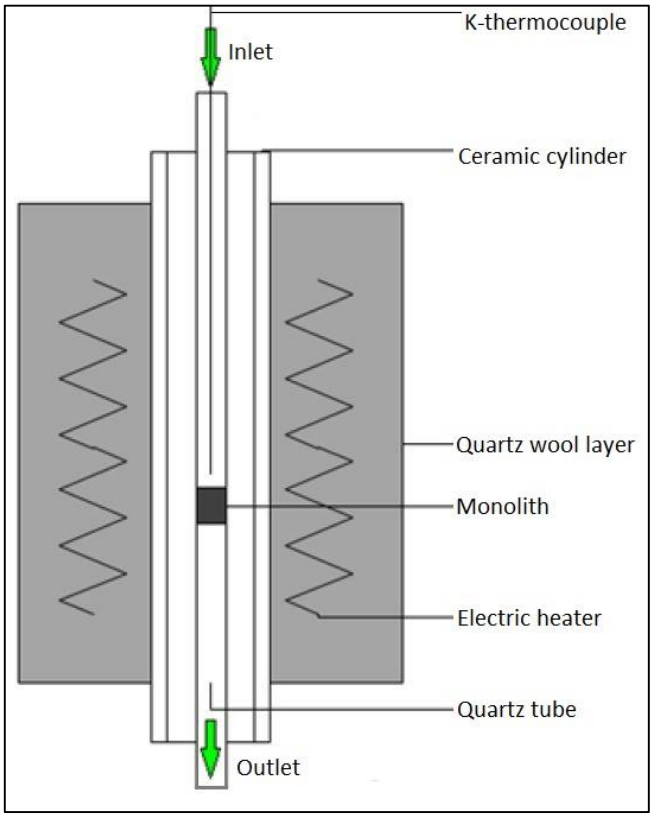

Figure 3. 6. *A schematic representation of the FFC reactor.*

Because of the considerable insulation layer, the thermal inertia of this reactor is greater than the inertia of the FFC reactor. This is an important difference when in terms of experimental time because the FFC reactor takes about 3 hours to cool down while the FF reactor takes twice that time. The global result is that the FFC reactor can perform more experiments than the FF reactor in the same time.

This reactor configuration is quite similar to Fernandes *et al.* (1999)'s and Behrendt *et al.* (1996)'s configuration because the inlet channel is larger than the catalyst. As described in § 3.2.1 and shown in Figure 3.8, the lateral streamlines can easily by-pass the catalyst and the central streamlines have different contact time with the catalyst. This geometry is not a proper stagnation-point flow geometry but it is the only way to continuously monitoring the temperature on the upper face of the catalyst during the course of the reaction.

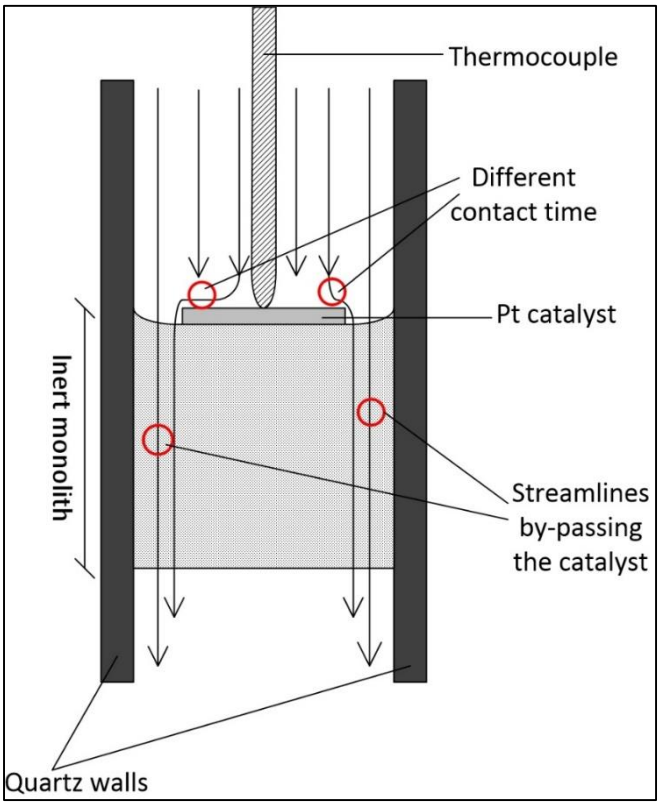

Figure 3. 7. *A schematic representation of the catalyst disposition inside the FF reactor. The phenomena of bypassing of the catalyst and different contact time are underlined.*

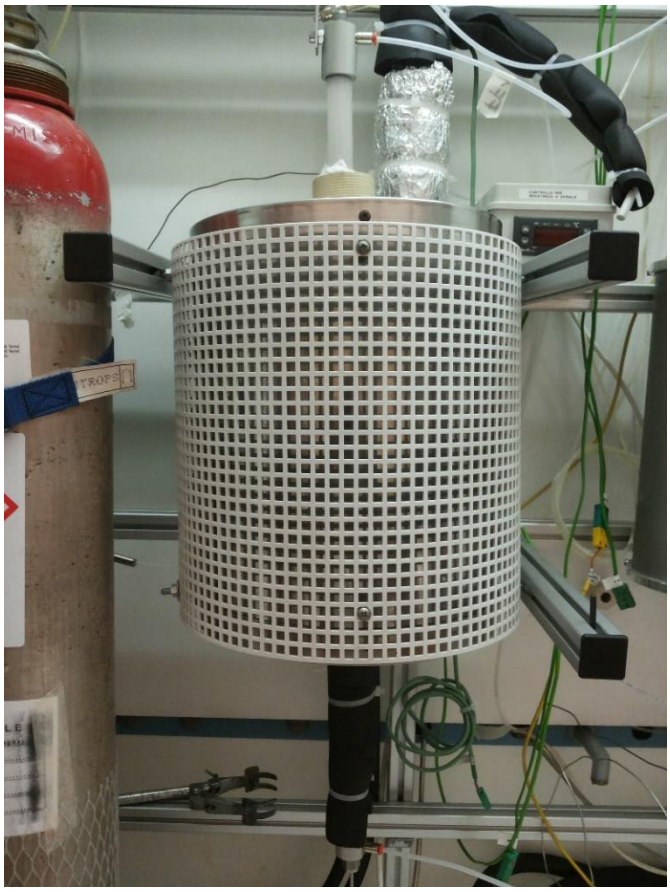

Figure 3. 8. *A picture of the FF reactor in the working conditions.*

3.3 The flow meters

The feeding system of the reactors is composed by gas tanks for each gas and 10 flow meters. The tanks are placed outside the laboratory and they are connected to the flow meters through a metal pipe with a pressure of 5 bars. The flow meters measurement is based on the mass of the fluid flowing. In particular, they have a heated metal wire and they measure the temperature variation of the wire. Since they thermal conductivity of the gas is known, the flow meters can calculate the flow rate by measuring the temperature variation of the wire. All flow meters are calibrated using nitrogen but different gases have different thermal conductivity so the same temperature variation corresponds to different flow rates for different gases. However, since this phenomenon is well known and easy to measure, the vendor sold with the flow meters also a table to convert the nitrogen calibration to a calibration useful for all used gases.
The used flow meters can be digital ("*Bronkhorst*" flow meters) or analogic ("*Brooks*" flow meters) and they have different maximum flow rate. Usually, one flow meter with a high maximum flow rate (2000 mL/min) and one or two with a low flow rate (10-50 mL/min) were used in this Thesis: the first one was used for air or the inert gas while the others were used for hydrogen or oxygen. Digital flow meters allow a more precise flow rate control so they were used in most of the experiments.

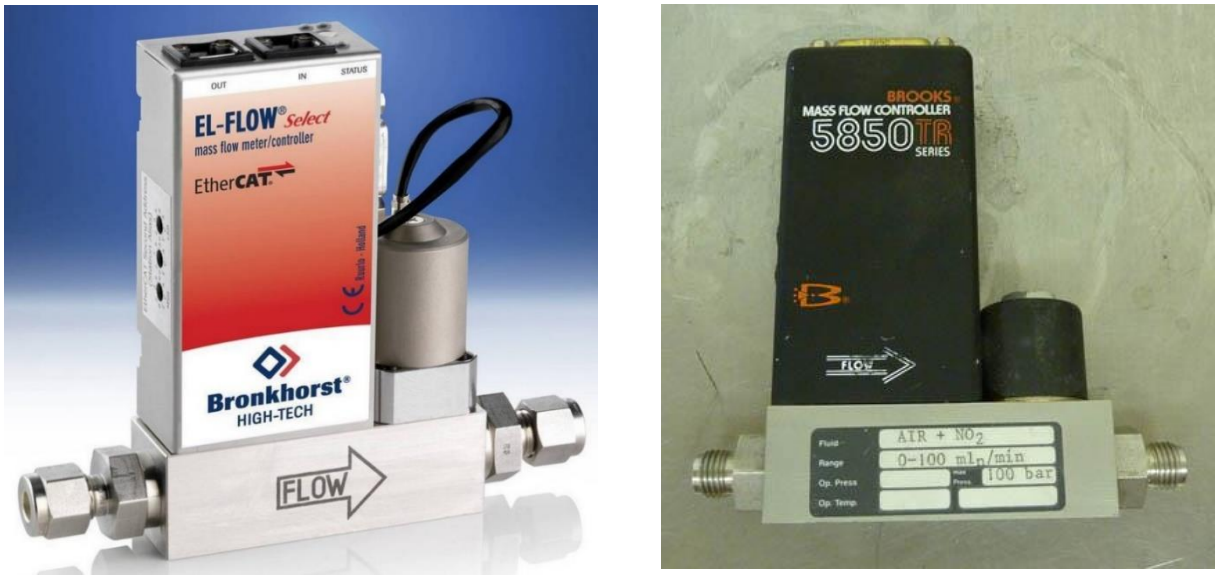

a. b.

Figure 3. 9. *A picture of the two types of the flow meters. a. is digital ("Bronkhorst") and b. is analogic ("Brooks").*

After the flow meters, gases are carried into low-density polyethylene (LDPE) tubes until they reach the reactor. These tubes has an inner diameter of 4 mm and an outer diameter of 6 mm and gases are mixed together through proper connectors. For safety reasons, one reagents is mixed with the inert gas before it reaches the other reagent.

The FFC reactor is connected with the LDPE tubes through standard connectors while the connectors for the FF reactor are more complex because they need to connect a quartz tube with a LDPE tube. They have the geometry shown in Figure 3.11: the LDPE tube is connected laterally and a thermocouple may enter the connector from the top. Quartz tubes are connected at the bottom part where there is a plastic O-ring that seals the connector to the tube.

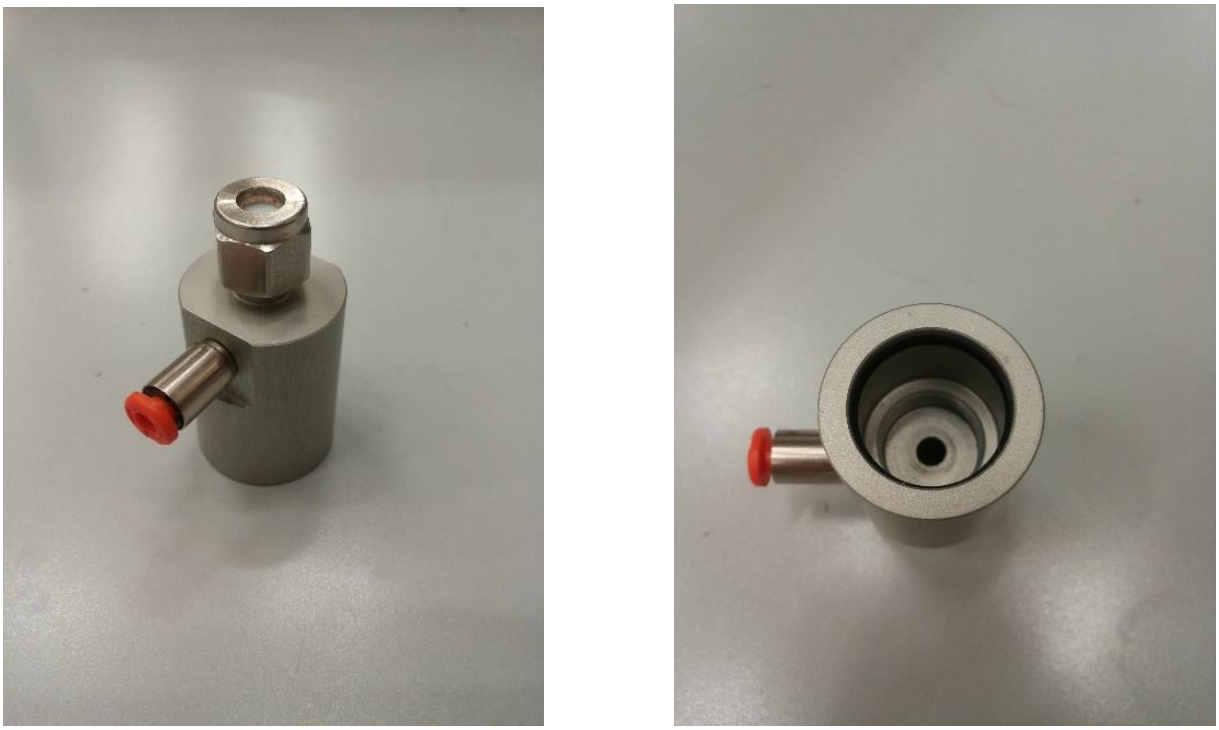

a. b.

Figure 3. 10. *Pictures of the connectors for the FF reactor. a. shows the connector for the LDPE tube on the left and the connector for the thermocouple on the top. b. shows the plastic O-ring used to seal the quartz tube with the connector.*

3.4 The analysis equipment

In order to analyze the products of the reaction, a gas chromatograph and/or a mass spectrometer has been used. The gas chromatograph is useful to get both a qualitative and quantitative analysis but it has long analysis times while the mass spectrometer performs fast but only qualitative analysis.

3.4.1 The gas chromatography equipment

In this work, only hydrogen, oxygen and water need to be analyzed so the analysis results quite easy. Since the gas chromatograph creates a peak for each component with an area proportional to its concentration, it is very easy to associate the peak with the correct compound. This is the

reason why the gas chromatograph (*GC*) can perform qualitative analysis while quantitative analyses are performed by integrating the area of the *GC* peaks.

Most of experiments were carried out with the *Agilent GC7820* that is composed by three main parts: the valves, the columns and the detectors. At first, there is a sampling valve with a *loop* containing a sample exiting the reactor. Before the analysis (*LOAD position*), only an inert gas ("*carrier*") is flowing in the columns and, when the analysis begins (*INIECT position*), the valve switches so the carrier passes through the *loop* carrying the sample to the first column (Figure 3.12).

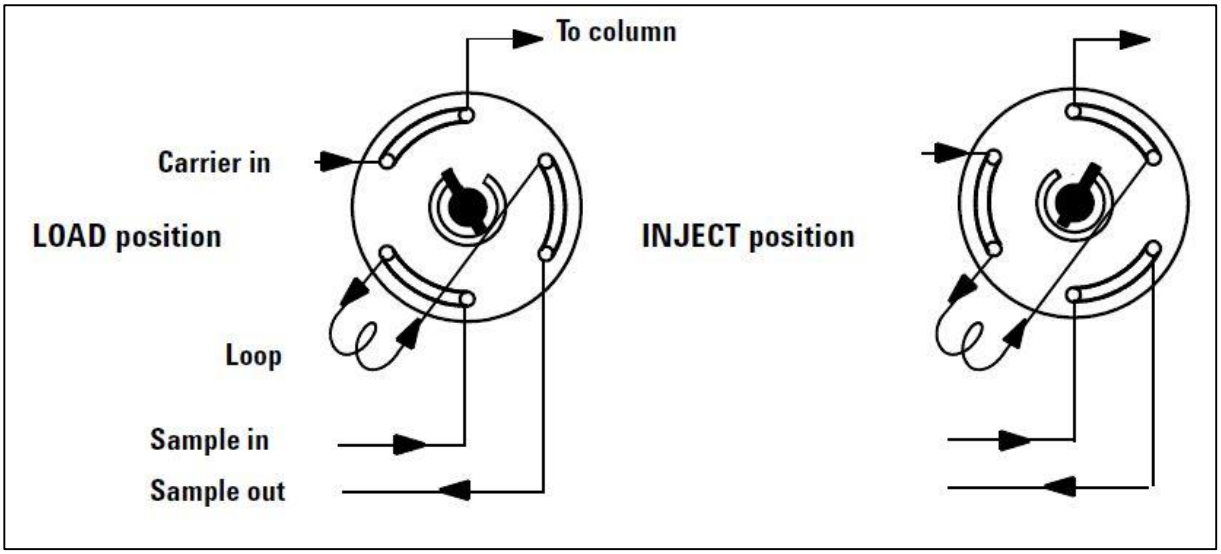

Figure 3. 11. *The position of the sampling valve before the analysis (LOAD position) and during the injection of the sample (INJECT position).*

Between the two columns that separate the components, there is the switching valve that excludes the second column. Indeed, for a certain valve position, the sample flows also in the second column while, for another valve position, the sample bypasses the second columns and it goes directly to the detector.

Figure 3. 12. *A picture of the Agilent GC7820.*

The columns that may be used in gas chromatography are divided in packed and capillary columns. The first ones have higher retention times and sample volumes and their performance in separating permanent gases is higher than the seconds. On the contrary, capillary columns can perform great analyses with complex liquid mixtures. However, the analyzed samples of this Thesis are always composed by a simple mixture of gases so there is no need to use capillary columns.

The chosen packed columns are placed inside the oven: the first one is an *Agilent PoraPak Q* and the second is an *Agilent MolSieve 5A*. The first columns is commonly used to separate light hydrocarbons but, during this project, it will separate water from oxygen and hydrogen. The second column separates permanent gases through its molecular sieves because different molecules have different retention time due to their dimension. It is important to notice that this column can easily adsorb water so the column exclusion is needed to ensure that the water left in the first column is not adsorbed. To remove adsorbed water from the *MolSieve 5A* a high-temperature (about 180 °C) regeneration is needed and usually it cannot restore the column to its initial separation power.

The *GC* has two detectors: the FID and the TCD. The first one analyzes compounds with C-H bonds (e. g. light hydrocarbons) so it will not be used in this Thesis. The TCD is a detector based on the different thermal conductivity of gases. In particular, the detector is composed by a heated wire that is maintained at a constant temperature in a carrier flow. When the analyzed gases reaches the wire, the thermal conductivity of the gas changes and so does the temperature of the wire. The electric conductivity of the wire varies with temperature so the detector

produces a signal proportional to the mass of the sample. The FID is a very sensitive detector but it is destructive and its use is limited while the TCD is less sensitive but it can analyze a wide range of compounds without damaging them.
During the analysis, the sampling valve are kept at 120 °C in order to avoid the condensation of water while the oven is initially at 60°C. In this way, when the sample is injected in the first column, all water condenses inside the column and permanent gases flows toward the second column. Then, the molecular sieves separates hydrogen and air components but nitrogen is not visible in the TCD because the carrier is also nitrogen. An operative temperature of 60 °C is the optimal compromise between low retention time and components separation while the relative pressure inside the column is increased up to 40 psi in order to avoid a long tail of the peaks. The first part of the analysis ends when the permanents gases reach the detector while water is still in the first column. To eliminate water from the system, the second part of the analysis begins with a switch of the valve between the columns. In this way, the second column is excluded and water goes directly to the detector because the oven temperature is simultaneously increase up to 120 °C. The oven heating rate is quite high (30 °C/min) in order to decrease the analysis time and pressure is increased too (60 psi) so water is more easily ejected from the column.
For the first experiments, the *Varian MicroGC CP 4900* was used: it has an operation very similar to the *GC7820* but it works on micro-volumes. Very small analysis volumes reduce the retention time of the peaks and the tail after the peaks but this instrument has its drawbacks. Since everything is *micro* inside the *MicroGC*, columns are grouped in packs so they cannot be easily changed because the whole pack needs to be changed. Furthermore, this instrument is more sensitive than the *GC7820* to pollutants in the analysis gases.
The *MicroGC* has a molecular sieve column (*MolSieve 5A*) to separate hydrogen from oxygen and it has a *backflush system* to separate water from permanent gases. This system is made by a pre-column that can separate water from permanent gases to avoid that it reaches and poisons the *MolSieve* column. After the components separation in the pre-column, a carrier flow goes backward to the pre-column and it pushes the water out from the system.
Because of its extremely small analysis volumes, this instrument has a great separation power. However, such a great power is not needed because only three components need to be analyzed. For this reason, the *MicroGC* was used only in the initial experiments and it has been used later on for other projects that need a better separation power.

Figure 3. 13. *A picture of the Varian microGC CP-4900.*

3.4.2 The mass spectrometer (MS)

The mass spectrometry is an analysis technique based on the samples ionization and the selection of ions. The instrument used in this Thesis is the "*Hiden HPR-20 QIC*" and it is composed by three main parts: the ionizing system, the quadrupole mass analyzer and the detectors.

Inside the first part, an electron beam hits the sample and it divides the components into ionized fragments. These fragments form a characteristic pattern that varies according to the ionization energy.

The quadrupole selects a specific ion according to its mass (*m*)/charge (*z*) ratio and it is composed by four cylindrical metal rods. Each opposing rod pair is connected together electrically, and a radio frequency voltage (RF) is applied between one pair of rods and the other. A direct current voltage is then imposed on the radio frequency voltage. All fragments derived from the first part are accelerated by an electric potential and they enter the space between the rods. Because of the direct current and radio frequency voltage, the fragments begin to have a sinusoidal trajectory according to their *m/z* ratio. Only the fragments with a particular mass have a stable path through the quadrupole and they reach the detector (Figure 3.15). However, a variation of the RF voltage may allow fragments with a different mass to have a stable path.

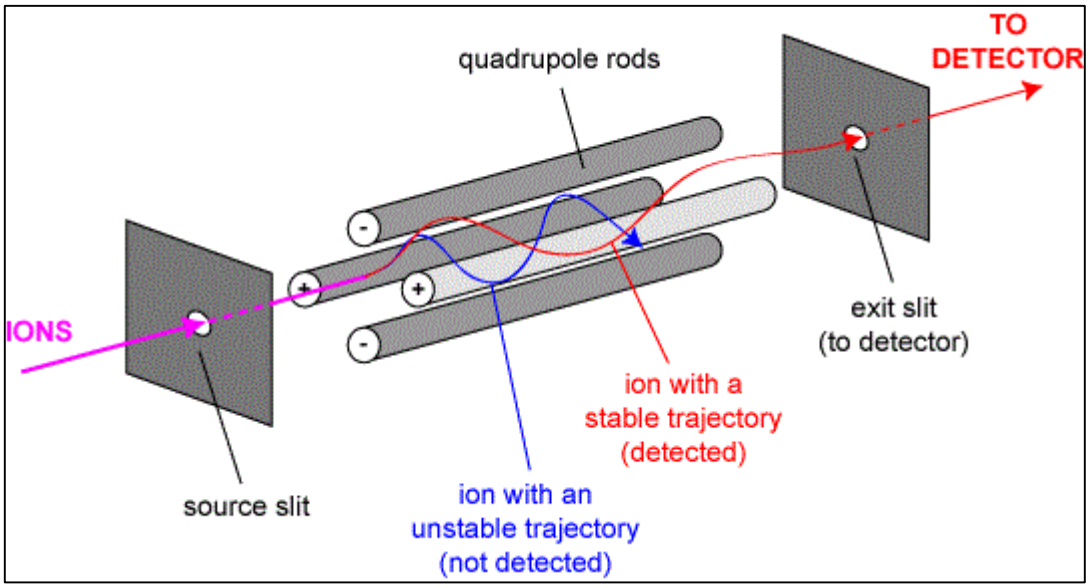

Figure 3. 14. *A schematic representation of the quadrupole and its operation (University of Bristol).*

The analyses performed with this equipment are faster than the GC analyses but they are only qualitative because different compounds can form the same fragment. In this way, the detector detects a particular fragment but it cannot know its original compound. However, since some compounds form unique fragments, quantitative analyses may be performed but, in most cases, quantitative data are produced through the *GC.*

The detector shows a signal correspondent to the partial pressure of the mass analyzed (p_i) and this signal compared to the total pressure (p_{TOT}) or the inert partial pressure (p_{IN}). The ratio:

$$\frac{p_i}{p_{TOT}\ (or\ p_{IN})} \tag{3.1}$$

is used to have semi-quantitative data by analyzing its variation during the course of the experiment.

Figure 3. 15. *A picture of the MS Hiden HPR-20 QIC.*

3.5 The results analysis

The results of the experiments are focused on the variation of the reaction conversion with time and temperature. To do that, the temperature of the proper thermocouple is continuously registered and it is coupled with the resulting data from the *GC7820 / microGC* or the *MS*. The *Labview* software monitors, controls and registers the temperature of all thermocouples. The temperature control is achieved by a PID controller but, since most of experiments need a quick temperature variation, only the proportional and derivative functions are implemented.
Both the gas chromatographs write, at the end of the analysis, a report (a *.Area* file) where there are the time of the analysis and the area of all peaks generated by the compounds. These data and the thermal data from *Labview* are elaborated through a MATLAB script ("*analisi_gc7820*" for the *GC7820* and "*analisi_ugc*" for the *microGC*) that calculates the reaction conversion:

$$X = 1 - \frac{M_{out}}{M_{in}} = 1 - \frac{N_{out}}{N_{in}}. \tag{3.2}$$

where M_{in} and M_{out} refers to the inlet and outlet hydrogen mass flow rate while N_{in} and N_{out} refers to the inlet and outlet hydrogen molar flow rate. M_{in} and M_{out} are related to the area of the

GC peaks before and after the reaction since the *GC* measurement is based on the difference of thermal conductivity. This technique produces a signal proportional to the mass of the sample, as described in §3.4.1.

The whole MATLAB script can be read in §A.1 (*GC7820*) and in §A.2 (*microGC*) and it is composed by several parts that:

1. read the day and the time of all analyses and all thermocouples;
2. couple all analyses with the correspondent temperature;
3. calculate the reaction conversion by substituting the area of the *GC* peaks in the (3.2) equation;
4. plot the value of conversion varying the temperature and time.

Unlike the *GC*, the output file of the *MS* is a *.csv* file where the partial pressures of all compounds are present. This *.csv* file is continuously updated every new analysis and it is elaborated with a MATLAB script ("*Analisi*") similar to the *GC* ones.

The post-processing part of the *MS* analyses is quite complex because the total pressure of the system may vary during the analysis. To proper compare the compounds partial pressure at different analysis time, we need to compare the ratio:

$$\frac{p_i}{p_{TOT}} \tag{3.3}$$

where p_i is the partial pressure of the component and p_{TOT} is the total pressure. In this way, the variation of the total pressure is taken into account.

The tasks of the *MS* MATLAB script are:

1. reading of the day and the time of all analyses and all thermocouples;
2. coupling all analyses with the correspondent temperature;
3. calculation of the (3.3) ratio;
4. selection of the partial pressure values when there is no reaction;
5. calculation of the conversion by substituting partial pressure values in the (3.2) equation;
6. plotting the value of conversion varying the temperature and time.

Like the *GC* scripts, the *MS* script can be read in §A.3.

Chapter 4

The CFD simulation

The forth Chapter presents a CFD model of the FFC reactor. This model was built with the COMSOL CFD program and its aim is the evaluation of the fluid and species transport inside the reactor. In particular, we would like to elucidate why the reaction never achieves 100% H_2 conversion and what are the effects of *gap* and inlet flow rate in terms of fluid dynamics.
First, the aim of the simulation is deeply described, then the developing of the model is presented and the Chapter ends with the calculated results and their critical analysis.

4.1 Introduction of the CFD simulation

Since mass transfer phenomena are very important in the evaluation of reaction conversion (§2.5), a deep study of the fluid dynamics is needed. In particular, we would like to simulate the reactor behavior in a mass transfer regime with different *gaps* and total inlet flow rate. For all these cases we would like to evaluate what are the mass transfer phenomena that may limit the hydrogen conversion. We also would like to find the reactor and fluid configuration that could increase the conversion. The simulated cases are:

- *Gaps* = 1, 3, 5 mm;
- Total inlet flow rates= 50, 75, 100, 200, 250 mL/min;

and the simulation is performed for a combination of all these cases. The choice of using these parameters values is consistent with the experimental data that are simulated (§5.2).
The CFD tool used for this simulation is COMSOL Multiphysics. The model is based on the steady state "Reacting Flow, Concentrated Species" (*rfcs*) and "Heat Transfer in Fluids" (*ht*) physics. The flow regime was assumed laminar, since the Reynolds number never exceed the value of 400.

4.2 The model

To develop the model, several parameters and variables are implemented to define the initial conditions (Tables 4.1 and 4.2).

Table 4. 1. *List of all parameters used in the CFD simulation with reference values (may change later).*

Parameter name [-]	Expression	Description [-]
Ri	1e-3 [m]	inlet radius
d	1e-3 [m]	gap
H	5e-2 [m]	total height
kin	0.8 [m/s]	kinetic constant
rcat	5e-3 [m]	catalyst radius
Vdot	0.05 [L/min]	total inlet flow rate
R	2.4e-2 [m]	reactor radius
Ru	3e-3 [m]	exit radius
MH2	2 [g/mol]	hydrogen molar weight
MO2	32 [g/mol]	oxygen molar weight
MN2	28 [g/mol]	nitrogen molar weight

Table 4. 2. *List of all variables used in the CFD simulation.*

Variable name [-]	Expression	Description [-]
xH2	0.01[-]	hydrogen molar fraction
vin	Vdot/(π·Ri^2) [m/s]	inlet flow velocity
xO2	0.21·(1-xH2) [-]	oxygen molar fraction
xN2	1-xH2-xO2 [-]	nitrogen molar fraction
wH2	$\frac{xH2 \cdot MH2}{MH2 \cdot xH2 + MO2 \cdot xO2 + MN2 \cdot xN2}$ [-]	inlet H2 mass fraction
wO2	$\frac{xO2 \cdot MO2}{MH2 \cdot xH2 + MO2 \cdot xO2 + MN2 \cdot xN2}$ [-]	inlet O2 mass fraction
wN2	$\frac{xN2 \cdot MN2}{MH2 \cdot xH2 + MO2 \cdot xO2 + MN2 \cdot xN2}$ [-]	inlet N2 mass fraction

The geometry is assembled based on an axisymmetric model that reduces the computational needs; only the inner part of the reactor, where the fluid flows, is modelled. The solid part of the reactor is not modelled because it is considered isotherm, inert and impervious. The reaction on the reactive catalyst surface is described as a "*reacting boundary*" with the *rfcs* physics. The dimensions of the CFD model are the same of the real FFC reactor and they are shown in Figure 4.1.

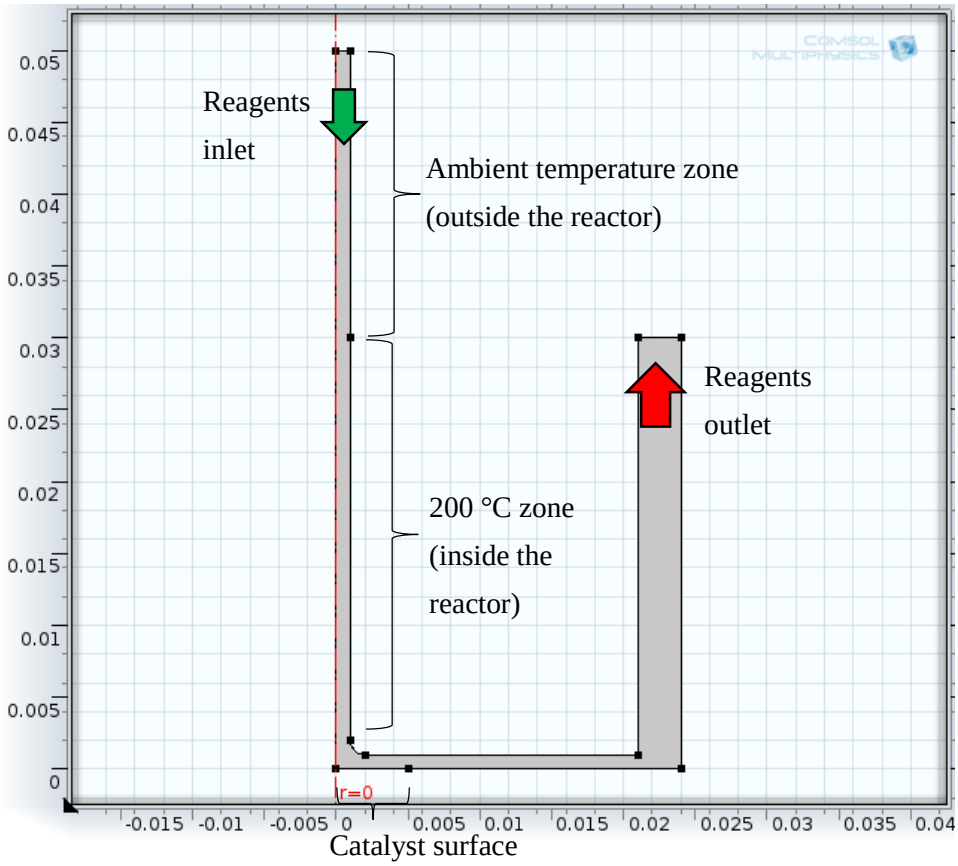

Figure 4. 1. *Geometry of the FFC reactor used for the CFD simulation. Dimensions are in meters. Size and proportion of this geometry reproduce those of the real FFC reactor. It is simulated only the inner part of the reactor, where the fluid flows.*

Since the inlet volumetric flow rates are set at ambient temperature, the simulated model includes a first part at ambient temperature, then temperature is raised up to the reactor temperature so the fluid velocity is increased according to temperature. We can also check if the fluid can actually heat up uniformly before reaching the catalyst. The simulation is performed with a temperature of the reactor = 200 °C because experimental evidences suggest that a mass transfer regime could prevail at this temperature .
Conversion is estimated with the equation:

$$X = 1 - \frac{W_{out}}{W_{in}} \tag{4.1}$$

where W_{out} is the outlet mass flow rate and W_{in} is the inlet mass flow rate (ks/s).
The hydrogen mass flow is calculated at the inlet and outlet boundaries. It was determined through the integral of the total H_2 flow in the z-direction (kg/s/m^2), provided by Comsol, multiplied by $2*r*\pi$ (where r is the distance from the symmetry axis):

$$W_{in/out} = \int_{r_1}^{r_2} n_{z,H2}\ 2\pi r dr \tag{4.2}$$

So the total flow rate of inlet and outlet hydrogen is calculated. For the bulk material of the model, nitrogen has been chosen since it is the most abundant compound.

4.2.1 Boundary conditions

The model uses 2 submodels ('physics'): the "Reacting Flow, Concentrated Species" and the "Heat Transfer in Fluids". On the inlet boundary, we set the *vin* velocity inlet condition and the hydrogen and oxygen concentrations (*wH2* and *wO2* variables) for the first physics,. For the outlet boundary, the condition of no viscous stress on pressure was chosen.
On all boundaries different from the inlet, the outlet and the reacting boundary, the conditions of *no flux* and of *no slip* are imposed since there is no mass, neither momentum transfer through these surfaces.
The reaction on the catalyst surface is simulated through a mass flow [kg/(m^2·s)] boundary conditions on the surface:

$$R = -kin\cdot(\rho\cdot wH2)\cdot(\rho\cdot wO2)^{0.5} \quad (4.3)$$

where the '-' indicate a flux of H_2 to outwards of the flow domain (inwards the surface)kin is the kinetic constant and ρ [kg/m^3] is the mass density of the system. This is a very simplified model to describe the reaction because it does not take into account any feature of the reaction mechanism (adsorption/desorption, radicals formation, etc…). However, with this CFD simulation, we would like to evaluate only the fluid dynamics aspects that may influence the conversion, so a first simplified description of the kinetic features is sufficient. The value of kin was fitted using the experimental data obtained in §5.2 and at §5.2.3 a comparison between CFD and experimental data in terms of conversions is reported. The initial guess of variables in the domain reproduce an air atmosphere.
The "Heat Transfer in Fluids" physics is used to simulate the thermal effects and solve the energy balance equations. Since the reactor walls are assumed isothermal, at 200 °C, the most important contribution of this physics is the increase of flow rate from the inlet condition at ambient temperature to the reactor conditions at 200 °C. For the thermodynamics of the system, the ideal gas fluid type is accurate enough and it also allows for a low computational need. The thermal boundary condition for the ambient temperature zone (Figure 4.1) is a 20 °C temperature while, inside the reactor, the imposed temperature is 200 °C. The initial temperature of the system is 20 °C. Even the reactive boundary is assumed isothermal and an expression of the reaction heat is not implemented because we believe, in the simulated steady state conditions, that the reactive surface may be assumed isothermal with a good degree of approximation. However, the implementation of the reaction heat may be useful to evaluate the effect of the ignition on the system with a transitory simulation. Also, later observation on the difference between temperature above and below the catalyst and measurements of large

temperature increase on the surface by means of FF reactor (see Chapter 5) suggest a revision of this initial assumption.

4.2.2 Mesh construction

For the construction of the mesh, an user-controlled mesh is implemented. At first, an *extra fine* mesh is used for the whole domain, then the mesh at all boundaries is refined with an *extremely fine* mesh precision. Since the reactive surface is the most important part of the system, mesh is furthermore refined close to this particular boundary. Indeed, all specifications of an *extremely fine* mesh are implemented but the maximum element size is decreased from 1.61e-4 to 6e-5 m. There is also another refinement for all boundaries because a "boundary layer" condition is implemented. In this way, there is a structured mesh composed by 3 rectangles in each boundary before that the unstructured triangular mesh starts. With this kind of mesh, there are 17698 elements and it is possible to achieve a high degree of mesh definition, as shown in Figure 4.2, that should ensure a satisfactory precision in the results.

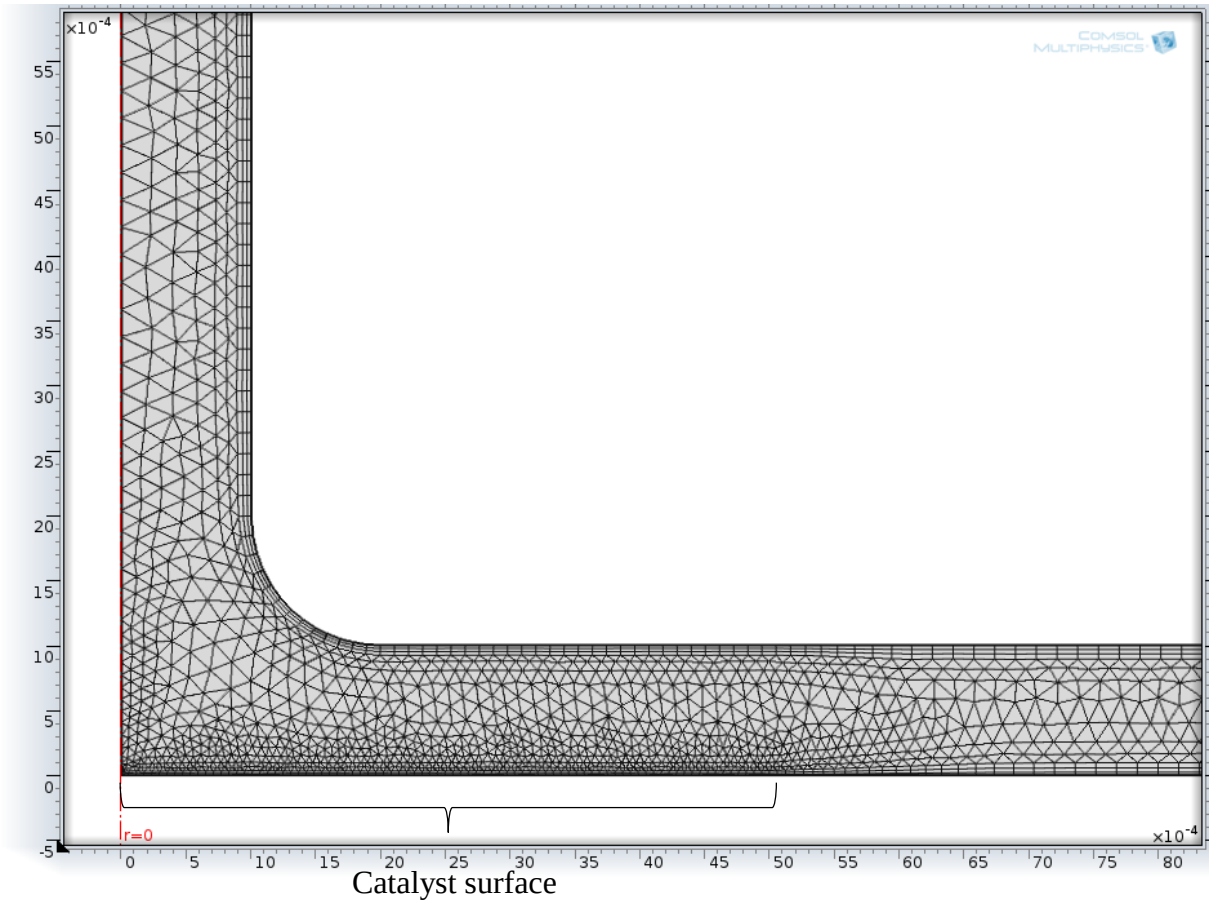

Figure 4. 2. *Representation of the mesh used in the simulation. Dimensions are in meter and the Figure is zoomed on the catalyst surface. It is possible to see the mesh refinement on all boundaries and on the catalyst surface in particular. It is also possible to see the structured mesh on the boundaries.*

Since the modelled system is small and it is in a laminar regime, a higher degree of mesh accuracy can be achieved without affecting the resolution time. Indeed, a singular steady state case is resolved in about 20-25 s, so the parametric sweep (i.e. calculation of all the combinations of inlet velocities and gaps) implemented in this simulation takes about 6 minutes to be solved on a PC with an Inlet processor i7-2630QM and 6 GB of RAM.

4.3 Results

The first result that should be observed is the temperature plot because it shows that, for low inlet flow rates, reagents are immediately heated up to 200 °C (Figure 4.3) while, for high flow rates, reagents reach the catalyst at about 180 °C (Figure 4.4). This observation suggests that also limitations to heat transfer from the reactor walls to the flowing gas may contribute to keep the conversion below the 100% expected at high temperature, in addition to the mass transfer limitations experimentally observed already at 180 °C (Figure 5.9).

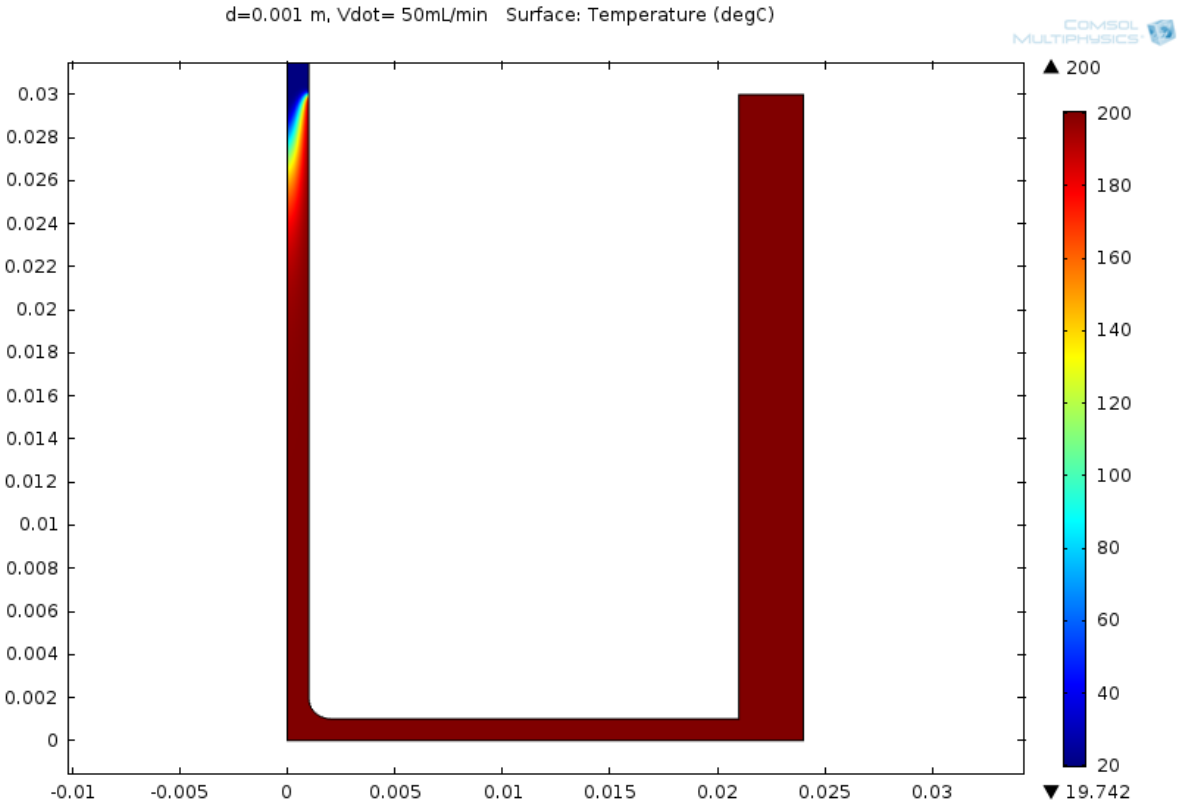

Figure 4. 3. *The computed temperature plot for a 50 mL/min flow rate and a 1 mm gap.*

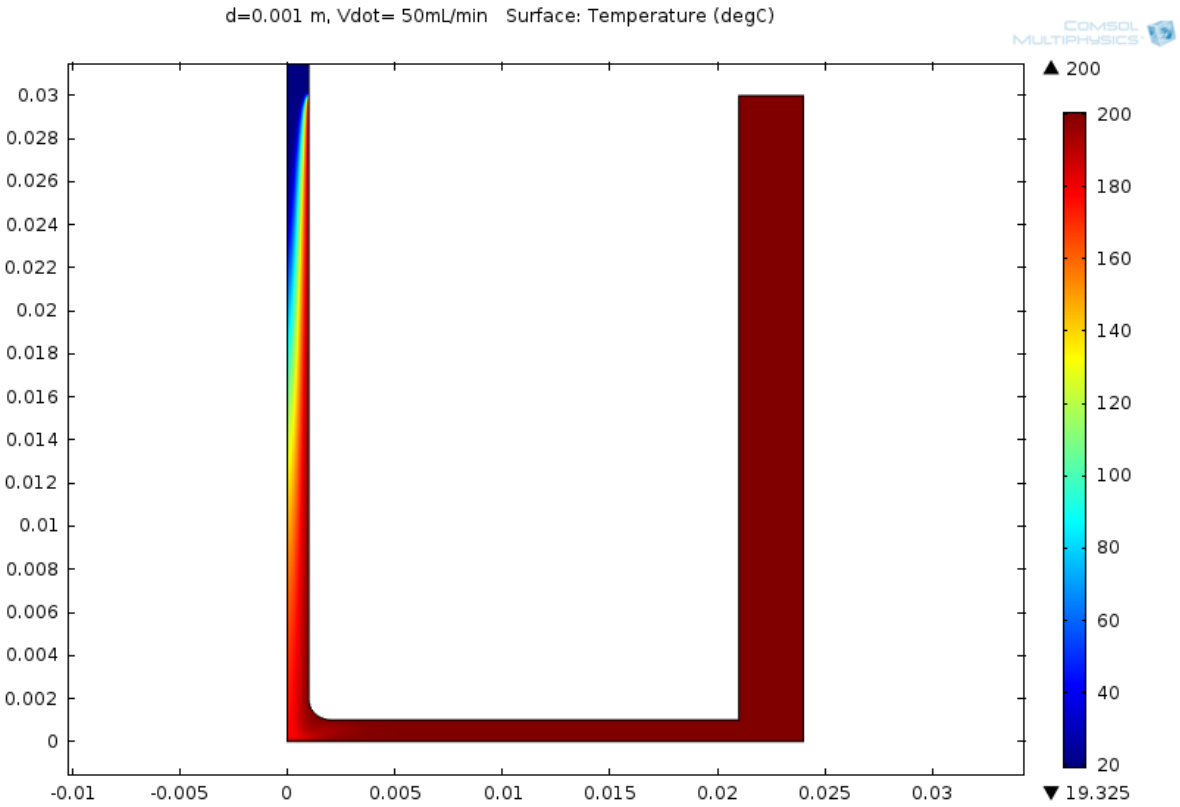

Figure 4. 4. *The computed temperature plot for a 250 mL/min flow rate and a 1 mm gap.*

The gas velocity strongly depends on the inlet flow rate and it is also increased when reagents enter the reactor because of the thermal effect. For the lowest flow rate (50 mL/min) the maximum fluid velocity is 0.81 m/s while, for 250 mL/min, it is 3.9 m/s (Figures 4.5 and 4.6).

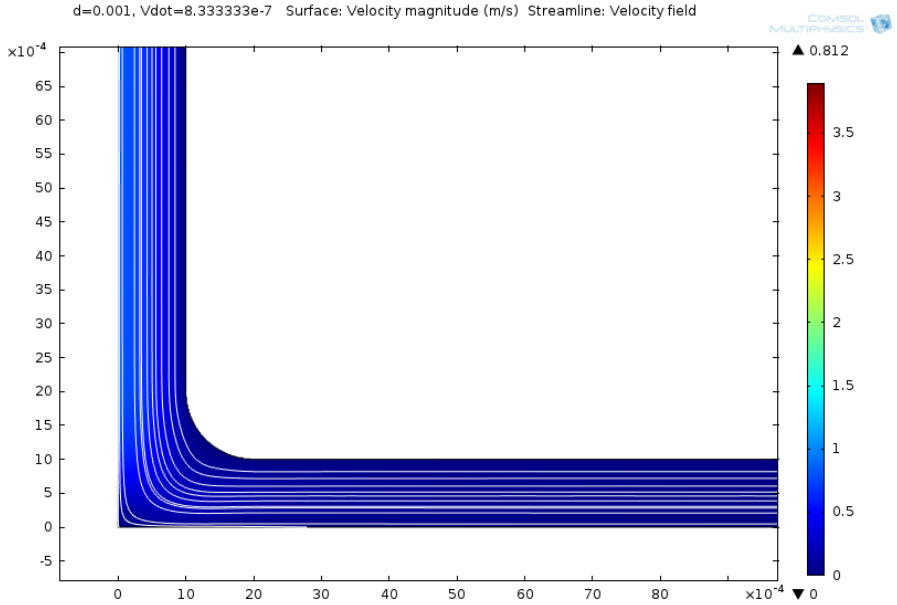

Figure 4. 5. *Velocity plot of the simulated case with a 50 mL/min inlet flow rate and a 1 mm gap.*

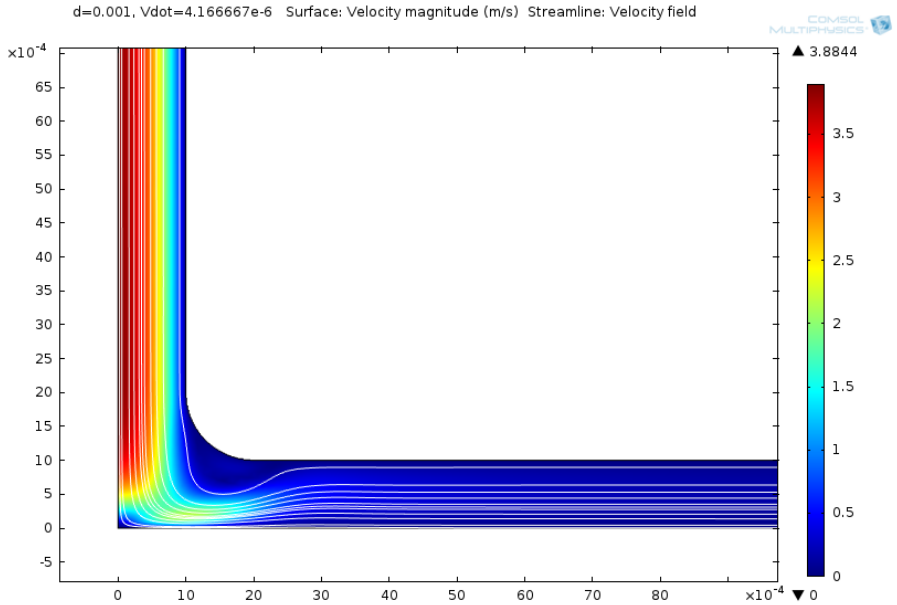

Figure 4. 6. *Velocity plot of the simulated case with a 250 mL/min inlet flow rate and a 1 mm gap.*

As expected, the fluid velocity immediately decreases once the catalyst is reached because the fluid spreads radially from the center of the reactor to the exit, using a progressively larger cross section.

The value of the local Reynolds number based on the inlet radius and local velocity was computed and shown in (Figure 4.7).

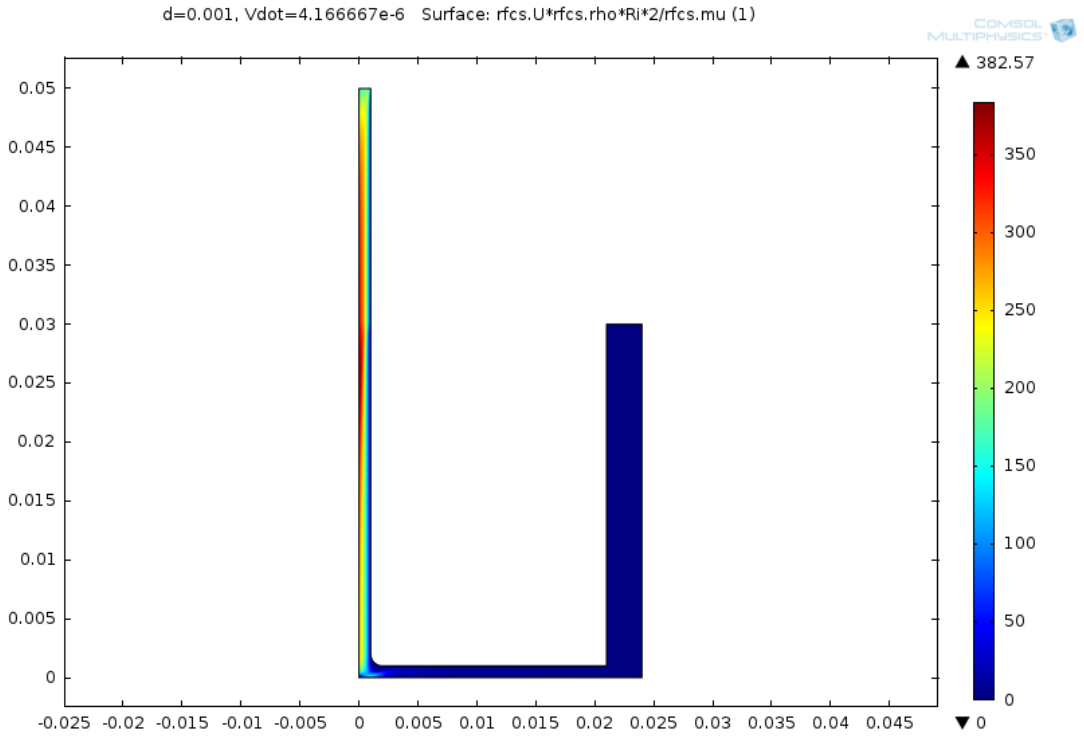

Figure 4. 7. *Plot of the computed local Reynolds number inside the reactor. It confirms the laminar regime of the system.*

The average Re based on the mean velocity and the diameter of the inlet pipe (were the velocity is higher) results 124 and 596, at the lower and the higher flow rate. We believe that these values, together with Figure 4.7, support the assumption of laminar regime

The focus of our simulation is on the hydrogen mass transfer because, as previously mentioned, we would like to elucidate if it affects the hydrogen conversion. The total hydrogen flux at different *gaps* and flow rates is plotted in Figures 4.8, 4.9, 4.10 and 4.11.

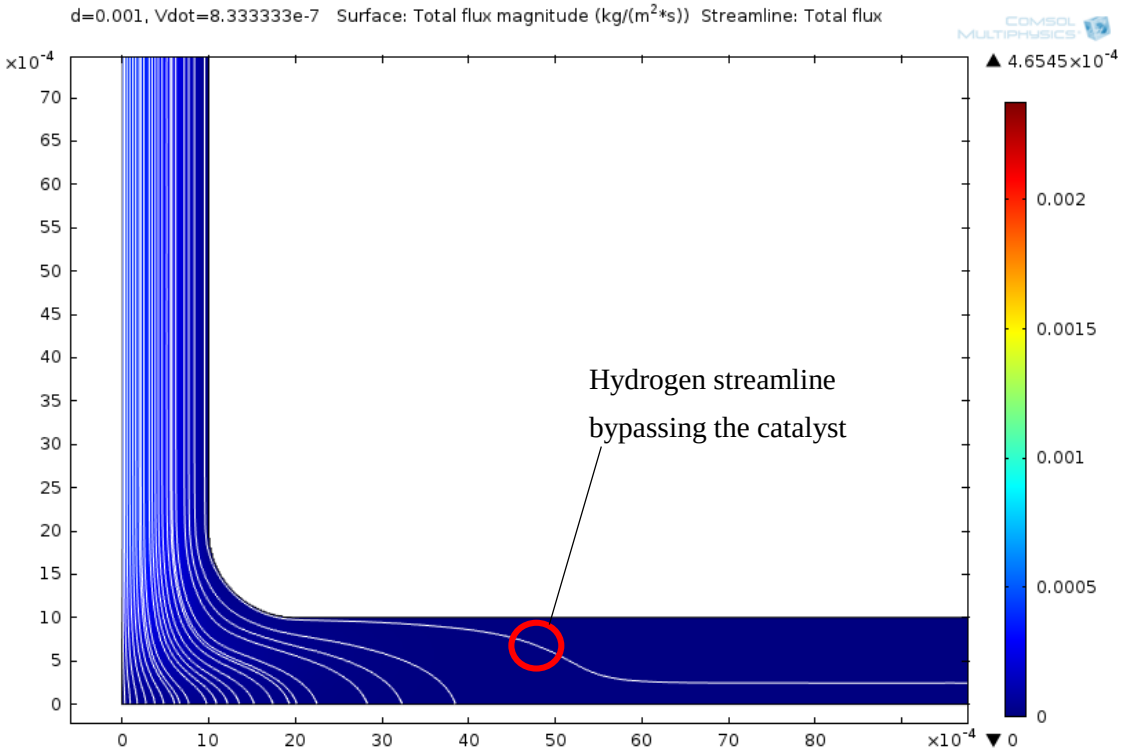

Figure 4. 8. *Plot of the hydrogen total flux with streamlines with a 50 mL/min inlet flow rate and a 1 mm gap.*

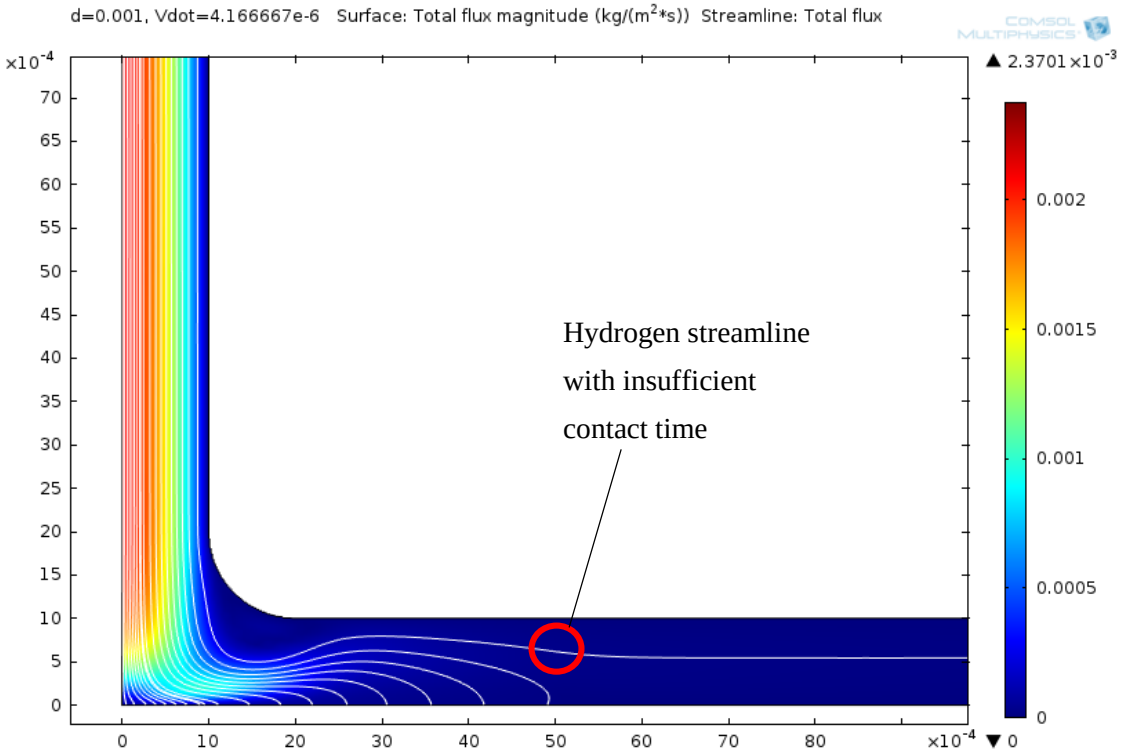

Figure 4. 9. *Plot of the hydrogen total flux with streamlines with a 250 mL/min inlet flow rate and a 1 mm gap.*

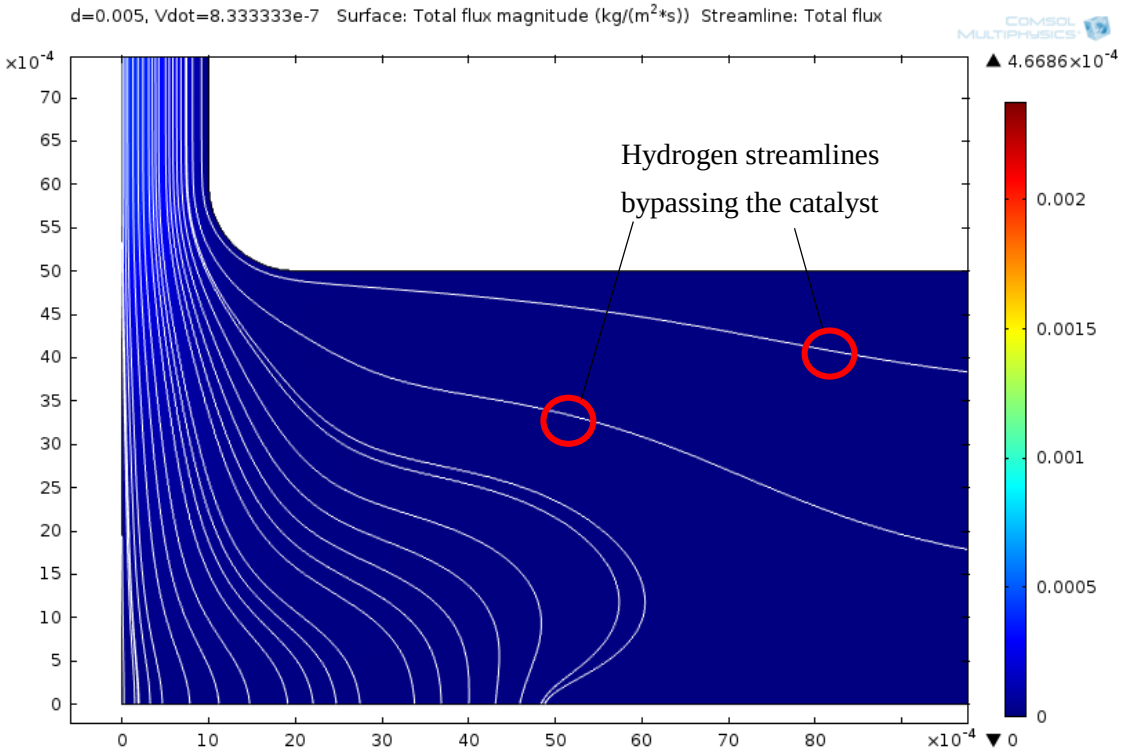

Figure 4. 10. *Plot of the hydrogen total flux with streamlines with a 50 mL/min inlet flow rate and a 5 mm gap.*

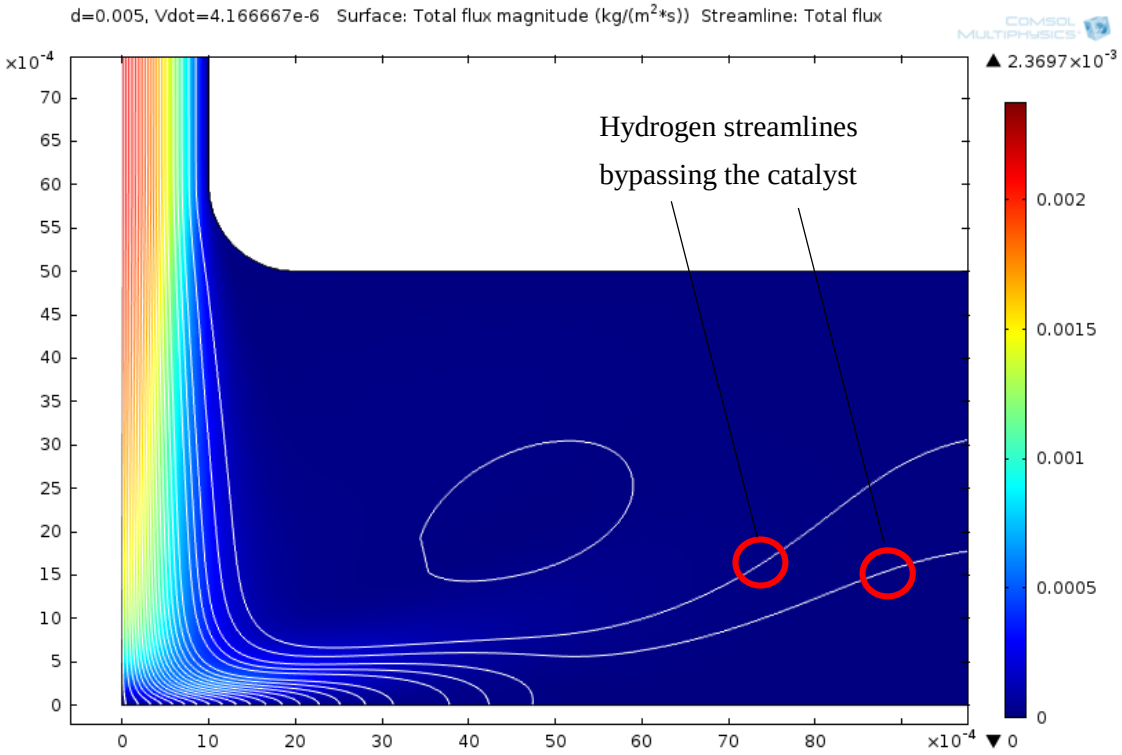

Figure 4. 11. *Plot of the hydrogen total flux with streamlines with a 250 mL/min inlet flow rate and a 5 mm gap.*

The results show that the reaction is never complete because of different flow-related phenomena. At low flow rates, hydrogen is not forced to reach the catalyst by convection, so it can easily bypass it flowing above the surface, in the distance (Figures 4.8 and 4.10). The situation changes significantly at high flow rates because reagents are forced towards the catalyst (Figures 4.9 and 4.11) but, at the same time, the contact time of reagents with the catalyst is smaller because of larger velocities. To get an idea of which phenomenon mainly affects the reaction, a conversion diagram is plotted (Figure 4.12).

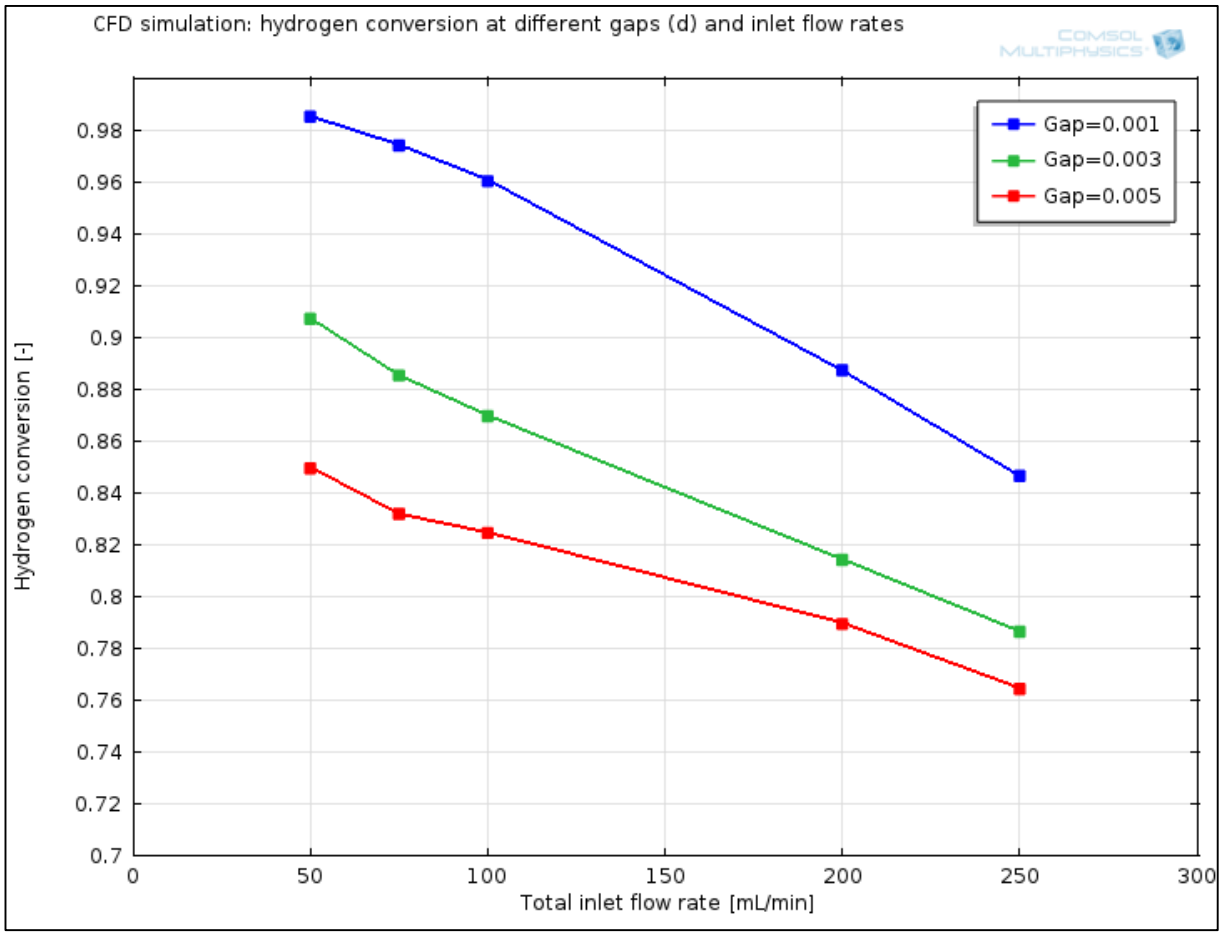

Figure 4. 12. *Hydrogen conversion plot for all gaps and inlet flow rates considered. Conversion is decreasing with the increase of gap and flow rate.*

According to the Figure 4.12, the effect of the reduced contact is more important on conversion than the catalyst bypass observed at low flow rate. Both these phenomena are increased at higher *gaps*, significantly reducing the achievable conversion as the gap increases.

A deep study of convection and diffusion transport mechanism in proximity of the catalyst was carried out to establish their influence on hydrogen mass transfer towards the catalyst. The convective flux of hydrogen along the *z* axis, immediately useful for feeding the catalyst, is plotted in Figures 4.13 and 4.15. It must be compared with the corresponding diffusive flux, shown in Figures 4.14 and 4.16. Note that the Fick's law is used to describe diffusion.

Since these fluxes do not vary significantly with the *gap*, we show and discuss only the case of 1 mm *gap*, at different flow rates.

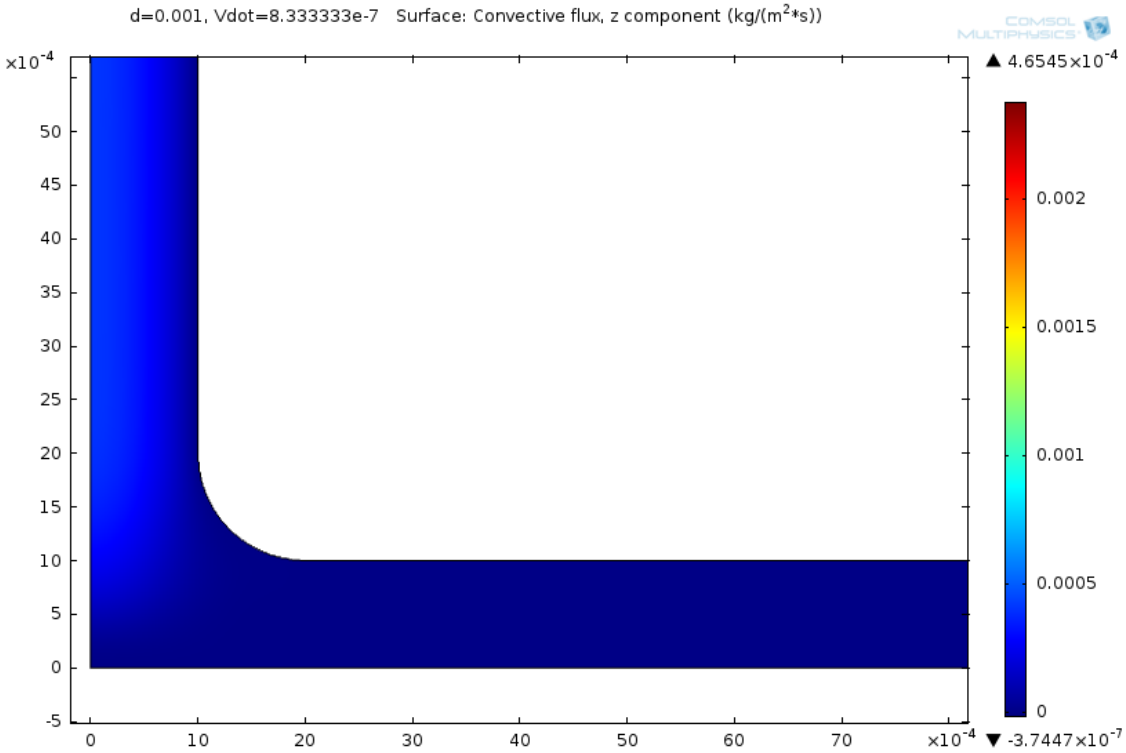

Figure 4. 13. *Plot of the hydrogen* ***convective*** *flux along the z axis with a 50 mL/min inlet flow rate and a 1 mm gap.*

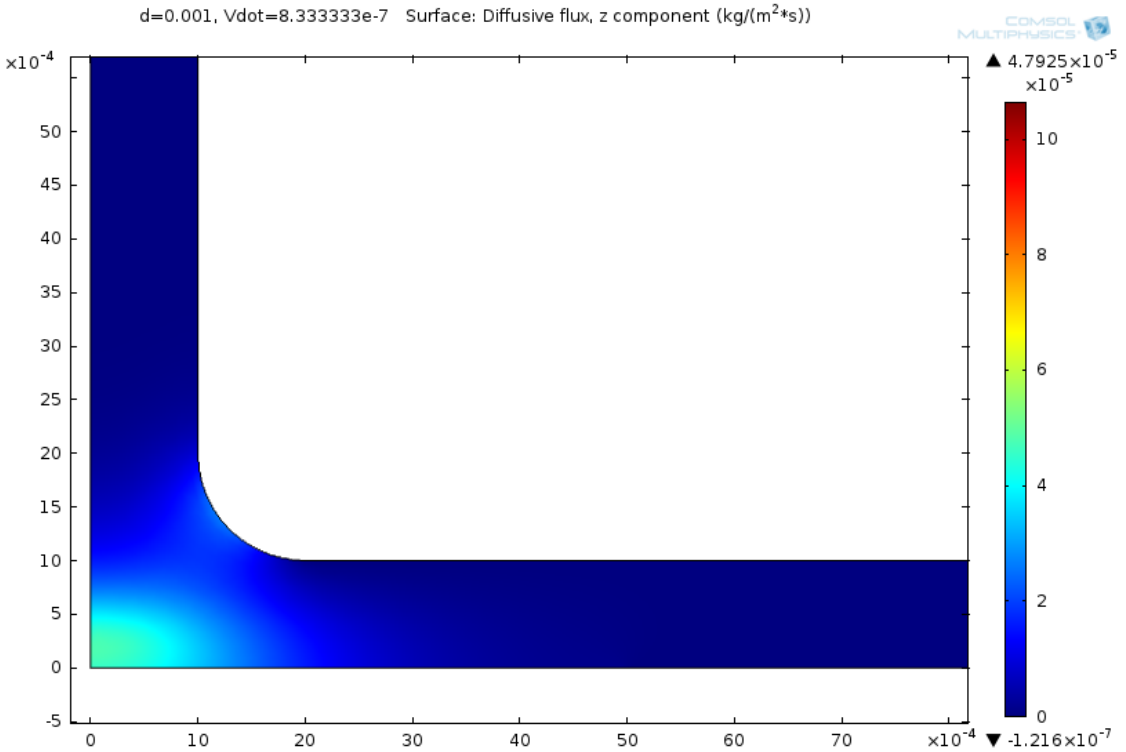

Figure 4. 14. *Plot of the hydrogen* ***diffusive*** *flux along the z axis with a 50 mL/min inlet flow rate and a 1 mm gap.*

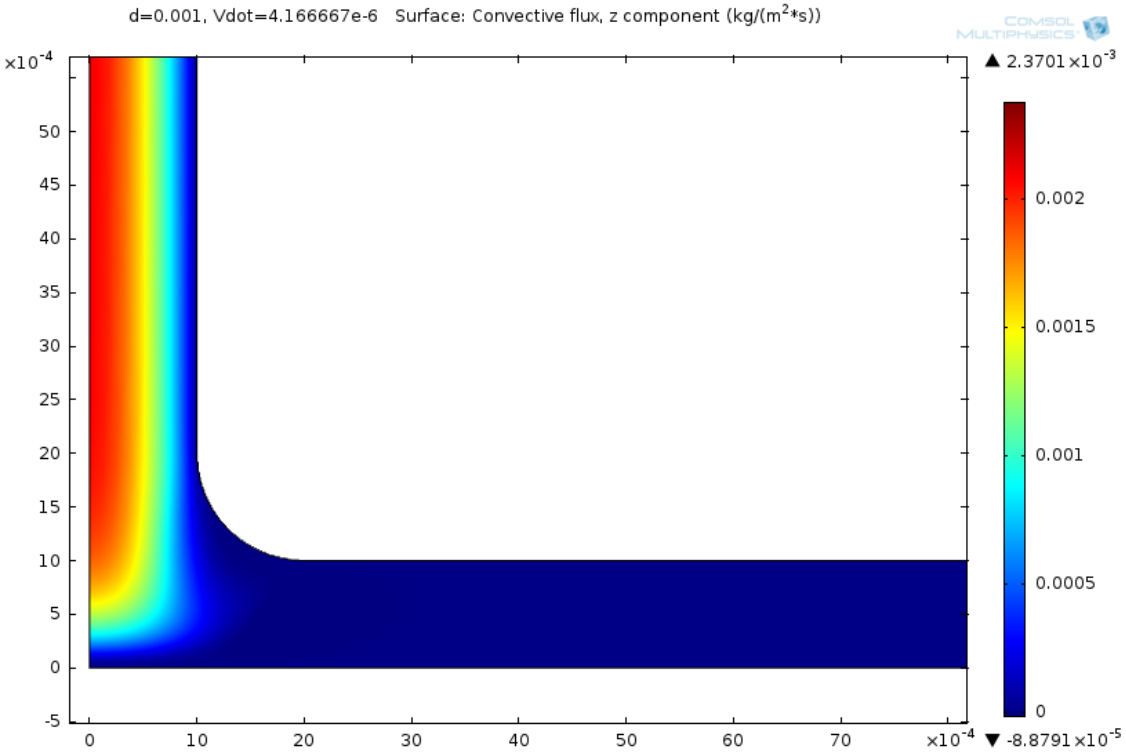

Figure 4. 15. *Plot of the hydrogen* ***convective*** *flux along the z axis with a 250 mL/min inlet flow rate and a 1 mm gap.*

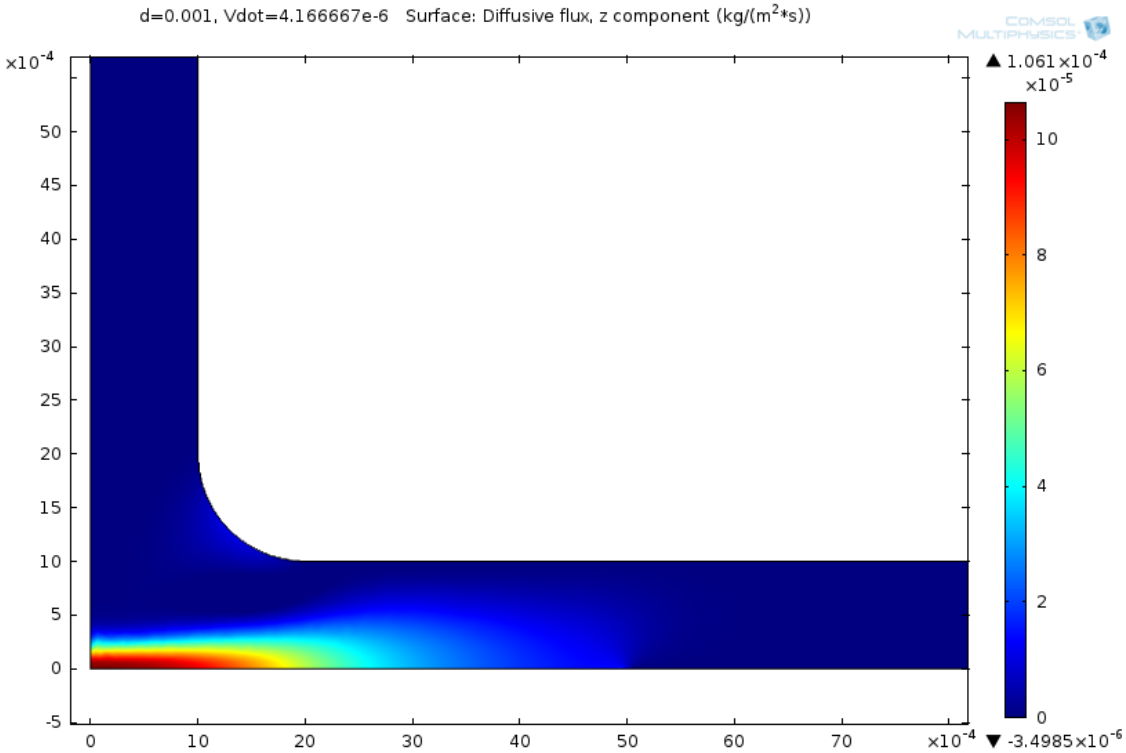

Figure 4. 16. *Plot of the hydrogen* ***diffusive*** *flux along the z axis with a 250 mL/min inlet flow rate and a 1 mm gap.*

These results show that both convection and diffusion towards the catalyst are enhanced at higher flow rates. In particular, at higher flow rates, hydrogen is transported only by convection until 0.5 mm from the catalyst then the fluid velocity decreases significantly. Diffusion is greatly promoted by convection since hydrogen is convectively transported very close to the catalyst, where it rapidly reacts, causing a large concentration gradient close to the surface, which supports diffusion (Figures 4.15 and 4.16).

On the other hand, at lower flow rates, hydrogen transport by diffusion compares with the convective transport, much farther in the catalyst region. Apparently, Figure 4.13 suggests that convection barely affects the hydrogen transport to the catalyst at the lowest flow rate, so diffusion gives the main contribution. It is significantly active since the reagents nozzle but its contribution never reaches the value of the high flow rate case. This is because the concentration gradient is lower in this case since the compound is not transported by convection.

Observing the normal total flux values at the reactive surface as a function of the radial coordinate up to the catalyst edge, it is possible to validate all previous arguments (Figures 4.17, 4.18, 4.19 and 4.20). Note that the normal total flux of H_2 is exactly equal to its surface consumption rate.

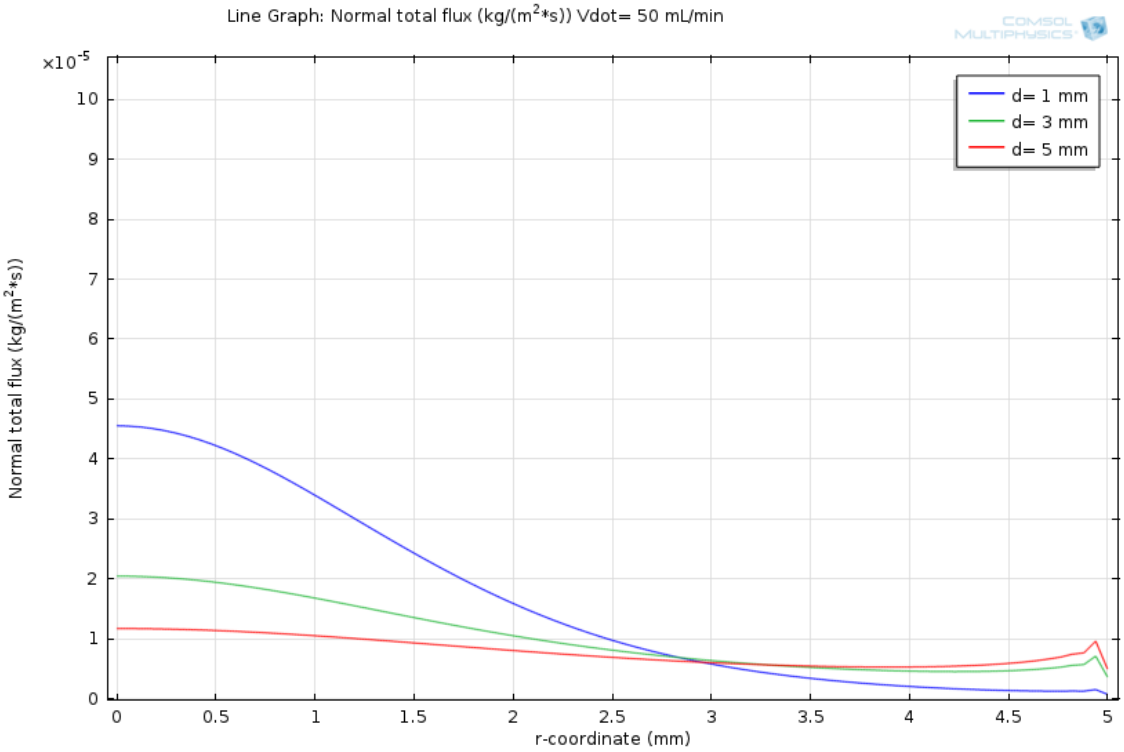

Figure 4. 17. *Normal hydrogen total flux on the reactive surface with a 50 mL/min inlet flow rate.*

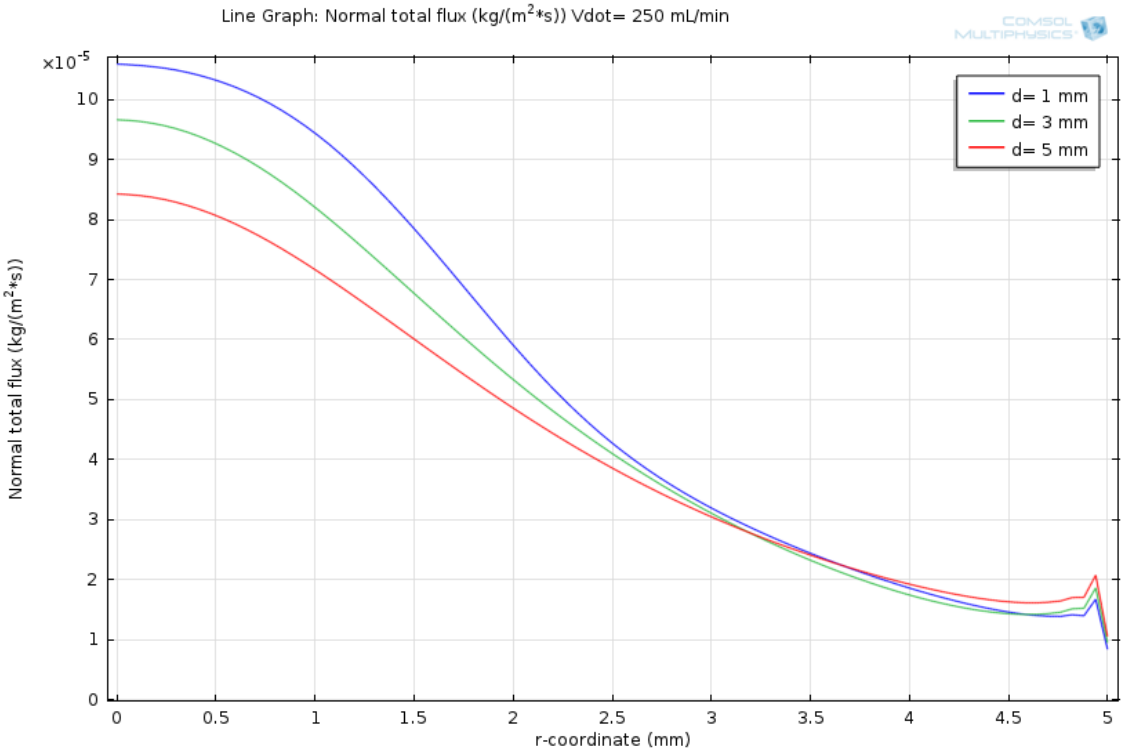

Figure 4. 18. *Normal hydrogen total flux on the reactive surface with a 250 mL/min inlet flow rate.*

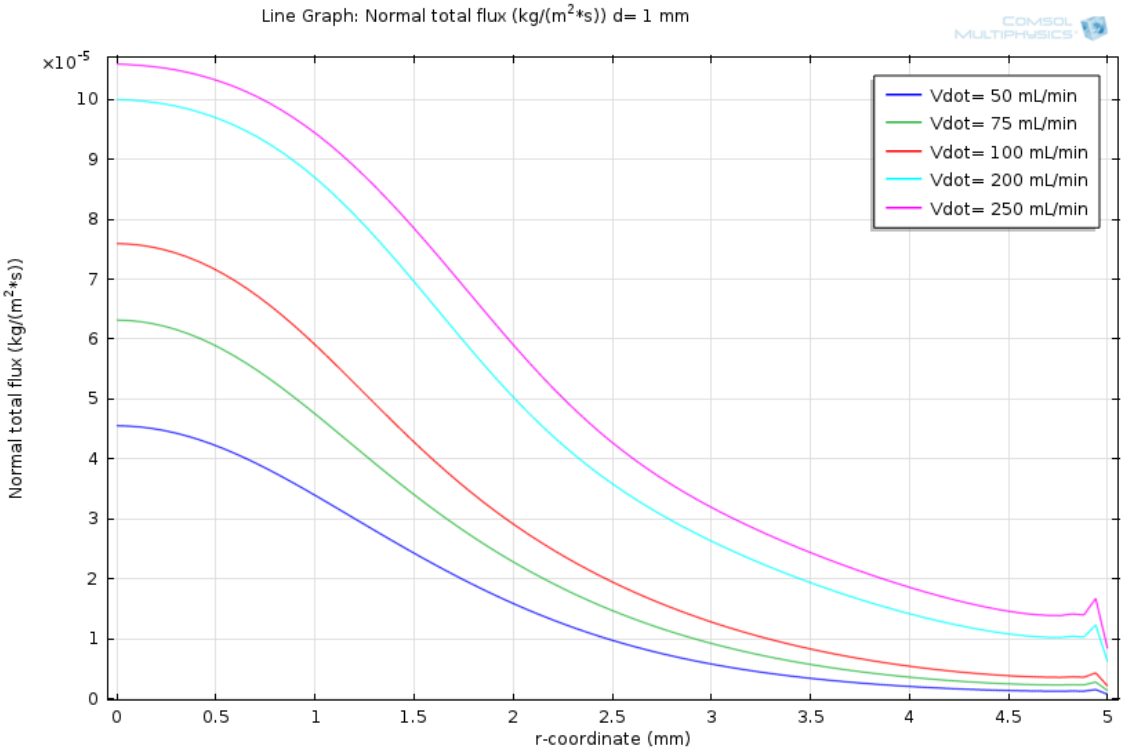

Figure 4. 19. *Normal hydrogen total flux on the reactive surface with a 1 mm gap.*

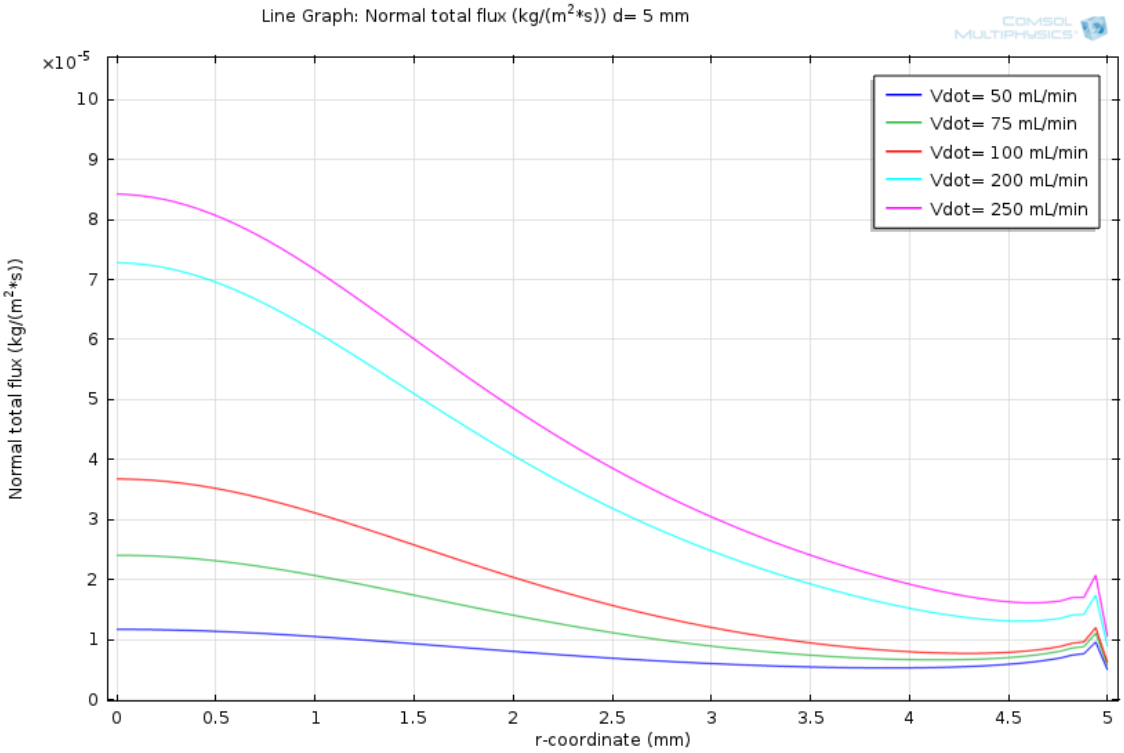

Figure 4. 20. *Normal hydrogen total flux on the reactive surface with a 5 mm gap.*

Figures 4.17 and 4.18 shows that, at any inlet flow rate, the lower is the *gap*, the higher is the hydrogen consumption rate at the catalyst surface.

On the other hand, Figures 4.19 and 4.20 show that, at any *gap*, the reacting hydrogen increases with the inlet flow rate, as argued with the observations maps on convective and diffusive fluxes of Figures 4.13-4.16.

It is interesting to note that most of hydrogen reacts in the central part of the catalyst (0 – 2 mm) because it is the stagnation point: the residence time is virtually infinity; that also causes the larger gradients with respect to the bulk, thus attracting H_2 by diffusion.

Finally, the initial assumption of isothermal catalyst has been removed and replaced by an adiabatic surface with local heat release due to the reaction as

$$\dot{Q}_R = -R\Delta H_R \tag{4.4}$$

Where $\Delta H_R = \Delta H^f$ of water (-57.8 kcal/mol). In addition to calculating the heat developed by the reaction, we must account for its effect on the kinetics. Consistent with the approximation of k=0.8 m/s we used a tentative Arrhenius model as $k(T)=2.58\cdot10^5\cdot\exp(-6000/T)$, which approximately gives $k(200°C)$ = 0.8 m/s, based on an activation energy of approx. 48 kJ/mol. For consistency of the comparison, also the calculations with adiabatic (not isothermal) catalyst have been carried out, with the same function *k(T)*.

The results show that the reaction can significantly rise the temperature in front of the catalyst, as shown in Figure 4.21 to 4.24, consistently with the observations reported in Chapter 5, 4th topic.

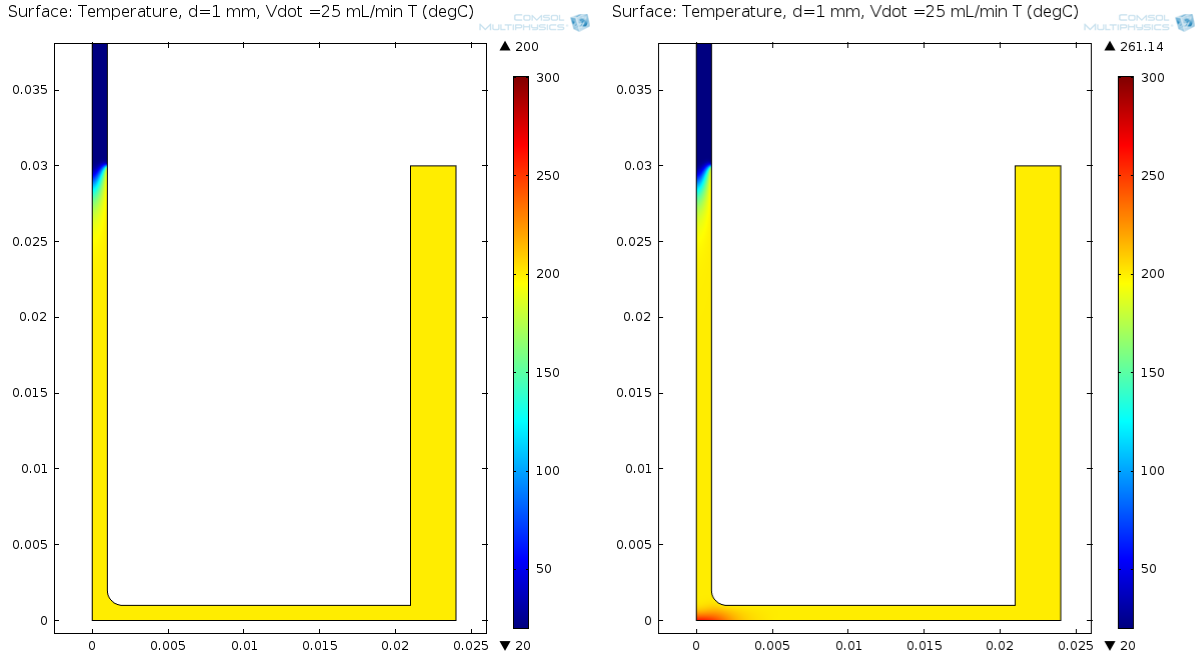

Figure 4.21. *Gas temperature at small flow rate and gap. Adiabatic catalyst. With (right) and without (left) account for heat of reaction. Reactor at T=200°C.*

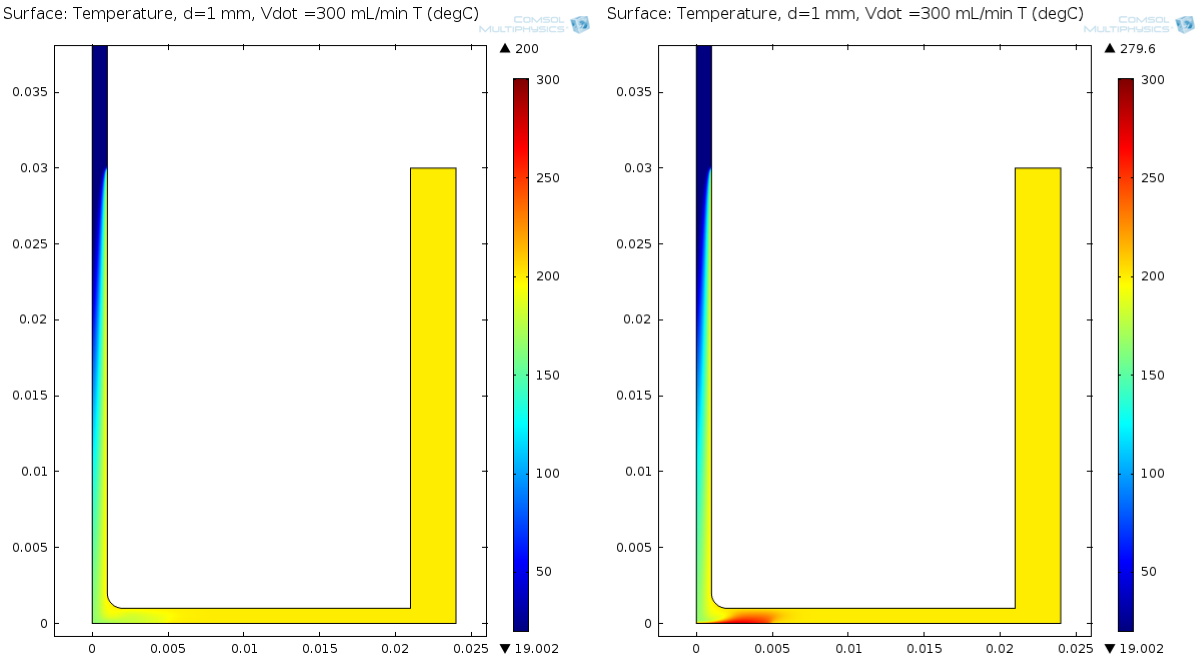

Figure 4.22. *Gas temperature at large flow rate in a small gap. Adiabatic catalyst. With (right) and without (left) account for heat of reaction. Reactor at T=200.*

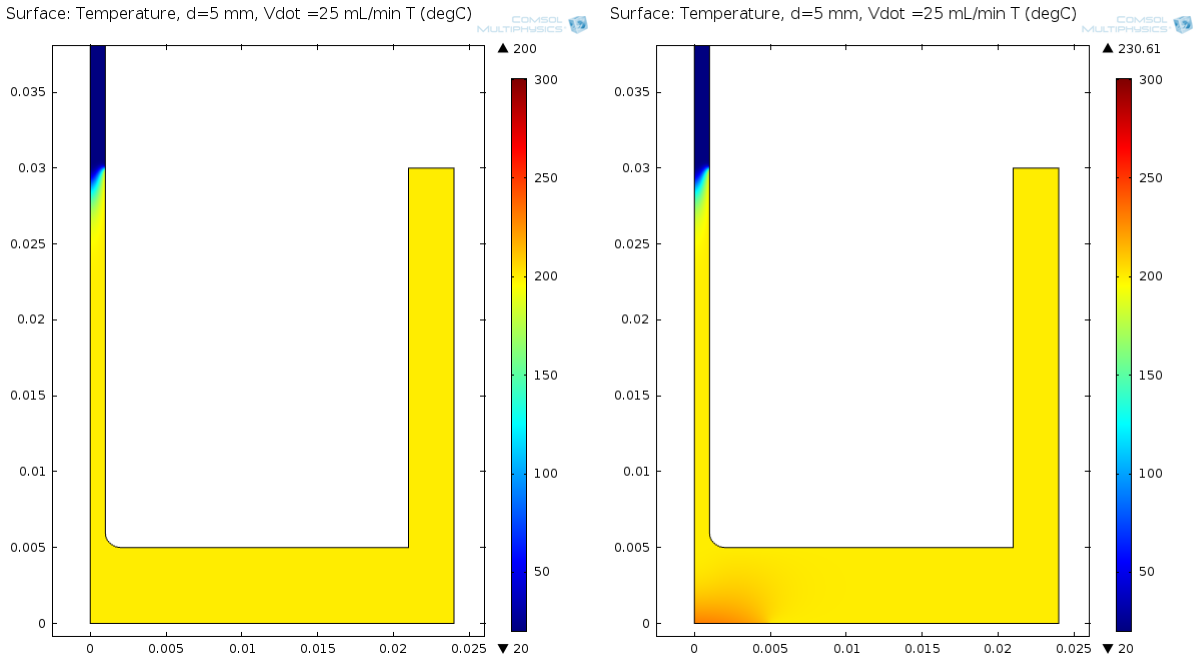

Figure 4.23. *Gas temperature at small flow rate in a large gap. Adiabatic catalyst. With (right) and without (left) account for heat of reaction. Reactor at T=200°.*

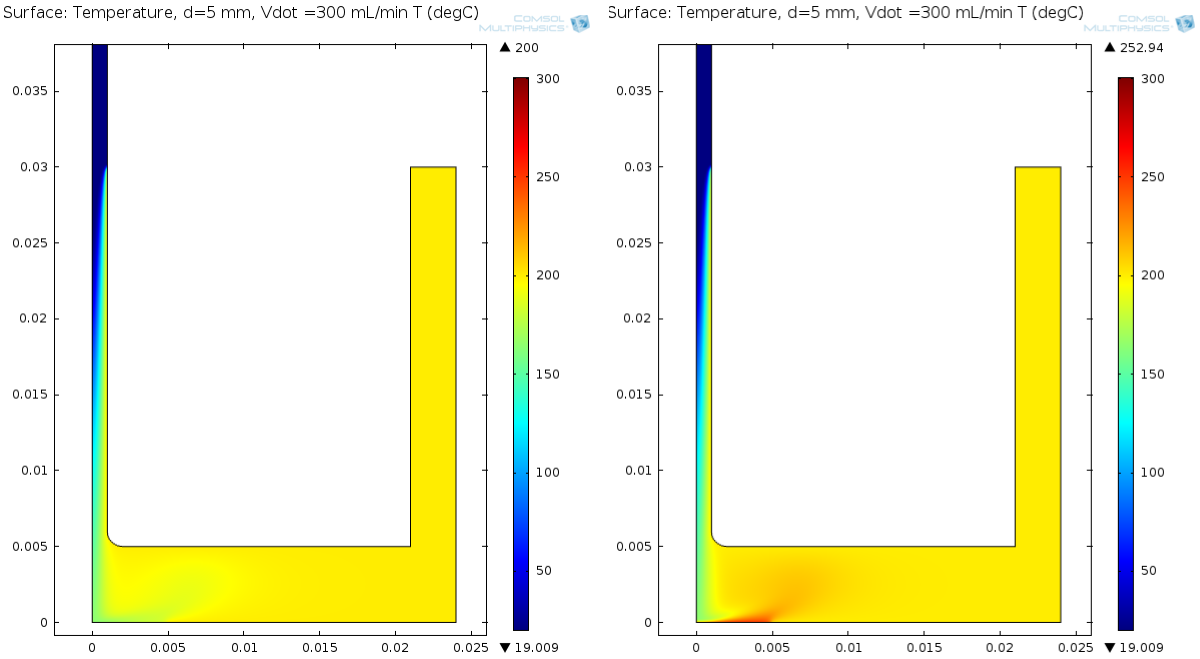

Figure 4.24. *Gas temperature at large flow rate in a small gap. Adiabatic catalyst. With (right) and without (left) account for heat of reaction. Reactor at T=200°C.*

At small gaps above the catalyst, the temperature can locally rise dramatically, more than 50°C. The larger the flow rate, the larger the temperature increase, notwithstanding the stronger convective cooling by the cold feed. At larger gaps, the local overheating spreads and dissolve, with a limited temperature rise.

The influence on the conversion is quite impressive, as shown in Figure 4.25.

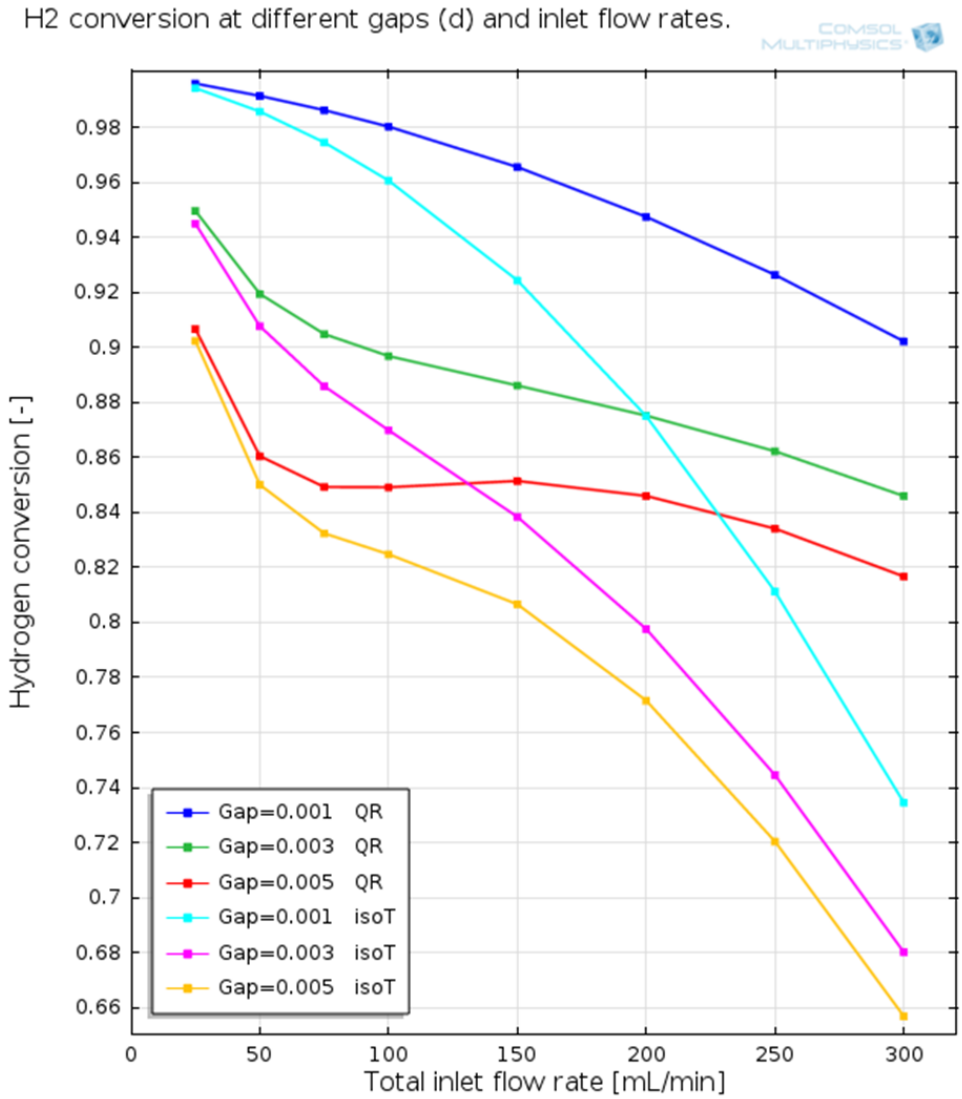

Figure 4.25. *Effect of flow rate and gap on the conversion. Adiabatic catalyst. With (QR) and without (nearly isoT) account for heat of reaction. Reactor at T=200°C.*

The heat of reaction keep the conversion fairly high even at large flow rates. The extreme reduction of the gap brings the conversion very close to 100%. Note that nearly isothermal operation leads to a depression of the conversion with increasing temperature not very comparable to the experimental observation, much better represented by the non-isothermal simulation

That definitely stimulates further investigations, also accounting for the heat transfer capacity of the Pt disk with its surrounding, which could be a key factor.

Chapter 5

The experimental results

The aim of the fifth Chapter is the description of the experimental results and their discussion. The experimental work is divided into 4 main topics that regards the evaluation of:

1. the variations of the catalyst activity due to thermal and thermochemical treatments;
2. the maximum conversion varying key geometry parameters (distance reagents nozzle-catalyst and total inlet flow rate);
3. the ignition temperature and reaction advancement varying the hydrogen composition in air;
4. the reaction heat on the reactive surface.

5.1 The variations of the catalyst activity

The first experimental topic of this Thesis regards the 1.evaluation of the variations of the catalyst activity based on the idea that a restructuring of the surface can increase the activity (§2.2.2). According to §2.2, the faceting process can be induced by thermal and thermochemical treatments. 3 types of thermal treatments were then performed on the Pt surface:

- in an inert atmosphere;
- in hydrogen atmosphere (surface reduction);
- in oxygen atmosphere (surface oxidation).

The temperature of all treatments is between 200 °C and 350 °C. Treatments at higher temperature are not allowed in the FFC reactor because the TiN coating may be damaged.
Since we would like to enhance the Pt activity for oxidation reactions at low temperature, the conversion is always evaluated at 120 °C.
In all experiments, the reaction is performed with the following flow conditions:

- total inlet flow rate (Vdot)= 75 mL/min;
- hydrogen volumetric composition= 5 %vol, hydrogen inlet flow rate= 3.75 mL/min;
- oxygen volumetric composition= 2.5 %vol, oxygen inlet flow rate= 1.87 mL/min;
- argon volumetric composition= 92.5 %vol, argon inlet flow rate= 69.38 mL/min.

The reagents composition is stoichiometric and the reaction conditions are diluted in an argon atmosphere to facilitate the GC analysis of H_2.

.

In all experiments, the reactor used is the FFC reactor, the heating rate is always 3 °C/min and conversion is calculated through the *microGC*.

5.1.1 Thermal treatments

As a first step, we verified the thesis of Kraehnert and Baerns (2007). They suggested that a thermal treatment is not sufficient to restructure the platinum surface, so the activity should not vary after a treatment.
The conditions for the treatments performed are shown in Table 5.1 and the results shown in Figures 5.1, 5.2, 5.2, 5.4. We first discuss test #1 and #2, where treatments were purely thermal, in an inert atmosphere. They differ by the Pt exposure before the tests, test #1 was on a sample previously exposed to air, while test #2 was carried out on a sampled previously kept under an inert atmosphere.

Table 5.1. *List of the thermal treatments performed in this research step.*

Thermal treatment number [-]	Test number [-]	Temperature [°C]	Time [h]
1	40	200	2
2	40	350	2
3	42	200	1
4	42	300	1
5-7	43	300	1
8	45	200	1

The reagents conversion was tested before and after each treatment. The results are shown in Figure 5.1 and 5.2 After an air exposure (atmospheric or synthetic), Figure 5.1, the conversion dropped almost to zero, but it raises during the reaction test, up to about 15%. The evolution was quite fast. Because of these rapid changing of activity, we set a standard duration for the reaction phase, of 30min, to prevent dramatic, irreversible transformations of the Pt surface, that might affect all the following tests. Figure 5.1 also shows that a first thermal treatment under inert atmosphere reestablished quite a good activity, leading to an appreciable conversion of approx. 55%. The conversion was monitored for 30 min and it shows an unexpected drop. At first, it is about 60% and it decreases quickly in the first minutes until it reaches a value of ~40% in 30 min. A second thermal treatment restores the same initial activity (of approx. 60%), but also the same rapid loss of activity is observed. Such a dramatic increase occurs only after the first treatment; all the following treatments, extending also to Test 42 (Figure 5.2), always in an inert atmosphere, do not significantly modify the sample activity, nor its inclination to rapidly loosing it.

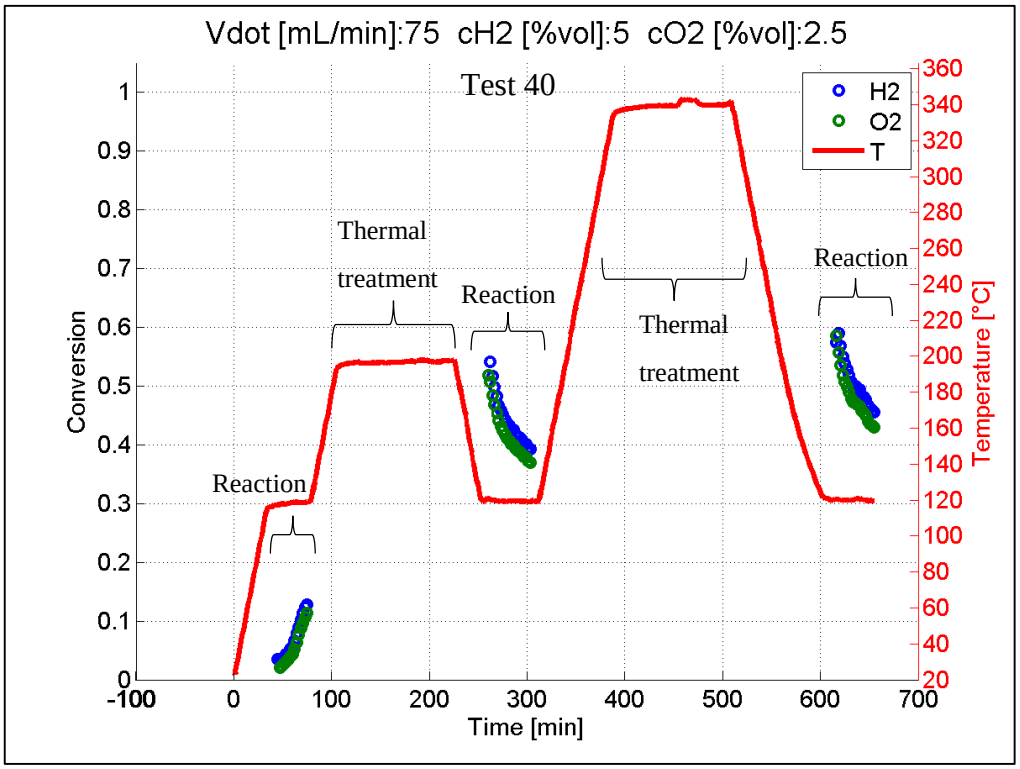

Figure 5. 1. *The results of 2 thermal treatments in inert after an initial exposure to air.*

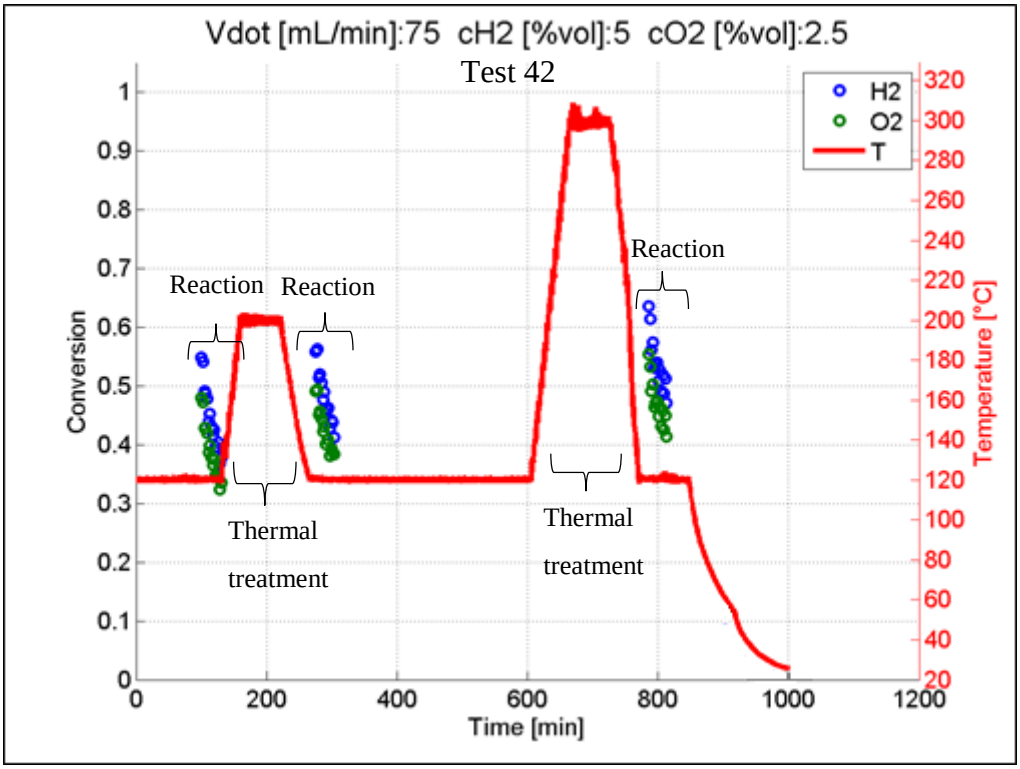

Figure 5. 2. *Experimental results of 2 thermal treatments in inter gas after an initial exposure to an inert atmosphere.*

So far, we confirm the thesis of Kraehnert and Baerns (2007). Thermal treatment alone do not modify the surface reactivity. The reason why a thermal treatment increases the conversion after an air exposure may be the cleaning of the surface. A high temperature process in an inert

atmosphere helps to desorb all species previously adsorbed on the catalyst. Then, the surface would easier adsorb hydrogen atoms so the conversion improves.
The decreasing behavior of conversion may be explained considering that, at the begin of the reaction, all Pt sites are available to adsorb the species and react. However, during the course of reaction there may be a site competition between all the involved compounds. In this way, the system tends to an equilibrium where conversion is much lower.

5.1.2 Reduction thermochemical treatments

High temperature reduction treatments, tests #43, were performed to vary the catalyst activity that is expected to raise because of the restructuring process, according to literature (§2.2.2).
These tests were conducted at 300-350 °C and the gas composition is:

- total inlet flow rate (Vdot)= 73.13 mL/min;
- hydrogen volumetric composition= 5.1 %vol, hydrogen inlet flow rate= 3.75 mL/min;
- argon volumetric composition= 94.9 %vol, argon inlet flow rate= 69.38 mL/min.

When the conversion is tested, components have the same flow rate and the only difference is the presence of oxygen.
Table 5.2 summarizes all reduction treatments.

***Table 5.2**. List of the reductive treatments performed in this research topic.*

Thermal treatment number [-]	Test number [-]	Temperature [°C]	Time [h]
1	39	350	1
2-9	43	300	1

Despite the expectations, hydrogen treatments do not show any enhancement of conversion even if 8 consecutive treatments were performed (Test 43). The effect is similar to thermal treatments. We speculate that treatments are effective purely because of temperature, independently of the reducing atmosphere. They apparently just clean the surface from adsorbed species without restructuring it. Even in this case, conversion rapidly drops from 60% to 40% in 30 min.

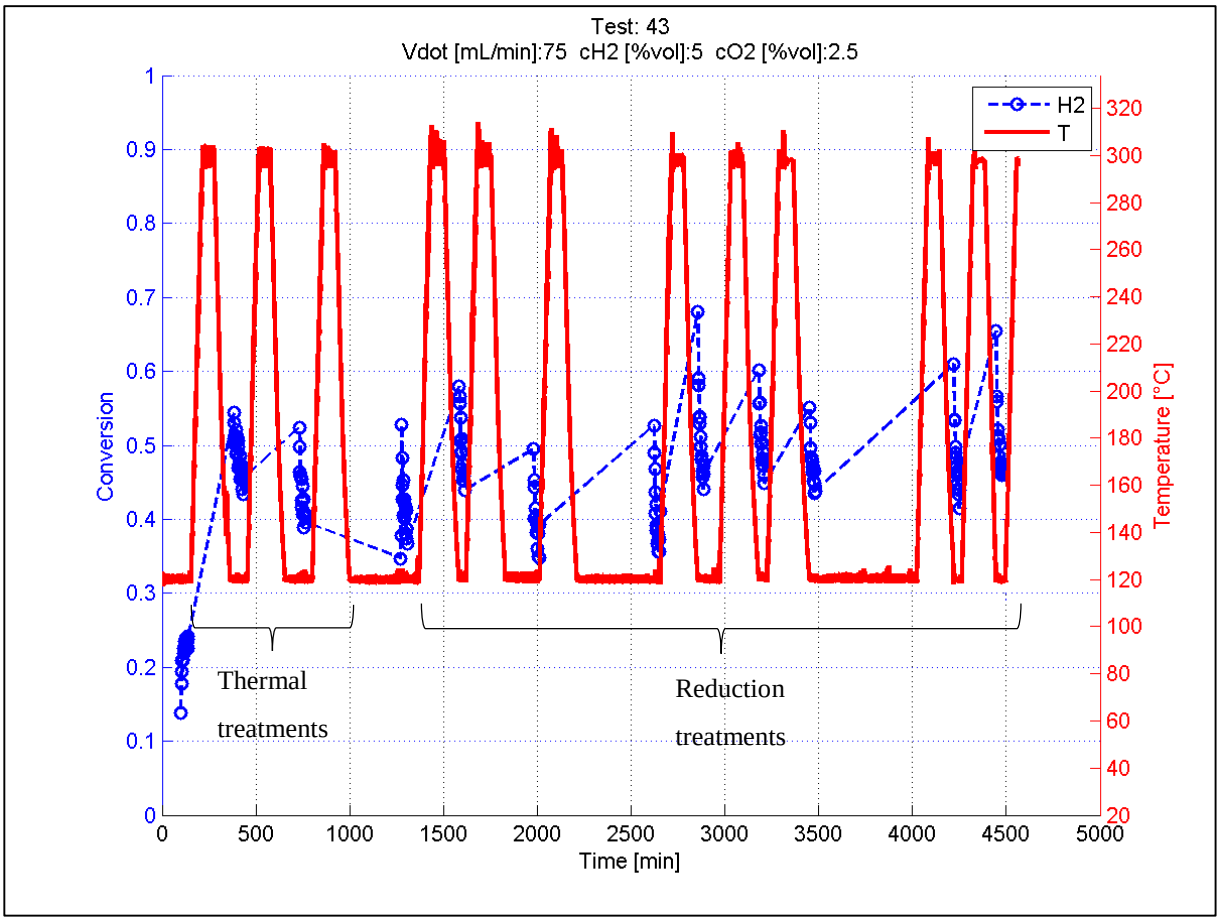

Figure 5. 3. *Experimental results of 3 thermal treatments and 8 reductive treatments.*

5.1.3 Oxidation thermochemical treatments

The final treatment tested to evaluate the activity modifications is a high temperature oxidation. Like the reduction case, the enhancement of conversion is expected because of the surface restructuring, following both literature indications and previous experiments in our lab, not reported here.

The experiments were conducted at 300 °C and the gas composition is:

- total inlet flow rate (Vdot)= 71.25 mL/min;
- oxygen volumetric composition= 2.6 %vol, oxygen inlet flow rate= 1.87 mL/min;
- argon volumetric composition= 97.4 %vol, argon inlet flow rate= 69.38 mL/min.

When the conversion is tested, components have the same flow rate and the only difference is the presence of hydrogen.

Table 5.3 summarizes all oxidation treatments.

Table 5.3. *List of the oxidative treatments performed in this research topic.*

Thermal treatment number [-]	Test number [-]	Temperature [°C]	Time [h]
1-3	44	300	1
4	45	300	1

The oxidation treatment produces a great increase of the initial conversion (from 60% to 85%). The obtain conversion is still decreasing with time from a value of 85% to 55%.

During the same test 44, three treatments were conducted and, while the first one greatly increases the conversion, the following 2 simply restore the initial activity already observed after the first oxidative treatment (Figure 5.4).

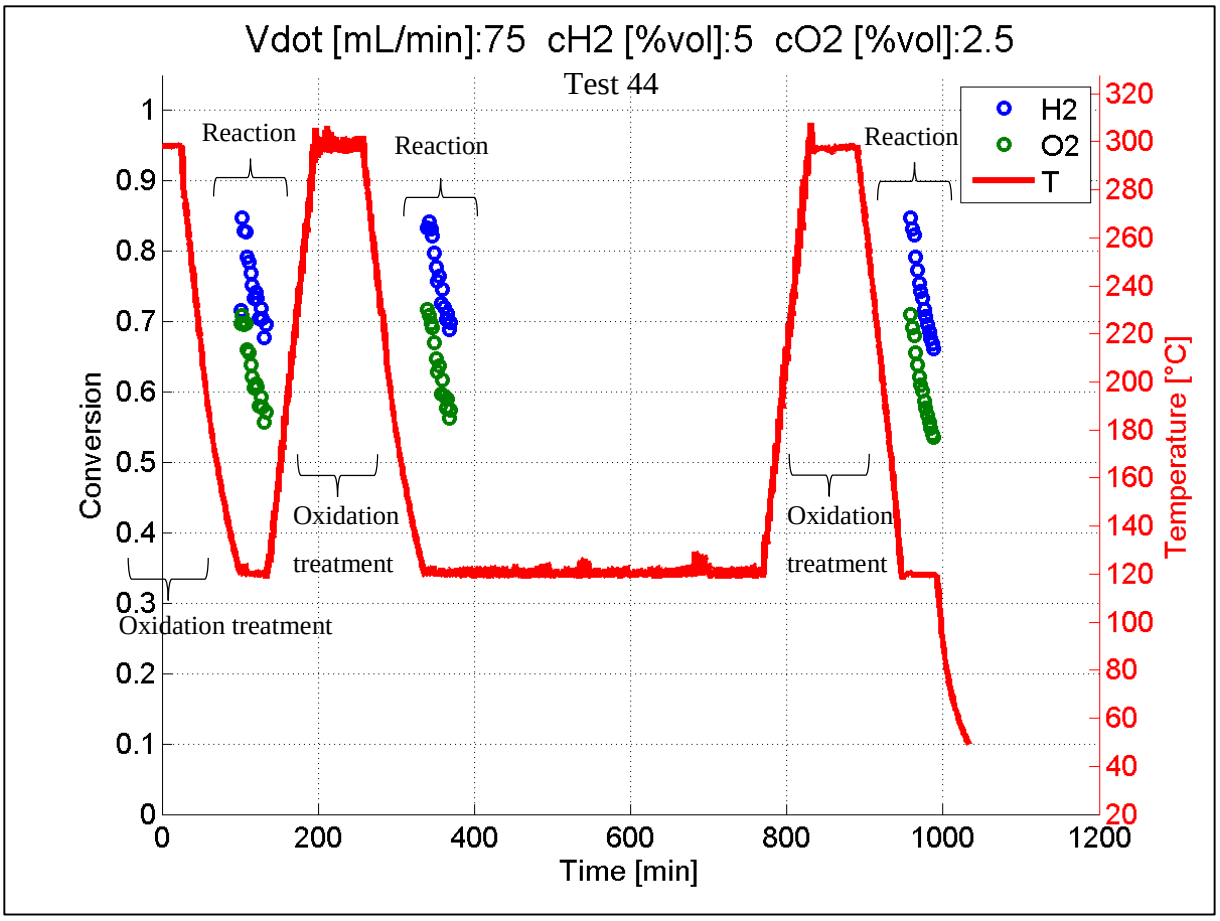

Figure 5. 4. *Experimental results of 3 oxidative treatments.*

The experimental results suggest that an oxidation treatment is much more effective than a thermal or reduction treatment in terms of enhancement of conversion. An oxidation may improve the cleaning the Pt surface, like the previous treatments. It may also promote the oxygen adsorption. In this situation, when the reaction begin, only hydrogen needs to be adsorbed because oxygen is already present on the surface. This situation can enhance the conversion since the oxygen adsorption energy is higher than the hydrogen energy (§2.1), so the activation energy of the global reaction is reduced. However, it looks like the surface

availability of oxygen is rapidly replaced by hydrogen, easier to adsorb, leading again to a slower surface reaction.

5.1.4 Conclusions of the first experimental topic

One of the aim of this research topic is the modification of the Pt surface with reduction and oxidation. However, as shown in Figure 5.5, the surface does not show any kind of restructuring process.

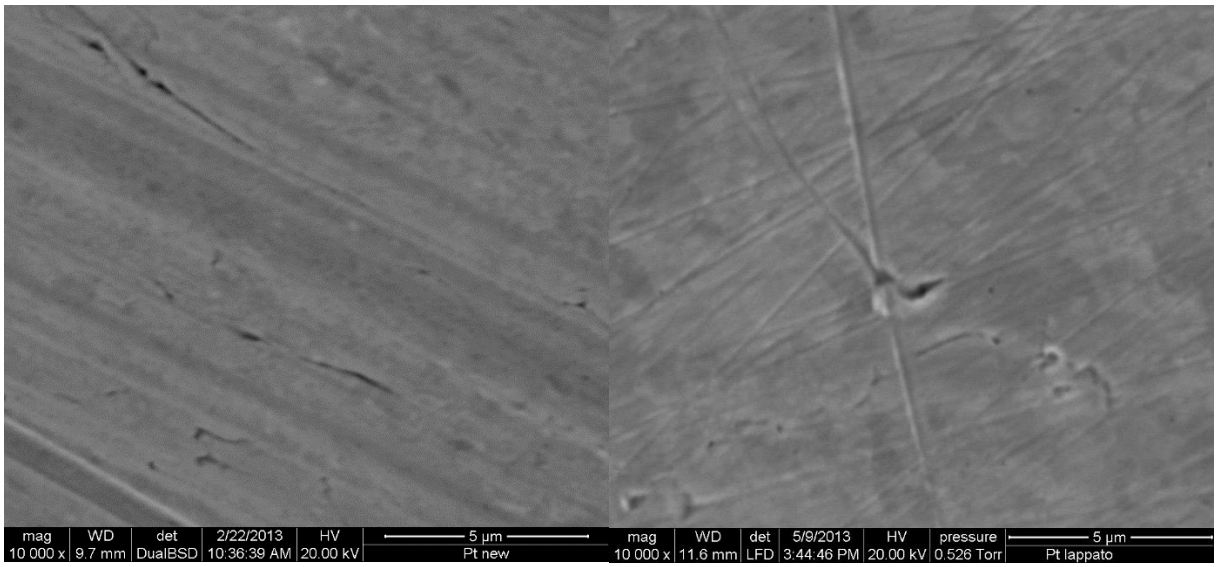

a. b.

Figure 5. 5. *A SEM picture of the catalyst surface before (a.) and after (b.) all treatments.*

This result suggests that, to induce the surface faceting, observed in the past after the use of Pt disk in a different reactor up to 600°C, a higher temperature and a higher oxygen or hydrogen concentration are needed. However, a temperature above 350 °C cannot be achieve with the FFC reactor without damaging its coating. To confirm this idea and validate literature paper, more investigations are needed.

The enhancements of conversion observed in these experiments appears related only to a process of surface cleaning from the adsorbed species. After this process, hydrogen adsorb more easily and, as shown in Figure 5.4, an oxidation treatment is much more effective than any other treatment because it may also promote the oxygen adsorption.

To conclude the research topic, the steady state value of conversion at the end of its decreasing behavior was evaluated (Figure 5.6). After both a reductive and an oxidative treatment, conversion tends to reach about the same steady state value (between 10-15 %) that may represent the equilibrium point of a site competition.

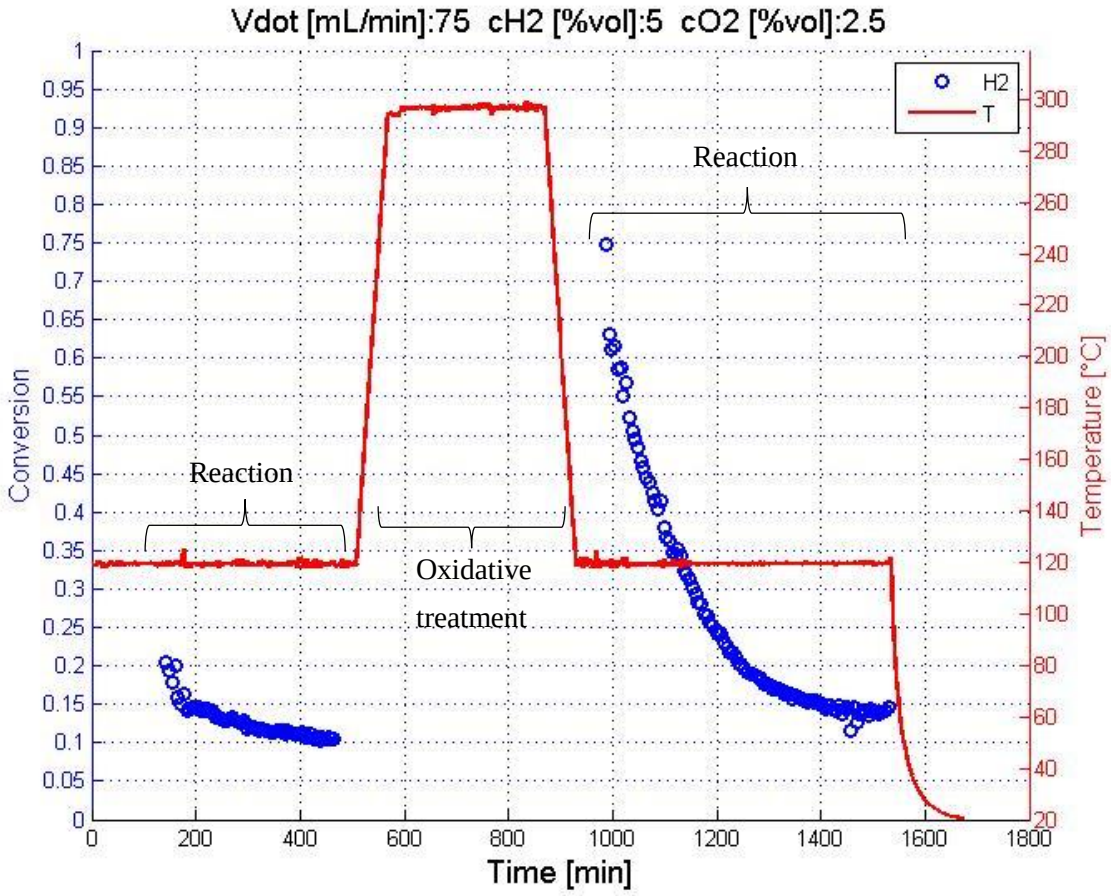

Figure 5.6. *The evaluation of the steady state conversion after a reductive treatment (on the left) and an oxidative treatment (on the right).*

The conclusion of this research topic is that the activity of the catalyst depends greatly on its history (~20% of conversion after an air exposure and ~80% after an oxidation treatment). Because of that, experimental results may be not consistent. To avoid this problem and maximize the catalyst activity, a reagent atmosphere with a large excess of oxygen will be used during the next research topics. The excess of oxygen should also avoid the decrease of conversion during the course of reaction seen in this first topic.

5.2 The geometric and fluid dynamics influences on maximum conversion

An important kinetic feature that needs to be evaluated is the maximum H_2 conversion achievable and particularly how key geometric parameters of the reactor and fluid dynamics affect it. The experiments show that above a relative high temperature, say approx. 200°C, the conversion does not increases further. We speculate that this could be an indication of mass transfer control and now we wish to investigate this issue.

5.2.1 Experimental results

Experiments were performed at 3 different gaps (Figure 2.20) (1 – 3 – 5 mm) and at 5 different inlet flow rate (50 – 75 – 100 – 200 – 250 mL/min) so the influence of the flow patterns can be investigated. All the experiments were carried out in a steady state condition, at 200 °C. Due to the excess of oxygen in the inlet mixture, we do not observe the large conversion variations of the previous research topic so the steady state condition was reached in only a few minutes.
The experimental results are shown in Figure 5.7.

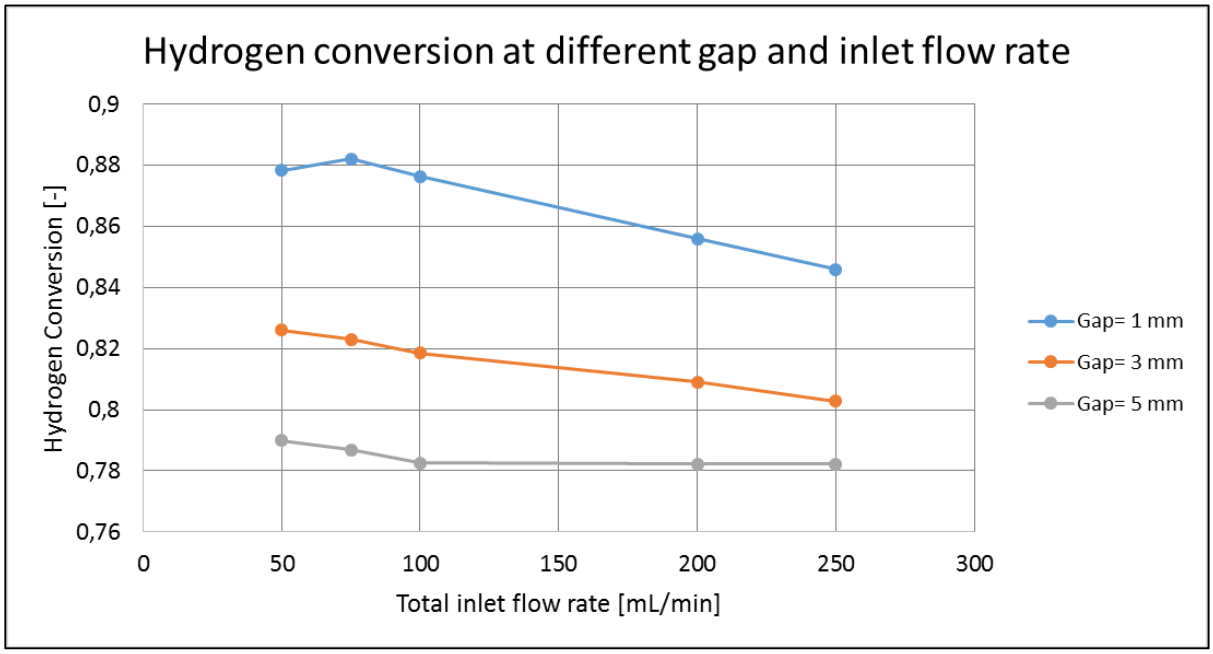

Figure 5. 7. *Experimental results of the second research topic. Maximum conversion is evaluated at 3 different gaps and 5 different inlet flow rates. Hydrogen never reacts completely and conversion decreases with the flow rate and the gap.*

The most important elucidated result is that conversion never exceeds 90% in this reactor configuration and range of operating conditions, so hydrogen does not react completely. The gap has another important effect because conversion decreased monotonically and significantly (up to 10%) when the gap increases from 1 to 5 mm.
The variation of the inlet flow rate has a minor effect on the system but in all cases conversion decreases with the flow rate. The highest effect is observed with the lowest gap (1 mm) and conversion decreases from 88% to 85%.

5.2.2 Discussion

As shown by the experimental results, fluid flow patterns affect the reactor performance, because the reaction is never complete.
Based on these results validated by the CFD simulation (§4), we formulated several explanations about internal the mass transfer. At first, the conversion cannot reach 100% at

lower flow rates (50 – 75 mL/min) because reagents can easily bypass the catalyst, flow at a distance above it, without really touching it. The fluid right above the catalyst is fairly stagnant and diffusion prevails and controls the reagents transfer to the surface. The phenomenon of catalyst bypassing is more important for higher gaps so conversion is understandably lower for them.

When the flow rate is increased, the reagents are convected towards the catalyst, where they react heterogeneously. At the same time, a larger flow rate determinies a reduced reagents-catalyst contact time and the global effect is a reduction of conversion. The lower the gap, the higher the flow rate effect because the tangential velocity on the catalyst surface increases more significantly.

5.2.3 Comparison of CFD and experimental results

Once that experimental data are measured and CFD simulations are performed, it is possible to compare the results in terms of conversion. It is important to remind that the kinetics used in the CFD calculation is simplified. The reaction detailed simulation is not the leading idea of the CFD investigation because it is mainly focused on the fluid dynamics. Kinetics was adapted to these data, and the same rate equation and parameters used for all the configurations and conditions. The comparison is shown in Figure 5.7. It allow some qualitative indications.

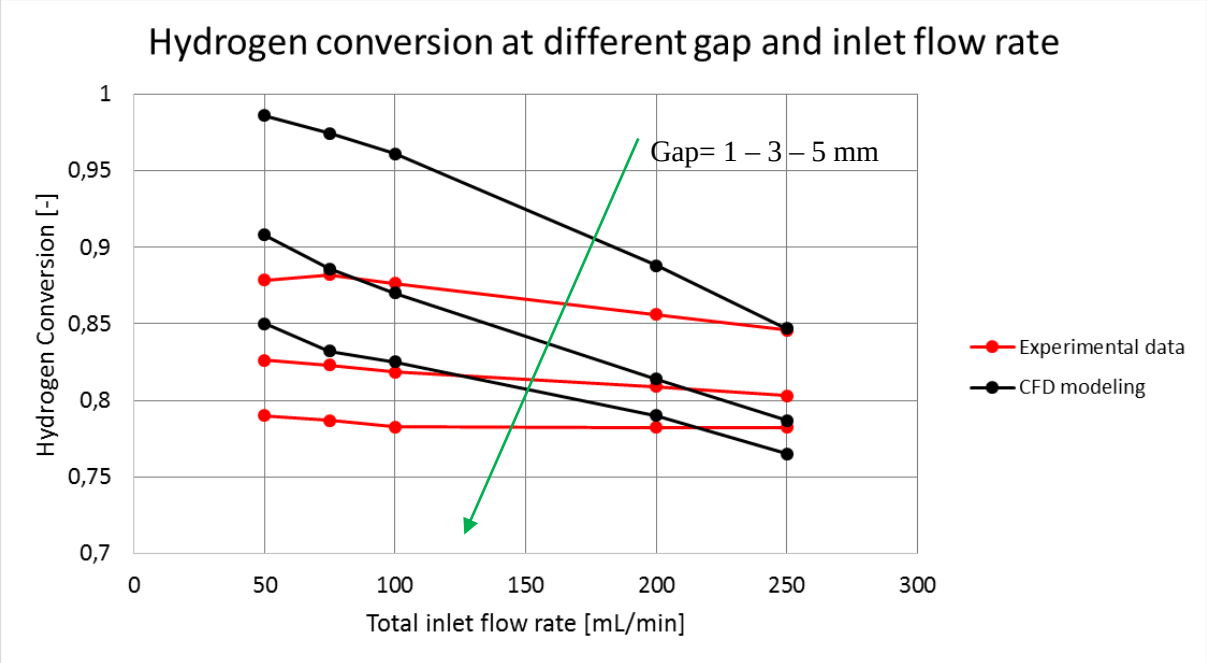

Figure 5.8. *A comparison between the experimental and CFD data in terms of hydrogen conversion.*

Even if the model overestimate the conversion for inlet flow rates ≤ 100 mL/min, the decreasing trend of conversion with flow rate is confirmed in both cases. Another point of agreement

between the CFD model and the experiments is the decrease of conversion with the increase of the gap because both cases show about the same decrease for any considered point.
A difference in term of conversion between the experiments and the simulation is expected since the CFD reaction kinetics model is extremely simple; it does not take into account any adsorption/desorption phenomena or radicals formation. That affects mostly the data at larger flow rate, where the reagents appear to reach the catalyst more easily, thus a kinetic regime prevails. A better kinetics is expected to modify the slope of the CFD curves, particularly at high flow rate, where the catalyst contact time is the key parameter. Consequently, also the low flow rate predictions might get closer to the experiments. However, the semi-quantitative agreement between the experiments and CFD calculations is satisfactory for a description of the fluid dynamics inside the reaction. To refine the CFD data, the implementation of a detailed kinetic mechanism is needed. Subsequently, a fitting of the kinetic parameters may be necessary to find the best fit between the simulation and the experiments, as suggested by Vlachos and Bui (1996).
Finally, we should stress that the measured differences in the final conversion at different gap and flow rate values are fairly small. Approx, the range spans between 78% and 88%. This make the identification of marked effects quite delicate, particularly the flow rate effect.
Also, Figure 5.11 shows that the maximum achievable conversion varies with H_2 inlet concentration, by about 3%, which is comparable to the span of a single curve in Figure 5.6, at a given gap value.

5.3 The ignition temperature and the reaction advancement

The third topic of this Thesis evaluates ignition temperature, reaction advancement and maximum conversion for different inlet hydrogen compositions. The most important aspect is the ignition temperature because Literature reports a wide range of not consistent results that are also used to tune detailed surface chemistry models. The reactor modelling is affected by experimental inaccuracies described in (§2.5) so we would be surprised that the models could apply to different geometries with the same success degree. Some simulation carried out in the group indeed proved that severe errors arise from the application of a detailed model to experimental data different from those used to tune the mechanism.
The evaluation of the FFC performance and the comparison with Literature is one of the leading ideas of this research topic.

5.3.1 Experimental results

To evaluate the ignition temperature, a temperature ramp was performed from 25 °C to 200 °C with a low heating rate (0.2 °C/min) and conversion is evaluated for each °C. This heating rate

allows monitoring the ignition temperature with a good precision and it allows the system to reach an equilibrium situation. Since after 200 °C the conversion does not increase anymore, the temperature rise is stopped, because the limitations discussed in the previous sections arise. With this kind of experiment, we can simultaneously evaluate the advancement of the reaction with temperature and its maximum conversion.

For all experiments in this topic, the following features are kept constant:

- *gap* between reagents inlet and catalyst= 1 mm;
- total inlet flow rate = 200 mL/min;
- conversion calculated with the *GC7820*;
- reactor: FFC reactor;
- maximum T = 200°C;
- heating rate = 0.2 °/min.

All experiments are conducted in an hydrogen-air atmosphere and the tested hydrogen compositions are shown in Table 5.4.

Table 5.4. *List of test numbers and inlet hydrogen concentrations in the experiments of the third research topic.*

Test number [-]	**Hydrogen concentration in air [%vol]**
74	0.4
77	1
77	2
84	3
86	4
90	7
92	10
93	15

Figure 5.9 shows a comparison of the course of reaction with temperature for all hydrogen concentrations tested. To do this comparison, the MATLAB script "*confronto*" was used (§A.4).

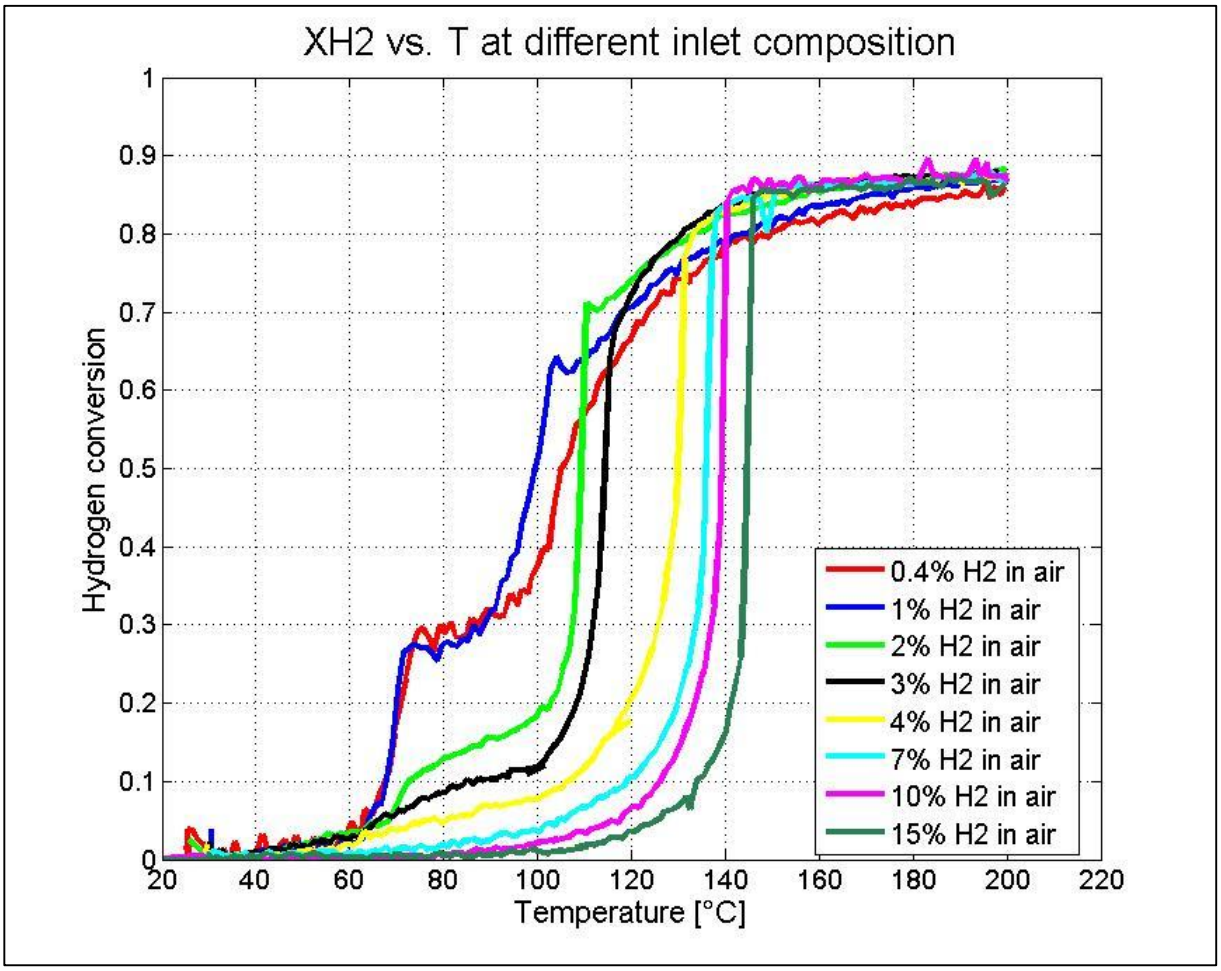

Figure 5. 9. *The increase of hydrogen conversion with temperature is shown at different inlet hydrogen compositions. As previously discuss (§5.2) hydrogen never reacts completely and the reaction behavior differs significantly between all compositions.*

5.3.2 Discussion

The main difference between the experimental results concerns the advancement of conversion with temperature. For hydrogen compositions < 2%, conversion increases gradually and the ignition temperature cannot be uniquely defined. Indeed, at 70 °C conversion swiftly reaches 30% but, after that, it is quite stable for ~15 °C. Then, it slowly increases again until it reaches its maximum value (85-87 %). The reaction seems to progress in two different steps: the first one is at 70 °C and the second at 90 °C. However, this may be a misleading conclusion. Remember that the temperature on the figure is the one reported by the thermocouple just below the Pt disk. There might be a difference between such a measured temperature and the one prevailing on the catalyst surface. This difference would explain the particular behavior of conversion: right after the ignition, the reactive surface may be heated up to 90 °C due to the surface reaction heat while the thermocouple would be still monitoring the temperature of the whole reactor (related to the temperature ramp). The conversion would be now stable until the

reactor temperature exceeds 90 °C. This investigation will be the forth research topic, described in §5.4.

Because the heating rate is so low, one may argue that there is enough time to allow the heat to propagate across the disk, from the upper surface to the lower side of the disk. A 30° interval (e.g. 70→100°C) requires 150 min, i.e. 2.5 h. However, the heat production by the surface reaction also depends on the reaction rate, which is quite weak at the lowest H_2 concentration.

For hydrogen compositions > 2%, the ignition temperature can be easily defined because conversion has a sharp increase with temperature. However, even in this composition range there are significant differences.

For compositions < 7%, the conversion increases slightly (< 15%) before the ignition and, after the ignition, the maximum of conversion is not immediately achieved. On the contrary, for higher compositions, there is no reaction until the ignition and, after the ignition, the maximum of conversion is immediately reached. We believe that such a behavior after the ignition may be still explained with the difference between the reaction and measured temperature. For the higher hydrogen concentration, the heat generated with the ignition may be enough to markedly increase the temperature of the reactive surface and the bulk of the disk, up to the thermocouple on its bottom. In this way, the reaction temperature right after the ignition would be close enough to the temperature needed for the maximum conversion.

After this first conclusion, it is now possible to compare the observed ignition temperatures with the literature ones (Figure 5.10).

The experimental results confirm some Vlachos and Bui (1996)'s results for hydrogen compositions ≤ 2% while, for higher H_2 concentration, our measurements totally disagree with those of Literature. Brady et al. (2010)'s and Behrendt et al. (1996)'s temperatures are always much lower from the experimental ones. In particular, Brady et al. (2010) observed that, for a hydrogen composition < 7%, the ignition occurs at room temperature. Such evidence has not been observed in any experiments that we carried out.

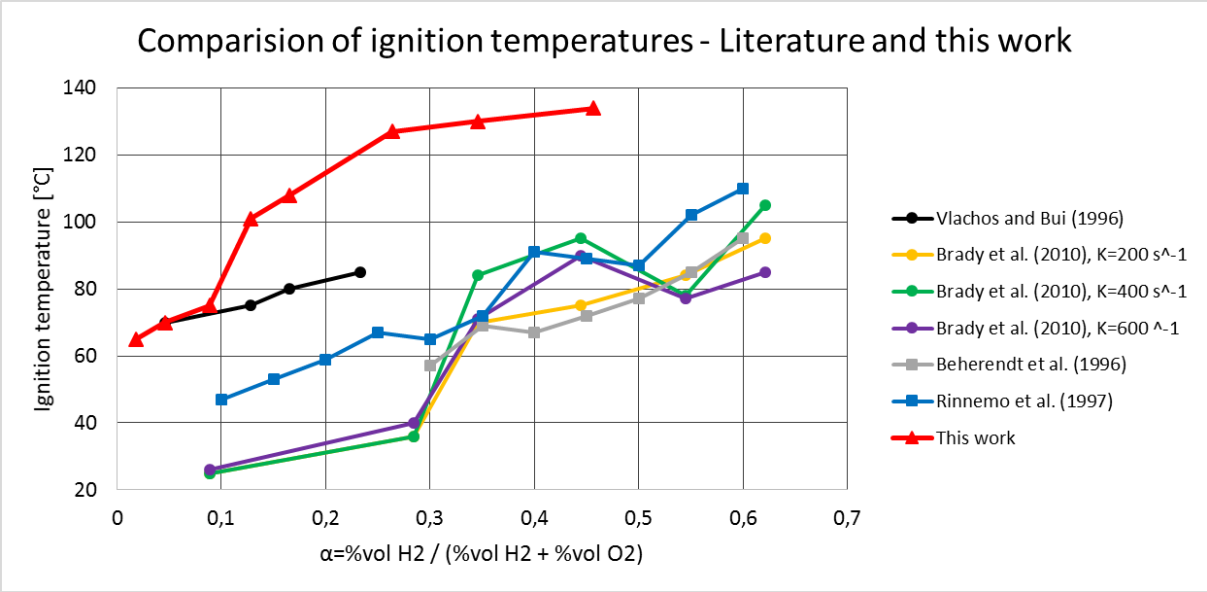

Figure 5. 10. *Comparison between the ignition temperatures observed in this work and the literature ones. An accord is found only for low hydrogen compositions (α<0.05) while, for other compositions, results are discordant.*

Since the reactor geometry (§2.5 and §3.2.1) and the *strain rate* of the experiments is very different from the literature values, differences in the results can be expected. In particular, high values of *strain rate* reduce the contact time of the reagents with the catalyst so the ignition may be inhibited. To confirm this hypothesis, a further investigation with a lower inlet flow rate (and consequently a lower *strain rate*) is needed.

The maximum conversion (X) is very similar for all hydrogen compositions ($85\% < X < 88\%$) (Figure 5.11).

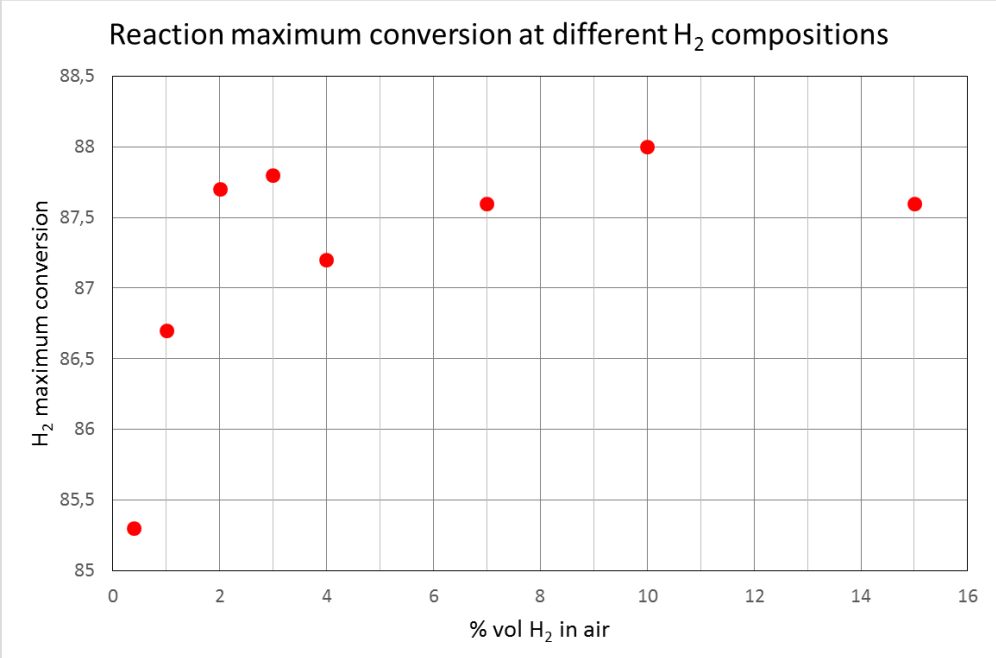

Figure 5. 11. *Experimental maximum conversion at different inlet hydrogen compositions. Observed values slightly differ.*

The maximum conversion for all compositions is always 87% < X < 88%, beside the case of hydrogen < 1% that have a lower maximum conversion (Figure 5.9). Once again, the weakness of the reaction might be a factor in temperature distribution, for the lowers H2 concentrations.
Since consistency of experimental data was problematic in the first research topic (§ 5.1.4), the experiments were reproduced to ensure their consistency. We believe that experimental reproducibility is a major issue, and it is questionable also in literature works; several papers (Brady et al., 2010; Vlachos and Bui, 1996; etc…) do not report any detail about reproducibility; so are afraid that it was overlooked.
In this topic, the operating under excess of oxygen in the inlet composition always ensure a good consistency. Indeed, the ignition temperature may vary but its variation is always < 2 °C.

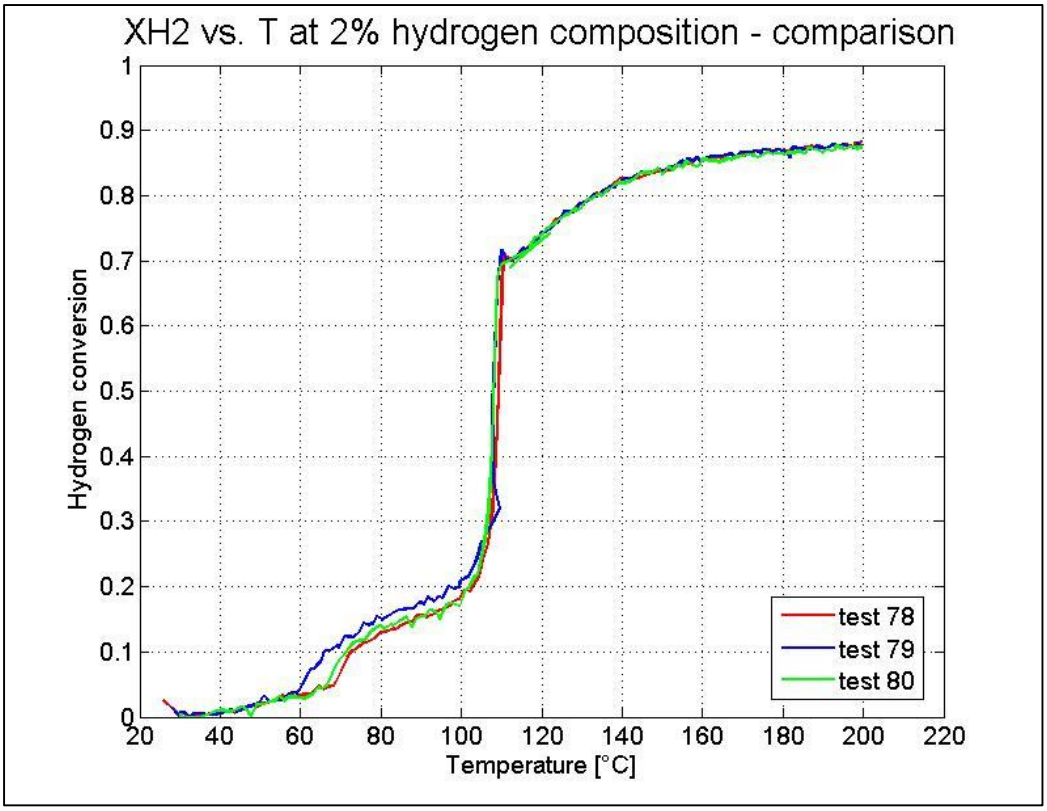

Figure 5. 12. *Three replications of test at 2% inlet hydrogen composition in air. Total inlet flow rate = 200 mL/min. Heating rate = 0.2 °/min.*

Figure 5.10 shows very consistent tests for the 2% hydrogen composition and it proves the very good reproducibility of our results, even at low H_2 concentration.

5.4 The surface reaction heat

The results of the third research topic suggest the idea that there may be a difference between the temperature of the upper catalyst surface (reactive surface) and the temperature of the lower surface (measured temperature).

The aim of the forth research topic is an attempt to experimentally evaluate the reaction heat on the reactive surface. However, the geometry of the FFC reactor does not allow that measurement so the FF reactor is used.

5.4.1 Experimental results

Since we would like to evaluate the reaction heat in the experiments of the third topic, the experimental conditions are kept constant apart from the effort of measuring the temperature and the reactor used.

The experimental features of this topic are:

- slow temperature ramp (0.2 °C/min) from 25 °C to 200 °C;
- total inlet flow rate= 200 mL/min;
- conversion and heat effects calculated with the *MS* and the *GC7820*;
- reactor used= FF reactor (thermocouple in contact with the reactive surface).

Two experiments were performed with this setup with a hydrogen inlet composition of 1 % and 5 % in air respectively.

Two experiments were performed with this setup with a hydrogen inlet composition of 1 % and 5 % in air respectively.

The first experiment is (1% H_2) includes only one temperature ramp, from ambient temperature until the ignition is reached and the conversion starts raising. The second experiment includes 2 temperature ramps; the reactor is cooled down right after the ignition and it is maintained at a lower temperature (90 °C) until the reaction is clearly stopped (about 2 hours). Then the temperature is raised again with the same heating rate to evaluate the reproducibility of the temperature of ignition.

The results of these experiments are shown in Figures 5.13 and 5.14.

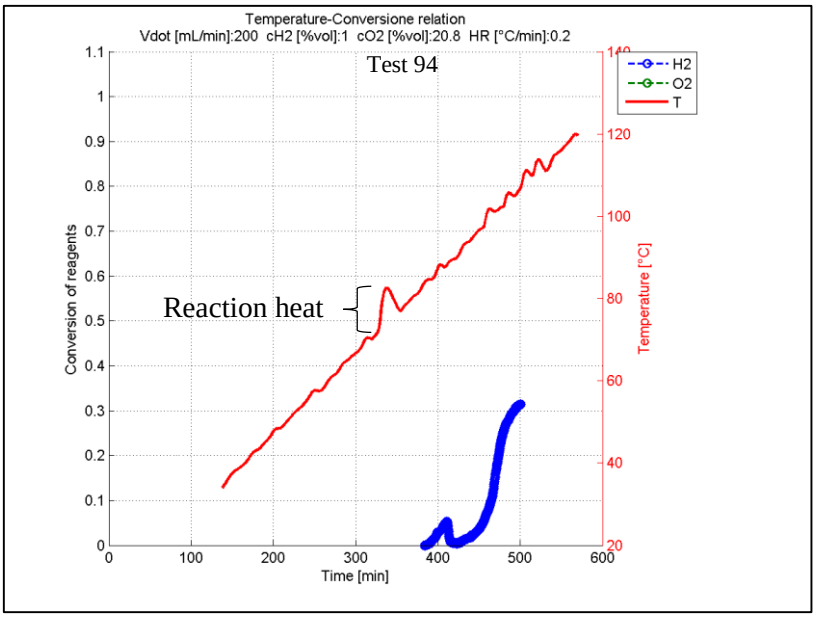

Figure 5. 13. *Experimental measurement of the reaction heat produced with ignition at 1% of inlet hydrogen composition. As expected, there is a thermal effect of about 15 °C right after the ignition.*

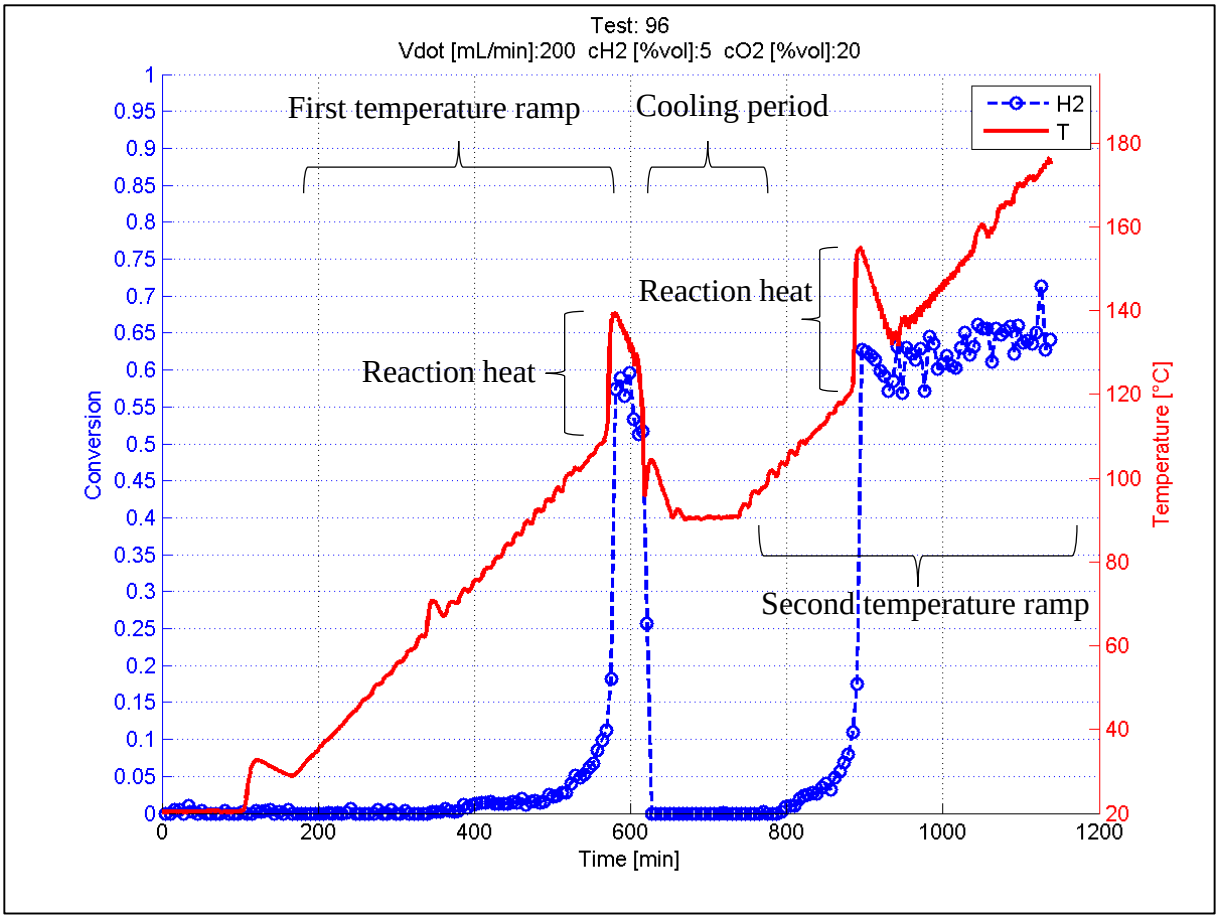

Figure 5. 14. *Experimental measurement of the reaction heat produced with ignition at 5% of inlet hydrogen composition. In the same experiment, the reaction heat was evaluated two times and the results show a thermal effect of 35 °C because of ignition.*

The result of Test 94 (1% of H_2) shows the onset of a rapid heating of the surface, overtaking the heating by the oven, at 70 °C of about +15 °C. That confirms the expectations: the onset of reaction causes a significant (see Figure 5.9 to appreciate the relevance) increase of surface temperature. That occurs even before appreciable conversion could be measured.
The effect at 5% of H_2 (Test 96) is more evident since the temperature increase reaches about 35 °C. The second ramp after the intermediate cooling proves a good reproducibility because both ignitions happen in a 10 °C range (110-120 °C) with a comparable magnitude (temperature increase of about 35 °C).

5.4.2 Discussion

The results of the previous research topic suggest that, for a 1% inlet hydrogen composition, there is a heating effect due to the ignition of about 20 °C. This effect should be reasonably proportional to hydrogen composition and it should not be measured by the thermocouple in the FFC reactor since there is not an increase in the measured temperature during the ignition.
This idea is confirmed by these results and, especially for higher hydrogen composition, there is an important temperature difference between the measured platinum surface and the reactive surface when the ignition happens. The way of measuring the temperature in the FFC reactor is still valid to evaluate the ignition temperature and the maximum conversion but there are thermal effects not observed that may influence the system behavior during the course of reaction. These effects explain why the conversion reaches its maximum value right after the ignition for hydrogen compositions > 10% and why reaction seems to have a "2 step behavior" for hydrogen compositions < 1% (Figure 5.9). If we always would like to couple the conversion with the right and reactive temperature, a measurement of the upper surface of the catalyst is needed.
Comparing the ignition temperatures found in this research topic with those found in the third one, there is a very good agreement between the results (Figures 5.9, 5.13 and 5.14) even if a different reactor was used.
With the FFC reactor, the reaction conversion at temperatures >150 °C is always higher than 80%, while, with the FF reactor, the conversion is about 65% even in a 150 °C – 170 °C temperature range. This is a confirmation that flow patterns in different reactors affect significantly the performances and that, with the FF reactor geometry, the reagents can bypass the catalyst laterally and subtract to the effect of catalyst as they would do in the more appropriately designed FFC reactor.

Conclusions

The first aim of this Thesis is the evaluation of the catalyst activity variations due to surface treatments. Thermal treatments as well as reductive and oxidative treatments were performed expecting, according to literature papers, a structural change of the catalyst surface. Unfortunately, this effect is significant only for treatments at higher temperature and for longer times and it was not observed in the current study. However, an increase of conversion is still noticeable. During thermal and reductive treatments, the reaction conversion was increased because of a surface cleaning process due to the high temperature reached. A greater increase of conversion was achieved through oxidation treatments because of both the surface cleaning and the favored adsorption of oxygen. Since its adsorption has an activation energy higher than the hydrogen energy, a high temperature oxidation treatment promotes significantly the reaction.

In all experiments of this research topic, conversion has a decreasing behavior during the course of reaction because, after a first situation where all active sites are available, there is a site competition between the compounds involved in the reaction.

The first conclusion of this topic is that the activity of the catalyst is strongly influenced by its history. Because of this behavior, there may be a lack of experimental reproducibility. To always ensure a good reproducibility in following research topics, the reagent composition changed from a stoichiometric one to an atmosphere with a large excess of oxygen.

The importance of mass transfer phenomena is elucidated during the second topic and the main attention is focused on the influence of the *gap* and the inlet flow rate. Conversion reaches its maximum value for the lowest *gap* and for flow rates < 100 mL/min. It decreases mainly because of a *gap* increase (about 10%) but also because of a flow rate increase (about 2-4%). The performed CFD simulation show the same decreasing behavior and it also gives an inner view of all the involved mass transfer phenomena. In particular, it shows that, at low flow rates, hydrogen does not reacts completely because it is not forced towards the catalyst and it can flow above the surface without reaching it. When the flow rate is increased, hydrogen is forced towards the surface but the contact time between the reagents and the catalyst is reduced. The final effect of these phenomena is a conversion decrease. With a higher *gap*, the bypass phenomenon is more important so the conversion is reasonably lower.

The CFD simulation deals with the mass transfer phenomena involved to transport hydrogen until the catalyst. At low flow rates, diffusion has a significant importance from the reagents nozzle until the catalyst surface while convection has a scarce influence especially in the 0.5 mm right above the catalyst. At high flow rates, the situation is different because hydrogen is transported only by convection until 0.5 mm from the catalyst surface. Then, the fluid velocity

decreases swiftly and mass transfer is mainly due to diffusion that is more effective than in the low flow rate case because the concentration gradient is higher. A refinement of the model describing the reaction is implemented in the final part of the CFD simulation. This improvement leads to a different behavior of the calculated conversion data that become more in accord with the measured ones.

Since the ignition temperature is one of the most studied kinetic features, it is evaluated in the current work to compare it with the literature. The results show a general increase of the ignition temperature with the hydrogen concentration that confirms the literature results. This is because hydrogen adsorption has a low activation energy so, when its concentration is increased, the catalyst surface tends to be wholly occupied by hydrogen. So a higher temperature is needed to desorb hydrogen and favor the oxygen adsorption. However, even if the temperature trend is confirm, the observed ignition temperature is significantly higher than all temperatures found in literature. This is because the reactor configuration used in this work is different from all others, so this is another confirmation that the mass transfer and the reactor geometry has a great importance in the evaluation of all kinetic features. The results of this experimental topic suggest the idea that the ignition of the reaction produces a large amount of heat that is not correctly measured. In the last topic of this Thesis, the temperature of the reactive surface is monitored during the ignition and the results confirm the previous suggestion. Indeed, the ignition produces an important increase of temperature (proportional to the hydrogen concentration) that was not measured in the previous research topic.

The future developments of this Thesis regards both the experimental part and the simulation one. To monitor properly the temperature of the reactive surface, a different reactor configuration is needed. The geometry features (*gap*, diameter of reagents nozzle, etc…) should remain the same but a pyrometer should be included inside the reactor to measure the catalytic temperature.

The CFD simulation needs to be further refined in the description of the reaction, so a detailed reaction mechanism should be implemented in the COMSOL software using MATLAB and CANTERA. In this way, it would be possible to achieve a better accordance between the experiments and the simulation data in term of conversion.

Another future improvement that regards the kinetic mechanism is the development of a reaction mechanism that does not take into account the effect of mass transfer phenomena. We expect that the produced mechanism should have a general validity while all Literature mechanisms are valid only in the system where they are developed.

Appendix 1

analisi_gc7820.m

```
function analisi_gc7820_v3
% programma per analizzare misure da uGC
% associandogli T estratte da file di 8Tin2Vout
% versione che legge tutto uGC e poi le T

clear all
clc
close all

% ============= dati richiesti
nump = 97; % numero della prova da elaborare
% irif = 4; % file di riferimento
NT = 5;     % numero della TC da rilevare
negl = [0 0]; % definisce quale specie non va considerata nel calcolodi X:
0-->considera -10-->trascura
cut = 1; % limite superiore dei valori di X accettabili: elimina valori di
X da errori numerici
% ============= directory dei dati
% Nicola
% dir = 'C:\Users\utente\Dropbox\CreLab(3)\H2_pt\';
% Francesco
dir = 'W:\Users\Francesco\Dropbox\CreLab\Singoli Progetti\H2_pt\';
% Lab
% dir = 'C:\Documents and Settings\canu_lab\My
Documents\Dropbox\CreLab\H2_pt\';
% ============= fine dati richiesti

% ============= lettura dati
% info da Diario
excel='DiarioD.xlsx';
V=xlsread([dir excel],'Diario',strcat('Y',num2str(nump)));
cCmb=xlsread([dir excel],'Diario',strcat('AF',num2str(nump)))*100;
cO2=xlsread([dir excel],'Diario',strcat('AD',num2str(nump)))*100;
HR=xlsread([dir excel],'Diario',strcat('T',num2str(nump)));

f1 = strcat('prova',num2str(nump),'.Area');        % l'originale mancava di
misure di Area su alcune prove
f2 = strcat('TinTout',num2str(nump),'.dat');        % l'originale mancava
di misure di Area su alcune prove
f3 = strcat(['rif' num2str(nump)],'.Area');

% read GC file.Area
% estrae le info generali
fid1 = fopen([dir 'dati_gc7820\data\' f1]);
tline = fgetl(fid1);    % 1st line
tline = fgetl(fid1);    % 2nd line
dum=strread(tline,'%s','delimiter','\t');
Title=dum(2);
Nrec = str2num(cell2mat(dum(3)));    % N of uGC data
```

```
tline = fgetl(fid1);    % 3rd line (columns headings)
dum=strread(tline,'%s','delimiter','\t');
Ncol = length(dum);
Nc = Ncol-10;        % Numero di specie;assume che le prime 9 colonne siano
sempre tali e le specie siano dalla 10a in avanti
Nomi = dum(11:end);

% ciclo su tutte le analisi
for i = 1:Nrec
    tline = fgetl(fid1);    % first data row
    dum=strread(tline,'%s','delimiter','\t');
    d=strread(char(dum(1)),'%d','delimiter','/');       % date d/m/y
    h=strread(char(dum(2)),'%s','delimiter',' ');       % time h/m/s
    t=strread(char(h(1)),'%d','delimiter',':');

    if length(h)>1
        if strcmp(h(2),'PM') && t(1)~=12
            t(1) = t(1)+12;
        end
        if strcmp(h(2),'AM') && t(1)==12
            t(1) = 0;
        end
    end

    tGC(i) =datenum([d(3),d(1),d(2),t']);               % time as serial
number
    tGC(i) = tGC(i)+(60/1440);                          % correzione
dell'ora: openlab sincronizza con un'ora in anticipo. in termini seriali 2h
= 120/1440

    %     disp(sprintf(' %04.0f analysis time: %s
',i,datestr(tGC(i),'dd/mm/yyyy HH:MM:SS')));
    for j=1:Nc, Areas(i,j) = str2num(cell2mat(dum(10+j)));end
end

tGCm = min(tGC);
tGCM = max(tGC);
% plot(tGC-tGC(1))   % per verifica del vetore tempo tGC

% ricerca delle T corrispondenti
fid2 = fopen([dir 'dati_gc7820\data\' f2]);
ant = 0.1; % ant*1440 = minuti prima dell'acquisizione del primo segnale
uGC
post = 0.1; %post*1440 = minuti dopo l'ultima acquisizione del uGC
i=0;
while 1
    tline = fgetl(fid2);
    dum = strread(tline,'%s','delimiter','\t');
    d   = strread(char(dum(1)),'%d','delimiter','/');       % date d/m/y
    t   = strread(char(dum(2)),'%d','delimiter','.');       % time h/m/s
    t   = datenum([d(3),d(2),d(1),t',0]);                    % time as
serial number

    if t>tGCm-ant    % da circa 10 min prima del primno tempo di analisi
        i = i + 1;
        tT(i)= t;
        T(i) = str2num(cell2mat(dum(4+NT)));    % T dell NT-esima TC più
prossima all'analisi i-esima
        if t>tGCM+post     % fino a circa 10 min dopo l'ultimo tempo di
analisi
```

```
          break
        end
    end
end

% interpolazione dati per determinare l'accoppiamento (TGC,Areas)
[tGC,ix] = sort(tGC);         % riordina le analisi GC, nel caso non
fossero tutte successive
Areas = Areas(ix,:);          % riordina le aree secondo la nuova
indicizzazione
tGC = (tGC-tT(1))*1440;       % t dall'inizio prova, in minuti
tT = (tT-tT(1))*1440;         % tempo in minuti
TGC = interp1(tT,T,tGC);      % interpolazione delle T


% acquisizione del riferimento da database
fid3 = fopen([dir 'dati_gc7820\data\' f3]);
tline = fgetl(fid3);    % 1st line
tline = fgetl(fid3);    % 2nd line
dum=strread(tline,'%s','delimiter','\t');
Nrec = str2num(cell2mat(dum(3)));    % N of uGC data
tline = fgetl(fid3);    % 3rd line (columns headings)
dum=strread(tline,'%s','delimiter','\t');
Ncol = length(dum);  % numero di colonne dati
Nc = Ncol-10;        % numero di specie

% ciclo su tutte le analisi
for i = 1:Nrec
    tline = fgetl(fid3);     % first data row
    dum=strread(tline,'%s','delimiter','\t');
    for j=1:Nc, Areas_rif(i,j) = str2num(cell2mat(dum(10+j)));end
end

% segnale di riferimento della composizione in ingresso:
% rif = mean(Areas_rif); % valore medio come riferimento
rif = median(Areas_rif); % mediana come riferimento

% ============== graphics
figure(1)
[h_axes, A_lines, T_lines] = plotyy(tGC,Areas,tT,T);
legend([Nomi;'T']);

set(gca,'Box','off');
set(get(h_axes(1),'XLabel'),'String','Time [min]');
set(get(h_axes(1),'YLabel'),'String','Areas');
set(get(h_axes(2),'YLabel'),'String','Temperature [°C]');
set(h_axes(1),'YTick',0:0.1:1.1);
% set(h_axes(1),'Ylim',[0 1.1]);
set(h_axes(2),'YTick',20:20:max(T)+20);
set(h_axes(2),'Ylim',[20 max(T)+20]);
set(A_lines,'linestyle','--','linewidth',1.5,'marker','o');
set(T_lines,'linestyle','-','linewidth',2);
title(['Test: ',num2str(nump); strcat('Vdot [mL/min]:',num2str(V),strcat('
c',Nomi(1)),' [%vol]:',num2str(cCmb),strcat('  c',Nomi(2)),'
[%vol]:',num2str(cO2),'  HR [°C/min]:',num2str(HR))])
grid on

X = zeros(length(Areas),Nc);
for ins = 1:Nc
    X(:,ins) = 1-Areas(:,ins)/rif(ins);
```

```
    Xmedio= mean(X);
    X(find(X(:,ins)<0),ins)=0;
    X(:,ins) = X(:,ins)+negl(ins);
    X(find(X>cut))=0;

    figure(1+ins)
    title(['Test: ',num2str(nump); strcat('Vdot
[mL/min]:',num2str(V),strcat('  c',Nomi(1)),'
[%vol]:',num2str(cCmb),strcat('  c',Nomi(2)),' [%vol]:',num2str(cO2),'  HR
[°C/min]:',num2str(HR))])
    cm1 = colormap(jet);

    if length(X)>20
        numcolor = length(X)/10;
        style = '-';
    else
        numcolor = length(X);
        style = 'o';
    end

    for kcolor = 1:numcolor
            perc_avanz = kcolor/numcolor;
            icol = ceil(perc_avanz*(length(cm1)-1))+1;
            lA=TGC(length(TGC)/numcolor*(kcolor-
1)+1:length(TGC)/numcolor*kcolor);
            lB=X(length(TGC)/numcolor*(kcolor-
1)+1:length(TGC)/numcolor*kcolor,ins);

plot(lA,lB,'linestyle',style,'Color',cm1(icol,:),'LineWidth',1.5), hold on
    end

    xlabel('Temperature profile [°C]')
    ylabel('Reagent Conversion')
    axis([20 max(TGC)+20 0 1])
    fmt='%4.2f h';
    colorbar('YTick',[1 icol/2 icol]...
    ,'YTickLabel',{sprintf(fmt,0),sprintf(fmt,(tGC(end)-
tGC(1))/120),sprintf(fmt,(tGC(end)-tGC(1))/60)})
    grid on
end

cols = 'bgy';
for ins = 1:Nc
    figure(ins+3)
    [h_axes, A_lines, T_lines] = plotyy(tGC,X(:,ins),tT,T);
    legend([Nomi(ins);'T']);

    set(gca,'Box','off');
    set(get(h_axes(1),'XLabel'),'String','Time [min]');
    set(get(h_axes(1),'YLabel'),'String','Conversion');
    set(get(h_axes(2),'YLabel'),'String','Temperature [°C]');
    set(h_axes(1),'YTick',0:0.05:1.1);
    set(h_axes(1),'Ylim',[0 1]);
    set(h_axes(2),'YTick',20:20:max(T)+20);
    set(h_axes(2),'Ylim',[20 max(T)+20],'YColor','r');
    set(A_lines,'linestyle','--
','linewidth',1.5,'marker','o','Color',cols(ins));
    set(T_lines,'linestyle','-','linewidth',2,'Color','r');
    % title(['Test: ',num2str(nump); strcat('Vdot
[mL/min]:',num2str(V),strcat('  c',Nomi(1)),'
```

```
[%vol]:',num2str(cCmb),strcat('  c',Nomi(2)),' [%vol]:',num2str(cO2),'  HR
[°C/min]:',num2str(HR))])
    title(['Test: ',num2str(nump); strcat('Vdot
[mL/min]:',num2str(V),strcat('  c',Nomi(1)),'
[%vol]:',num2str(cCmb),strcat('  c',Nomi(2)),' [%vol]:',num2str(cO2))])
    grid on
end

figure(ins*2+2)
[h_axes, A_lines, T_lines] = plotyy(tGC,X,tT,T);
legend([Nomi;'T']);

set(gca,'Box','off');
set(get(h_axes(1),'XLabel'),'String','Time [min]');
set(get(h_axes(1),'YLabel'),'String','Conversion');
set(get(h_axes(2),'YLabel'),'String','Temperature [°C]');
set(h_axes(1),'YTick',0:0.1:1.1);
set(h_axes(1),'Ylim',[0 1.05]);
set(h_axes(2),'YTick',20:20:max(T)+20);
set(h_axes(2),'Ylim',[20 max(T)+20]);
set(A_lines,'linestyle','--','linewidth',1.5,'marker','o');
set(T_lines,'linestyle','-','linewidth',2,'Color','r');
% title(['Test: ',num2str(nump); strcat('Vdot
[mL/min]:',num2str(V),strcat('  c',Nomi(1)),'
[%vol]:',num2str(cCmb),strcat('  c',Nomi(2)),' [%vol]:',num2str(cO2),'  HR
[°C/min]:',num2str(HR))])
title(['Test: ',num2str(nump); strcat('Vdot [mL/min]:',num2str(V),strcat('
c',Nomi(1)),' [%vol]:',num2str(cCmb),strcat('  c',Nomi(2)),'
[%vol]:',num2str(cO2))])
grid on

figure(ins*2+3)
cvol = (1-X).*repmat([cCmb cO2],length(X),1);
cvol(find(cvol(:,1)>cCmb),1)=0;
cvol(find(cvol(:,2)>cO2),2)=0;
[h_axes, A_lines, T_lines] = plotyy(tGC,cvol,tT,T);
legend([Nomi;'T']);

set(gca,'Box','off');
set(get(h_axes(1),'XLabel'),'String','Time [min]');
set(get(h_axes(1),'YLabel'),'String','Concentration [%vol]');
set(get(h_axes(2),'YLabel'),'String','Temperature [°C]');
set(h_axes(1),'YTick',0:0.5:max(max(cvol))+.1);
set(h_axes(1),'Ylim',[0 max(max(cvol))+.1]);
set(h_axes(2),'YTick',20:20:max(T)+20);
set(h_axes(2),'Ylim',[20 max(T)+20]);
set(A_lines,'linestyle','--','linewidth',1.5,'marker','o');
set(T_lines,'linestyle','-','linewidth',2);
title(['Test: ',num2str(nump); strcat('Vdot [mL/min]:',num2str(V),strcat('
c',Nomi(1)),' [%vol]:',num2str(cCmb),strcat('  c',Nomi(2)),'
[%vol]:',num2str(cO2),'  HR [°C/min]:',num2str(HR))])
grid on

%inizio subplot finale=========================================
figure(ins*2+4)
subplot(2,3,1)
title(['Test: ',num2str(nump); strcat('Vdot [mL/min]:',num2str(V),strcat('
c',Nomi(1)),' [%vol]:',num2str(cCmb),strcat('  c',Nomi(2)),'
[%vol]:',num2str(cO2),'  HR [°C/min]:',num2str(HR))])
    cm1 = colormap(jet);
```

```
    if length(X)>20
        numcolor = length(X)/10;
        style = '-';
    else
        numcolor = length(X);
        style = 'o';
    end

    for kcolor = 1:numcolor
            perc_avanz = kcolor/numcolor;
            icol = ceil(perc_avanz*(length(cm1)-1))+1;
            lA=TGC(length(TGC)/numcolor*(kcolor-
1)+1:length(TGC)/numcolor*kcolor);
            lB=X(length(TGC)/numcolor*(kcolor-
1)+1:length(TGC)/numcolor*kcolor,1);

plot(lA,lB,'linestyle',style,'Color',cm1(icol,:),'LineWidth',1.5), hold on
    end

    xlabel('Temperature profile [°C]')
    ylabel('H2 Conversion')
    axis([0 max(TGC)+20 0 1])
    fmt='%4.2f h';
    colorbar('YTick',[1 icol/2 icol]...
    ,'YTickLabel',{sprintf(fmt,0),sprintf(fmt,(tGC(end)-
tGC(1))/120),sprintf(fmt,(tGC(end)-tGC(1))/60)})
    grid on
%seconda figura==========
subplot(2,3,2)
title(['Test: ',num2str(nump); strcat('Vdot [mL/min]:',num2str(V),strcat('
c',Nomi(1)),' [%vol]:',num2str(cCmb),strcat('  c',Nomi(2)),'
[%vol]:',num2str(cO2),'  HR [°C/min]:',num2str(HR))])
    cm1 = colormap(jet);

    if length(X)>20
        numcolor = length(X)/10;
        style = '-';
    else
        numcolor = length(X);
        style = 'o';
    end

    for kcolor = 1:numcolor
            perc_avanz = kcolor/numcolor;
            icol = ceil(perc_avanz*(length(cm1)-1))+1;
            lA=TGC(length(TGC)/numcolor*(kcolor-
1)+1:length(TGC)/numcolor*kcolor);
            lB=X(length(TGC)/numcolor*(kcolor-
1)+1:length(TGC)/numcolor*kcolor,2);

plot(lA,lB,'linestyle',style,'Color',cm1(icol,:),'LineWidth',1.5), hold on
    end

    xlabel('Temperature profile [°C]')
    ylabel('O2 Conversion')
    axis([0 max(TGC)+20 0 1])
    fmt='%4.2f h';
    colorbar('YTick',[1 icol/2 icol]...
```

```
    ,'YTickLabel',{sprintf(fmt,0),sprintf(fmt,(tGC(end)-
tGC(1))/120),sprintf(fmt,(tGC(end)-tGC(1))/60)})
    grid on
%terza figura====================
subplot(2,3,3)
[h_axes, A_lines, T_lines] = plotyy(tGC,X,tT,T);
legend([Nomi;'T']);

set(gca,'Box','off');
set(get(h_axes(1),'XLabel'),'String','Time [min]');
set(get(h_axes(1),'YLabel'),'String','Conversion');
set(get(h_axes(2),'YLabel'),'String','Temperature [°C]');
set(h_axes(1),'YTick',0:0.1:1.1);
set(h_axes(1),'Ylim',[0 1.05]);
set(h_axes(2),'YTick',20:20:max(T)+20);
set(h_axes(2),'Ylim',[20 max(T)+20]);
set(A_lines,'linestyle','--','linewidth',1.5,'marker','o');
set(T_lines,'linestyle','-','linewidth',2,'Color','r');
% title(['Test: ',num2str(nump); strcat('Vdot
[mL/min]:',num2str(V),strcat('  c',Nomi(1)),'
[%vol]:',num2str(cCmb),strcat('  c',Nomi(2)),' [%vol]:',num2str(cO2),'  HR
[°C/min]:',num2str(HR))])
title(['Test: ',num2str(nump); strcat('Vdot [mL/min]:',num2str(V),strcat('
c',Nomi(1)),' [%vol]:',num2str(cCmb),strcat('  c',Nomi(2)),'
[%vol]:',num2str(cO2))])
grid on
%quarta figura====================
subplot(2,3,4)
[h_axes, A_lines, T_lines] = plotyy(tGC,X(:,1),tT,T);
    legend([Nomi(1);'T']);

    set(gca,'Box','off');
    set(get(h_axes(1),'XLabel'),'String','Time [min]');
    set(get(h_axes(1),'YLabel'),'String','Conversion');
    set(get(h_axes(2),'YLabel'),'String','Temperature [°C]');
    set(h_axes(1),'YTick',0:0.05:1.1);
    set(h_axes(1),'Ylim',[0 1]);
    set(h_axes(2),'YTick',20:20:max(T)+20);
    set(h_axes(2),'Ylim',[20 max(T)+20],'YColor','r');
    set(A_lines,'linestyle','--
','linewidth',1.5,'marker','o','Color',cols(1));
    set(T_lines,'linestyle','-','linewidth',2,'Color','r');
    % title(['Test: ',num2str(nump); strcat('Vdot
[mL/min]:',num2str(V),strcat('  c',Nomi(1)),'
[%vol]:',num2str(cCmb),strcat('  c',Nomi(2)),' [%vol]:',num2str(cO2),'  HR
[°C/min]:',num2str(HR))])
    title(['Test: ',num2str(nump); strcat('Vdot
[mL/min]:',num2str(V),strcat('  c',Nomi(1)),'
[%vol]:',num2str(cCmb),strcat('  c',Nomi(2)),' [%vol]:',num2str(cO2))])
    grid on
%quinta figura=============
subplot(2,3,5)
[h_axes, A_lines, T_lines] = plotyy(tGC,X(:,2),tT,T);
    legend([Nomi(2);'T']);

    set(gca,'Box','off');
    set(get(h_axes(1),'XLabel'),'String','Time [min]');
    set(get(h_axes(1),'YLabel'),'String','Conversion');
    set(get(h_axes(2),'YLabel'),'String','Temperature [°C]');
    set(h_axes(1),'YTick',0:0.05:1.1);
```

```
    set(h_axes(1),'Ylim',[0 1]);
    set(h_axes(2),'YTick',20:20:max(T)+20);
    set(h_axes(2),'Ylim',[20 max(T)+20],'YColor','r');
    set(A_lines,'linestyle','--
','linewidth',1.5,'marker','o','Color',cols(2));
    set(T_lines,'linestyle','-','linewidth',2,'Color','r');
    % title(['Test: ',num2str(nump); strcat('Vdot
[mL/min]:',num2str(V),strcat('  c',Nomi(1)),'
[%vol]:',num2str(cCmb),strcat('  c',Nomi(2)),' [%vol]:',num2str(cO2),'  HR
[°C/min]:',num2str(HR))])
    title(['Test: ',num2str(nump); strcat('Vdot
[mL/min]:',num2str(V),strcat('  c',Nomi(1)),'
[%vol]:',num2str(cCmb),strcat('  c',Nomi(2)),' [%vol]:',num2str(cO2))])
    grid on
% sesta figura============
subplot(2,3,6)
cvol = (1-X).*repmat([cCmb cO2],length(X),1);
cvol(find(cvol(:,1)>cCmb),1)=0;
cvol(find(cvol(:,2)>cO2),2)=0;
[h_axes, A_lines, T_lines] = plotyy(tGC,cvol,tT,T);
legend([Nomi;'T']);

set(gca,'Box','off');
set(get(h_axes(1),'XLabel'),'String','Time [min]');
set(get(h_axes(1),'YLabel'),'String','Concentration [%vol]');
set(get(h_axes(2),'YLabel'),'String','Temperature [°C]');
set(h_axes(1),'YTick',0:0.5:max(max(cvol))+.1);
set(h_axes(1),'Ylim',[0 max(max(cvol))+.1]);
set(h_axes(2),'YTick',20:20:max(T)+20);
set(h_axes(2),'Ylim',[20 max(T)+20]);
set(A_lines,'linestyle','--','linewidth',1.5,'marker','o');
set(T_lines,'linestyle','-','linewidth',2);
title(['Test: ',num2str(nump); strcat('Vdot [mL/min]:',num2str(V),strcat('
c',Nomi(1)),' [%vol]:',num2str(cCmb),strcat('  c',Nomi(2)),'
[%vol]:',num2str(cO2),'  HR [°C/min]:',num2str(HR))])
grid on
% fine subplot finale=============
% save dei grafici
for i = 1:2*ins+4
    figure(i)
    print('-dpng','-noui',['.\fig\prova' num2str(nump) '_' num2str(i)] )
end


% salva i dati in una matrice uGC(nump)
save(strcat('prova',num2str(nump)))
```

This script does not take into account the molar contraction that happens during the reaction and, since the *GC* always analyzes the same volume, the conversion may be underestimated. However, using the calculated rough conversion, it is possible to estimate the molar contraction so the conversion may be adjusted to its real value. Even if this script does not take to account this effect, it is very easy to consider it manually and, in any case, the error on maximum conversion never exceeds 1%. The maximum conversion plot (Figure 5.11) is already adjusted taking into account the mentioned issue.

Appendix 2

analisi_ugc.m

```
function analisi_ugc_v4
% programma per analizzare misure da uGC
% associandogli T estratte da file di 8Tin2Vout
% versione che legge tutto uGC e poi le T

clear all
clc
close all


% ============= dati richiesti
nump = 43; % numero della prova da elaborare
NT = 3;     % numero della TC da rilevare
rif = [240 242;240 242]; % numero delle acquisizione su cui mediare il
valore di riferimento
negl = [0 -10]; % definisce quale specie non va considerata nel calcolodi
X: 0-->considera -10-->trascura
cut = 0.7; % limite superiore dei valori di X accettabili: elimina valori
di X da errori numerici
% ============= directory dei dati
% Nicola
% dir='C:\Users\utente\Dropbox\CreLab(3)\H2_pt\';
% Francesco
dir='W:\Users\Francesco\Dropbox\CreLab\Singoli Progetti\H2_pt\';
% ============= fine dati richiesti

% ============= lettura dati
% info da Diario
excel='DiarioD.xlsx';
V=xlsread([dir excel],'Diario',strcat('Y',num2str(nump)));
cCmb=xlsread([dir excel],'Diario',strcat('AF',num2str(nump)))*100;
cO2=xlsread([dir excel],'Diario',strcat('AD',num2str(nump)))*100;
HR=xlsread([dir excel],'Diario',strcat('T',num2str(nump)));

f1 = strcat('prova',num2str(nump),'.Area');        % l'originale mancava di
misure di Area su alcune prove
f2 = strcat('TinTout',num2str(nump),'.dat');        % l'originale mancava
di misure di Area su alcune prove

% read uGC file.Area
% estrae le info generali
fid1 = fopen([dir 'dati_ugc\processing\' f1]);
tline = fgetl(fid1);    % 1st line
tline = fgetl(fid1);    % 2nd line
dum=strread(tline,'%s','delimiter','\t');
Title=dum(2);
Nrec = str2num(cell2mat(dum(3)));    % N of uGC data
tline = fgetl(fid1);    % 3rd line (columns headings)
dum=strread(tline,'%s','delimiter','\t');
```

```
Ncol = length(dum);
Nc = Ncol-9;        % Numero di specie;assume che le prime 9 colonne siano
sempre tali e le specie siano dalla 10a in avanti
Nomi = dum(10:end);

% ciclo su tutte le analisi
for i = 1:Nrec
    tline = fgetl(fid1);     % first data row
    dum=strread(tline,'%s','delimiter','\t');
    d=strread(char(dum(1)),'%d','delimiter','/');       % date d/m/y
    t=strread(char(dum(2)),'%d','delimiter','.');       % time h/m/s
    tGC(i) =datenum([d(3),d(2),d(1),t']);               % time as serial
number
%     disp(sprintf(' %04.0f analysis time: %s
',i,datestr(tGC(i),'dd/mm/yyyy HH:MM:SS')));
    for j=1:Nc, Areas(i,j) = str2num(cell2mat(dum(9+j)));end
end

tGCm = min(tGC);
tGCM = max(tGC);

% ricerca delle T corrispondenti
fid2 = fopen([dir 'dati_ugc\processing\' f2]);
ant = 0.07; % ant*1440 = minuti prima dell'acquisizione del primo segnale
uGC
post = 0; %post*1440 = minuti dopo l'ultima acquisizione del uGC
i=0;
while 1
    tline = fgetl(fid2);
    dum = strread(tline,'%s','delimiter','\t');
    d   = strread(char(dum(1)),'%d','delimiter','/');       % date d/m/y
    t   = strread(char(dum(2)),'%d','delimiter','.');       % time h/m/s
    t   = datenum([d(3),d(2),d(1),t',0]);                    % time as
serial number

    if t>tGCm-ant    % da circa 10 min prima del primno tempo di analisi
        i = i + 1;
        tT(i)= t;
        T(i) = str2num(cell2mat(dum(4+NT)));    % T dell NT-esima TC più
prossima all'analisi i-esima
%         disp(sprintf('             T time: %s T=%4.1f
°C',datestr(t0T,'dd/mm/yyyy HH:MM:SS'),T(i)))
%     if length(T)==Nrec
%         break,break
%     end
        if t>tGCM+post     % fino a circa 10 min dopo l'ultimo tempo di
analisi
          break
        end
    end
end

% riordina le analisi GC, nel caso non fossero tutte successive
[tGC,ix] = sort(tGC);
Areas = Areas(ix,:);

tGC = (tGC-tT(1))*1440;       % t dall'inizio prova, in minuti
tT = (tT-tT(1))*1440;

% trova le T corrispondenti ai tempi delle analisi, per interpolazione
```

```
TGC = interp1(tT,T,tGC);

save(strcat('uGC',num2str(nump)))

% ============== graphics
figure(1)
[h_axes, A_lines, T_lines] = plotyy(tGC,Areas,tT,T);
legend([Nomi;'T']);

set(gca,'Box','off');
set(get(h_axes(1),'XLabel'),'String','Time [min]');
set(get(h_axes(1),'YLabel'),'String','Areas');
set(get(h_axes(2),'YLabel'),'String','Temperature [°C]');
set(h_axes(1),'YTick',0:0.1:1.1);
set(h_axes(1),'Ylim',[0 1.1]);
set(h_axes(2),'YTick',20:20:max(T)+20);
set(h_axes(2),'Ylim',[20 max(T)+20]);
set(A_lines,'linestyle','--','linewidth',1.5,'marker','o');
set(T_lines,'linestyle','-','linewidth',2);
title(['Test: ',num2str(nump); strcat('Vdot [mL/min]:',num2str(V),strcat('
c',Nomi(1)),' [%vol]:',num2str(cCmb),strcat('  c',Nomi(2)),'
[%vol]:',num2str(cO2),'  HR [°C/min]:',num2str(HR))])
grid on

X = zeros(length(Areas),Nc);
for ins = 1:Nc
    X(:,ins) = (1-Areas(:,ins)/mean(Areas(rif(ins,1):rif(ins,2),ins)));
    X(find(X(:,ins)<0),ins)=0;
    X(:,ins) = X(:,ins)+negl(ins);
    X(find(X>cut))=0;

    figure(1+ins)
    title(['Test: ',num2str(nump); strcat('Vdot
[mL/min]:',num2str(V),strcat('  c',Nomi(1)),'
[%vol]:',num2str(cCmb),strcat('  c',Nomi(2)),' [%vol]:',num2str(cO2),'  HR
[°C/min]:',num2str(HR))])
    numcolor = 15;
    cm1 = colormap(jet);
    for kcolor=1:numcolor
        lA=TGC(length(TGC)/numcolor*(kcolor-
1)+1:length(TGC)/numcolor*kcolor);
        lB=X(length(TGC)/numcolor*(kcolor-
1)+1:length(TGC)/numcolor*kcolor,ins);
        line(lA,lB,'Color',cm1(kcolor,:),'LineWidth',4), hold on
    end
    xlabel('Temperature profile [°C]')
    ylabel('Reagent Conversion')
    axis([0 max(TGC)+20 0 1])
    fmt='%4.0f h';
    colorbar('YTick',[1 numcolor/2 numcolor]...
    ,'YTickLabel',{sprintf(fmt,0),sprintf(fmt,(tGC(end)-
tGC(1))/120),sprintf(fmt,(tGC(end)-tGC(1))/60)})
    grid on
end

cols = 'bgy';
for ins = 1:Nc
    figure(ins+3)
    [h_axes, A_lines, T_lines] = plotyy(tGC,X(:,ins),tT,T);
```

```
    legend([Nomi(ins);'T']);

    set(gca,'Box','off');
    set(get(h_axes(1),'XLabel'),'String','Time [min]');
    set(get(h_axes(1),'YLabel'),'String','Conversion');
    set(get(h_axes(2),'YLabel'),'String','Temperature [°C]');
    set(h_axes(1),'YTick',0:0.1:1.1);
    set(h_axes(1),'Ylim',[0 1]);
    set(h_axes(2),'YTick',20:20:max(T)+20);
    set(h_axes(2),'Ylim',[20 max(T)+20],'YColor','r');
    set(A_lines,'linestyle','--
','linewidth',1.5,'marker','o','Color',cols(ins));
    set(T_lines,'linestyle','-','linewidth',2,'Color','r');
    % title(['Test: ',num2str(nump); strcat('Vdot
[mL/min]:',num2str(V),strcat('  c',Nomi(1)),'
[%vol]:',num2str(cCmb),strcat('  c',Nomi(2)),' [%vol]:',num2str(cO2),'  HR
[°C/min]:',num2str(HR))])
    title(['Test: ',num2str(nump); strcat('Vdot
[mL/min]:',num2str(V),strcat('  c',Nomi(1)),'
[%vol]:',num2str(cCmb),strcat('  c',Nomi(2)),' [%vol]:',num2str(cO2))])
    grid on
end

figure(ins*2+2)
[h_axes, A_lines, T_lines] = plotyy(tGC,X,tT,T);
legend([Nomi;'T']);

set(gca,'Box','off');
set(get(h_axes(1),'XLabel'),'String','Time [min]');
set(get(h_axes(1),'YLabel'),'String','Conversion');
set(get(h_axes(2),'YLabel'),'String','Temperature [°C]');
set(h_axes(1),'YTick',0:0.1:1.1);
set(h_axes(1),'Ylim',[0 1.05]);
set(h_axes(2),'YTick',20:20:max(T)+20);
set(h_axes(2),'Ylim',[20 max(T)+20]);
set(A_lines,'linestyle','--','linewidth',1.5,'marker','o');
set(T_lines,'linestyle','-','linewidth',2,'Color','r');
% title(['Test: ',num2str(nump); strcat('Vdot
[mL/min]:',num2str(V),strcat('  c',Nomi(1)),'
[%vol]:',num2str(cCmb),strcat('  c',Nomi(2)),' [%vol]:',num2str(cO2),'  HR
[°C/min]:',num2str(HR))])
title(['Test: ',num2str(nump); strcat('Vdot [mL/min]:',num2str(V),strcat('
c',Nomi(1)),' [%vol]:',num2str(cCmb),strcat('  c',Nomi(2)),'
[%vol]:',num2str(cO2))])
grid on

figure(ins*2+3)
cvol = (1-X).*repmat([cCmb cO2],length(X),1);
cvol(find(cvol(:,1)>cCmb),1)=0;
cvol(find(cvol(:,2)>cO2),2)=0;
[h_axes, A_lines, T_lines] = plotyy(tGC,cvol,tT,T);
legend([Nomi;'T']);

set(gca,'Box','off');
set(get(h_axes(1),'XLabel'),'String','Time [min]');
set(get(h_axes(1),'YLabel'),'String','Concentration [%vol]');
set(get(h_axes(2),'YLabel'),'String','Temperature [°C]');
set(h_axes(1),'YTick',0:0.5:max(max(cvol))+.1);
set(h_axes(1),'Ylim',[0 max(max(cvol))+.1]);
set(h_axes(2),'YTick',20:20:max(T)+20);
```

```
set(h_axes(2),'Ylim',[20 max(T)+20]);
set(A_lines,'linestyle','--','linewidth',1.5,'marker','o');
set(T_lines,'linestyle','-','linewidth',2);
title(['Test: ',num2str(nump); strcat('Vdot [mL/min]:',num2str(V),strcat('
c',Nomi(1)),' [%vol]:',num2str(cCmb),strcat('  c',Nomi(2)),'
[%vol]:',num2str(cO2),'  HR [°C/min]:',num2str(HR))])
grid on

% save dei grafici
for i = 1:2*ins+3
    figure(i)
    print('-dpng','-noui',['.\fig\prova' num2str(nump) num2str(i)] )
end

save(strcat('uGC',num2str(nump)))
```

Appendix 3

analisi.m

```
% Programma per analizzare i risultati di acquisione MID con Hiden a
% partire dal file .CSV
% avviare il programma una prima volta per definire tmin tmax e tcalib
%%%%%%%%%%%%%%%%%%%%%%%%%%%%%%%%%%%%%%%%%%%%%%%%%%%%%%%%%%%%%%%%%%%%%%%%%%%%


function Analisi
clc, close all, clear all, format compact
warning off all

%%%%%%%%%%%%%%%%%%%%%%%%%%%%%%%%%%%%%%%%%%%%%%%%%%%%%%%%%%%%%%%%%%%%%%%%%%%%
%Variabili da impostare
% massa dei reagenti di cui calcolare X(T)
reag=[2 32];    % massa dei reagenti di cui calcolare X(T)
nump = 95;              % numero della prova

% options
iRead = 1; % =1 per impostare i parametri, 0=per caricare i valori salvati
in prova(i).mat
xlsscrivi = 0; % =1 per scrivere i dati sul file Diario.xls

% parametri
if iRead
    winp = 6;            % Ampiezza del filtro
    tmin = 20;           % tempo minimo considerato
    tmax = 0;           % tempo massimo considerato (0=t(end))
    nTC = 1;            % numero di segnali di T acquisiti
    nTplot = 1;           % temperatura considerata per X(T): 1-->T1, 2--
>T2
    ncicliT = 1;          % definisci il numero di cicli termici

    method = 1; %metodo di valutazione della conversione
    switch method
        case 1
        %calcolo della conversione con riferimento al segnale iniziale
            tcalib = [200 500]; % tcalib(1) = segnale di cin

        case 2
        %calcolo della conversione con riferimento al segnale finale
            tcalib = [230 870]; % tcalib(2) = segnale di cin

        case 3
        %vettore intervalli t per la retta di riferimento
        tcalib=[165 420];
    end

    %matrice intervalli t per il riferimento allo zero strumentale
```

```
    %dimensioni: length(reag)x2
    onzrif = 0;
    zrif=[80 100];

    % opzione per la scelta manuale del riferimento
    rif=1;


else

load(strcat('prova',num2str(nump),'.mat'),'winp','tmin','tmax','nTC','nTplo
t','ncicliT','onzrif','zrif','tcalib','method')
end

%nome file Diario(i).xls
% Nicola
% ddir = 'C:\Users\utente\Dropbox\CreLab(3)\H2_pt\';
% Francesco
ddir = 'W:\Users\Francesco\Dropbox\CreLab\Singoli Progetti\H2_pt\';

excel='DiarioD.xlsx';

% Definizione del nome del file da utilizzare e della directory
file = strcat('prova',num2str(nump));
dir = [ddir 'dati_hiden\csv\'];


% Lettura dati
fid = fopen([dir, file, '.csv']);

while 1
  tline = fgetl(fid);

   N  = strfind(tline, 'scans');
   if N>0, Nt = (tline(1:N-2)); end     % N di scans = N tempi a cui ci
sono dati

   N = strfind(tline, '"Scans"');
   if N>0, Nseg = str2num(tline(9:end)); N=0; end  % Num di segnali
acquisiti

   N = strfind(tline, '"Time"');
   if N==1,
      nomi=strread(regexprep(regexprep(tline,'"',''),';',' '),'%s');
      nomi = nomi(3:end);  % elimina Time, ms..
   break
   end   % estrae i nomi delle colonne

end

    fmt='%d:%d:%d ;'; for i =1:Nseg+1, fmt = [fmt  ' %g ;'];end
    A = fscanf(fid,fmt,[Nseg+4 inf]);
    t = A(4,:)/1000/60; % converte il tempo da ms a min
    A = A(5:end,:); % ridefinisce la matrice A considerando solo le pi e la
T

%identificazione specie reagenti

%Riarrangiamento dati
iT=[0 0];
```

```
ip=ones(length(nomi),1);

for nT=1:length(iT)
    for i=1:length(nomi)
        if iT(1)==0
                if strcmp(nomi(i),'T1'),iT(1)=i;ip(i)=0;end % identifica
posizione T1
        end
        if iT(2)==0
                if strcmp(nomi(i),'T2'),iT(2)=i;ip(i)=0;end % identifica
posizione T2
        end
    end
end

iT=iT(iT>0);
T=A(iT,:)';

if length(iT)==1
    legT=[{'T1'}];
    nTC = 1; %numero di TC
else
    legT=[{'T1'} {'T2'}];
    nTC = 2; %numero di TC
end

nomi=nomi(ip>0);
p=A(ip>0,:)';
r=zeros(1,length(nomi));

for j=1:length(reag)
    mass=reag(j);
    for i=1:length(nomi)
        s=strcat('m',num2str(mass));
        ssem=strcat(s,'sem');
        if strcmp(nomi(i),s),r(i)=i;end % identifica posizione m(i)
        if strcmp(nomi(i),ssem),r(i)=i;end % identifica posizione m(i)sem

        if rif==0
            if strcmp(nomi(i),'Ptot'),rif=i;end % identifica posizione Ptot
        end
    end
end

rifname='Ptot';
r=r(r>0);
nomir=nomi(r);

% condizioni operative da Diario
switch reag(1)
        case 2
            sleg=[{'H2'} {'O2'}];
            cCmb=xlsread([ddir excel],'Diario',strcat('AF',num2str(nump)));
        case 16
            sleg=[{'CH4'} {'O2'}];
            cCmb=xlsread([ddir excel],'Diario',strcat('AG',num2str(nump)));
        case 28
            sleg=[{'CO'} {'O2'}];
            cCmb=xlsread([ddir excel],'Diario',strcat('AE',num2str(nump)));
end
```

```
    V=xlsread([ddir excel],'Diario',strcat('Y',num2str(nump)));
    cO2=xlsread([ddir excel],'Diario',strcat('AD',num2str(nump)));
    HR=xlsread([ddir excel],'Diario',strcat('T',num2str(nump)));
    cCmb=cCmb*100;
    cO2=cO2*100;

    % Verifica la presenza di Ptot all'interno dei dati
if rif==1
    mrif=input('Digitare massa del riferimento: ');
    rifname=strcat('m',num2str(mrif));
    for i=1:length(nomi)
        if strcmp(nomi(i),rifname),rif=i;end % identifica posizione rif(i)
    end
end
% Riscala i segnali rispetto al riferimento
p = p./repmat(p(:,rif),1,Nseg-nTC);

% creazione della legenda
    leg(1:size(T,2))=legT;leg(size(T,2)+1:length(nomi)+size(T,2))=nomi; %
crea la legenda considerando anche la T e importando la lista dalla
variabile nomi

% visualizzazione profili
    figure(1)
    set(1,'NumberTitle','off','Name','Pi & T');
    set(1,'DefaultAxesColorOrder');  % crea nn gradazioni di colore per le
prossime nn linee

    [h_axes, h_lines] = plotyy(t,T,t,p,'plot','semilogy');
    legend(leg,'Location','NorthEastOutside');
    title(['Test: ' num2str(nump)]);

    set(gca,'Box','off'),xlabel('Time [min]')
    set(h_lines(1),'LineWidth',1.5,'Color','b');
    set(get(h_axes(1),'XLabel'),'String','t [min]');
    set(get(h_axes(1),'YLabel'),'String','T [°C]');
    set(get(h_axes(2),'YLabel'),'String',strcat('pi/',rifname));

    pause

    % filtro dati per diminuire il rumore, buon risultato con winp = 15-20
    p=filter(ones(1,winp)/winp,1,p);
    T=filter(ones(1,winp)/winp,1,T);

    % definire tmin e tmax da considerare
    if tmax==0
        tmax=t(end);
    end

    % definizione di un tempo iniziale tmin definito dall'utente
    itmin= t>tmin;  % calcola l'indice del tempo tmin digitato
    t=t(itmin);     % calcola il tempo minimo selezionato
    p=p(itmin,:);   % definisce il profilo di pressioni parziali
dall'istante di tempo tmin
    T=T(itmin,:);     % definisce la T di partenza in corrispondenza di
tmin

    % analogo alla definizione di tmin ma per un tempo tmax
    itmax= t< tmax;
    t=t(itmax);
```

```
    p=p(itmax,:);
    T=T(itmax,:);

    tmin=min(t);
    tmax=max(t);

close all

% Figura 1: andamento pressioni parziali riscalate
% creazione della legenda
leg(1:max(size(legT)))=legT;leg(max(size(legT))+1:length(nomi)+max(size(leg
T)))=nomi; % crea la legenda considerando anche la T e importando la lista
dalla variabile nomi

% visualizzazione profili
figure(2)
% set(1,'NumberTitle','off','Name','Pi & T');
% set(1,'DefaultAxesColorOrder');  % crea nn gradazioni di colore per le
prossime nn linee
[ax, h1,h2] =
plotyy(t',T,t',p,'plot','semilogy'),legend(leg,'Location','NorthEastOutside
');
title(['Test: ' num2str(nump)]);

set(gca,'Box','off');
set(h1,'LineWidth',1.5,'Color','b');
set(get(ax(1),'XLabel'),'String','Time[min]');
set(get(h1,'YLabel'),'String','Temperature [°C]');
set(get(h2,'YLabel'),'String',strcat('pi/',rifname));

if onzrif
    for j=1:length(r)
        tzrif1= find(t>zrif(1), 1 );  % calcola l'indice del tempo
triffzero min
        tzrif2= find(t<zrif(2), 1, 'last' );  % calcola l'indice del tempo
triffzero max

        mzrif=strcat('m',num2str(reag(j))); %trova la corrispondenza massa-
segnale all'interno di p
        p(:,r(j))=p(:,r(j))-mean(p(tzrif1:tzrif2,r(j)));  %calcola il
valore di riferimento per lo zero di p(j)
    end
end

xcmb = [] ; Tmpt = [] ; Xcmb = []; time = [];

switch method

    case 1
    amp = 5; % Definisce il numero di punti dell'intorno di it1 o it2 su
cui calcolare la media
    irifcmb = [find(t>tcalib(1),1) find(t>tcalib(2),1)];
    rifcmb = mean(p(irifcmb(1)-amp:irifcmb(1)+amp,r));
    Xcmb = 1-p(irifcmb(1):irifcmb(2),r)./repmat(rifcmb,(irifcmb(2)-
irifcmb(1))+1,1); %conversione regenti
    Tmpt = T(irifcmb(1):irifcmb(2)); %[°C], vettore temperatura
    time = t(irifcmb(1):irifcmb(2));

    case 2
```

```
    amp = 5; % Definisce il numero di punti dell'intorno di it1 o it2 su
cui calcolare la media
    irifcmb = [find(t>tcalib(1),1) find(t>tcalib(2),1)];
    rifcmb = mean(p(irifcmb(2)-amp:irifcmb(2)+amp,r));
    Xcmb = 1-p(irifcmb(1):irifcmb(2),r)./repmat(rifcmb,(irifcmb(2)-
irifcmb(1))+1,1); %conversione regenti
    Tmpt = T(irifcmb(1):irifcmb(2)); %[°C], vettore temperatura
    time = t(irifcmb(1):irifcmb(2));

    case 3
    for j=1:ncicliT
        t1=tcalib(j,1);
        t2=tcalib(j,2);
        it1=find(t>t1,1);
        it2=find(t>t2,1)-1;
        amp=5; % Definisce il numero di punti dell'intorno di it1 o it2 su
cui calcolare la media

        %Calcolo del punto iniziale
        % individua l'indice dei valori richiesti. Non possiamo determinare
        % direttamente il singolo punto ma bisogna determinare i valori
subito
        % minori o maggiori di quello desiderato
        pcmbm1=mean(p(it1-amp:it1+amp,r));

        % Calcolo del punto finale
        pcmbm2=mean(p(it2-amp:it2+amp,r));

        % Intervallo di tempo considerato
        tretta=t(it1:it2);

        % Calcolo dell'equazione della retta passante per i punti definiti
        % Combustibile
        mcmb=(pcmbm2-pcmbm1)/(t(it2)-t(it1));
        qcmb=pcmbm2-mcmb*t(it2);
        rifcmb =
repmat(tretta',1,2).*repmat(mcmb,length(tretta),1)+repmat(qcmb,length(trett
a),1);

        % Determina le conversioni per i diversi reagenti
        xcmb = 1-p(it1:it2,r)./rifcmb;

        Xcmb = [Xcmb; xcmb];
        tmpt = T(it1:it2,nTplot);
        Tmpt = [Tmpt; tmpt];
        tempo = t(it1:it2);
        time = [time;tempo'];

    end
end

dati.X = Xcmb; % vettore conversioni
dati.T = Tmpt; % vettore temperatura
dati.t = time; % vettore tempo

% Determina le temperature Tm (minima) e TM (massima) nell'intervallo
% definito dall'utente
[Tm,ITm] = min(dati.T);
[TM,ITM] = max(dati.T);
```

```
frmt='png'; % formato con cui salva le prove

% Figura 2: andamento della temperatura
figure(2)
plot(t,T,'LineWidth',1.5)
legend(legT,'Location','NorthEastOutside');
title(['Test: ',num2str(nump) '  Profilo di T ']);
xlabel('t [min]')
ylabel('T [°C]' )


% figure 3-->nr+2: X vs T
Tmpt=dati.T;
for nr=1:max(size(nomir))

    % Raccolta risultati
    X(:,nr)=dati.X(:,nr); % matrice coversione dei reagenti
    XM(nr)=max(X(:,nr))*100;

    yleg=nomir(nr);
    % Figura 3-->n-esima: plot conversioni
    figure(nr+2) % 2 si riferisce al # di figure precedentemente stampate
    cm1 = colormap(jet);

    if length(X)>20
        numcolor = length(X)/10;
        style = '-';
    else
        numcolor = length(X);
        style = 'o';
    end

    for kcolor=1:numcolor
        perc_avanz = kcolor/numcolor;
        icol = ceil(perc_avanz*(length(cm1)-1))+1;
        cm1 = colormap(jet(numcolor));
        lA=Tmpt(length(Tmpt)/numcolor*(kcolor-
1)+1:length(Tmpt)/numcolor*kcolor);
        lB=X(length(Tmpt)/numcolor*(kcolor-
1)+1:length(Tmpt)/numcolor*kcolor,nr);
        plot(lA,lB,'linestyle',style,'Color',cm1(icol,:),'LineWidth',1.5),
hold on
    end

    title(['Test: ',num2str(nump); strcat('Vdot
[mL/min]:',num2str(V),strcat('  c',sleg(1)),'
[%vol]:',num2str(cCmb),strcat('  c',sleg(2)),' [%vol]:',num2str(cO2),'  HR
[°C/min]:',num2str(HR))]) %     title([strcat('Prova-',num2str(vrb(1)))
strcat('Conversione-',yleg)]);
    xlabel('Temperature [°C]')
    ylabel(['Conversion of' sleg(nr)])
    axis([min(Tmpt) max(Tmpt) 0 1]);
    fmt='%4.2f h';
    colorbar('YTick',[1 icol/2 icol]...
    ,'YTickLabel',{sprintf(fmt,0),sprintf(fmt,(dati.t(end)-
dati.t(1))/120),sprintf(fmt,(dati.t(end)-dati.t(1))/60)})
    grid on
end

% figura nr+3: t vs T vs X
```

```
figure(2+nr+1)
set(2,'NumberTitle','off','Name','Pi & T');
set(2,'DefaultAxesColorOrder');  % crea nn gradazioni di colore per le
prossime nn linee
[h_axes, x_lines, T_lines] = plotyy(dati.t,dati.X,t,T(:,1));
legend([sleg,'T'],'Location','NorthEastOutside');
title(['Test: ',num2str(nump);'Temperature-Conversione relation';
strcat('Vdot [mL/min]:',num2str(V),strcat('  c',sleg(1)),'
[%vol]:',num2str(cCmb),strcat('  c',sleg(2)),' [%vol]:',num2str(cO2),'  HR
[°C/min]:',num2str(HR))]);

set(gca,'Box','off');
set(get(h_axes(1),'XLabel'),'String','Time [min]');
set(get(h_axes(1),'YLabel'),'String','Conversion of reagents');
set(get(h_axes(2),'YLabel'),'String','Temperature [°C]');
set(h_axes(1),'YTick',0:0.1:1.1);
set(h_axes(1),'Ylim',[0 1.1]);
set(h_axes(2),'YTick',20:20:max(T)+20);
set(h_axes(2),'Ylim',[20 max(T(:,1))+20]);
set(x_lines,'linestyle','--','linewidth',1.5,'marker','o');
set(T_lines,'linestyle','-','linewidth',2);
grid on

% figura nr+4: rapporto stechiometrico
figure(2+nr+2)
plot(dati.T,dati.X(:,1)./dati.X(:,2))
title(['Test: ',num2str(nump);'Verifica della stechiometria di reazione';
strcat('Vdot [mL/min]:',num2str(V),strcat('  c',sleg(1)),'
[%vol]:',num2str(cCmb),strcat('  c',sleg(2)),' [%vol]:',num2str(cO2),'  HR
[°C/min]:',num2str(HR))]);
xlabel('T [°C]')
ylabel(['Xreag/Xo2'])
% axis([min(dati.T) max(dati.T) 0 ceil(cCmb/cO2+3)]);

pause

% Salva le figure in files grafici
for kfig=1:2+nr+2
figure(kfig); print('-dpng','-
noui',strcat('.\fig\',strcat(num2str(file),strcat('_',num2str(kfig)))));
end

close all

Message=strcat('eseguita prova numero:',num2str(nump))

if xlsscrivi
    % Scrive i dati su xls (durata test,Xcomb,XO2,tmax,tmin,winp,Tmax,Tmin)
    Success = xlswrite([ddir
excel],max(t)/60,'Diario',strcat('E',num2str(nump)))
    Success = xlswrite([ddir
excel],size(reag,2),'Diario',strcat('CE',num2str(nump)))

    switch reag(1)
        case 2
            Success = xlswrite([ddir
excel],XM(1),'Diario',strcat('CF',num2str(nump)))
        case 16
            Success = xlswrite([ddir
excel],XM(1),'Diario',strcat('CG',num2str(nump)))
```

```
        case 28
            Success = xlswrite([ddir
excel],XM(1),'Diario',strcat('CH',num2str(nump)))
    end

    Success = xlswrite([ddir
excel],XM(2),'Diario',strcat('CI',num2str(nump)))
    Success = xlswrite([ddir
excel],tmin,'Diario',strcat('CN',num2str(nump)))
    Success = xlswrite([ddir
excel],tmax,'Diario',strcat('CO',num2str(nump)))
    Success = xlswrite([ddir
excel],winp,'Diario',strcat('CP',num2str(nump)))
    Success = xlswrite([ddir excel],TM,'Diario',strcat('R',num2str(nump)))
    Success = xlswrite([ddir excel],Tm  ,'Diario',strcat('S',num2str(nump
)))
end

% salva i dati
save(file)
```

Appendix 4

confronto.m

```
function confronto_francesco_v2
clc
clear all
close all

% prove = [74 77 78 84 86 90 92 93];
prove=[78 79 80]; %number of experiments to compare
mtime = 0;
leg1 = []; leg2 = []; leg3 = [];
color = 'rbgkycmr';

for k = 1:length(prove)
    load(strcat('prova',num2str(prove(k))))
    iTM=find(TGC==max(TGC))
    figure(1)
    plot(TGC(1:iTM),X(1:iTM,1),color(k),'Linewidth',2), grid on, hold on
    title('XH2 vs. T at different inlet composition', 'fontsize', 18)
    xlabel('Temperature [°C]', 'fontsize', 14)
    ylabel('Hydrogen conversion', 'fontsize', 14)
    axis([20 220 0 1])
    leg1 = [leg1;'test ',num2str(prove(k))];
    legend(leg1)
    leg= legend('Location','SouthEast');
    legend(leg);

    figure(2)
    plot(TGC,X(:,2),color(k),'Linewidth',1.5), grid on, hold on
    xlabel('Temperature [°C]')
    ylabel('Oxygen conversion')
    axis([20 220 0 1])
    leg2 = [leg2; 'test ' num2str(prove(k))];
    legend(leg2)

    for j = 1:Nc

        figure(j+2)
        subplot(1,length(prove),k)
        plot(tGC,X(:,j),color(k),'Linewidth',2), hold on
        title('Reagent conversion')
        leg3 = [(strcat('test ',num2str(prove(k)),' - ',Nomi(j)))];
        legend(leg3)
        xlabel('Time [min]')
        ylabel('Conversion')
        grid(gca,'minor')
        ylim([0 1])

%         subplot(1,3,2)
```

```
%         plot(time(index),1-
(Areas(index,j)./max(Areas(:,j))),strcat(symb(k),color(k)),'Linewidth',2),
hold on
%         title('Reagent conversion')
%         xlabel('Time [min]')
%         ylabel('Conversion')
%         grid(gca,'minor')

%         subplot(1,3,3)
%         plot(T,1-(Areas(:,j)./max(Areas(:,j))),color(k),'Linewidth',2),
hold on
%         title('Reagent conversion')
%         xlabel('Temperature [°C]')
%         ylabel('Conversion')
%         grid(gca,'minor')
    end

    T =[];
end

for i = 1:4
    figure(i)
    print('-dpng','-noui',['.\fig\confronti\prove ' num2str(prove) '_'
num2str(i)] )
end
```

Bibliography

- Baerns, M., Imbihl, R., Kondratenko, V.A., Kraehnert, R., Offermans, W.K., Van Santen, R.A., Scheibe, A. (2005). Bridging the pressure and material gap in the catalytic ammonia oxidation: Structural and catalytic properties of different platinum catalysts. *Journal of Catalysis* **232 (1)** , pp. 226-238.

- Behrendt, F., Deutschmann, O., Schmidt, R., Warnatz, J. (1996). Ignition and Extinction of Hydrogen-Air and Methane-Air Mixtures over Platinum and Palladium. *ACS Symposium Series* **638** , pp. 48-57.

- Brady, K., Sung, C.-J., T'Ien, J. (2010). Ignition propensity of hydrogen/air mixtures impinging on a platinum stagnation surface. *International Journal of Hydrogen Energy* **35 (20)**, pp. 11412-11423.

- Bui, P.-A., Vlachos, D.G., Westmoreland, P.R. (1996). Homogeneous ignition of hydrogen-air mixtures over platinum. *Symposium (International) on Combustion* **26 (1)**, pp. 1763-1770.

- Bui, P.-A., Vlachos, D.G., Westmoreland, P.R. (1997). Modeling Ignition of Catalytic Reactors with Detailed Surface Kinetics and Transport: Oxidation of H2/Air Mixtures over Platinum Surfaces. *Industrial and Engineering Chemistry Research* **36 (7)**, pp. 2558-2567.

- Cabié, M., Giorgio, S., Henry, C.R., Axet, M.R., Philippot, K., Chaudret, B. (2010). Direct observation of the reversible changes of the morphology of Pt nanoparticles under gas environment. *Journal of Physical Chemistry C* **114 (5)**, pp. 2160-2163.

- Deutschmann, O., Schmidt, R., Behrendt, F., Warnat, J. (1996). Numerical modeling of catalytic ignition. *Symposium (International) on Combustion* **26 (1)**, pp. 1747-1754.

- Diehl, M. (2003). Platinum Group Metals and Compounds, Section 10.4. In: *Ullmann's Encyclopedia of Industrial Chemistry* (John Wiley and Sons, Inc.).

- Fernandes, N.E., Park, Y.K., Vlachos, D.G. (1999). The autothermal behavior of platinum catalyzed hydrogen oxidation: Experiments and modeling. *Combustion and Flame* **118 (1-2)**, pp. 164-178.

- Försth, M., Gudmundson, F., Persson, J.L., Rosén, A. (1999). The influence of a catalytic surface on the gas-phase combustion of H2 + O2. *Combustion and Flame* **119 (1-2**), pp. 144-153.

- Försth, M., Eisert, F., Gudmundson, F., Persson, J., Rosén, A. (2000). Analysis of the kinetics for the H2 + 1/2O2 ⇌ H2O reaction on a hot Pt surface in the pressure range 0.10-10 Torr. *Catalysis Letters* **66 (1-2)**, pp. 63-69.

- Försth, M. (2002). Sensitivity analysis of the reaction mechanism for gas-phase chemistry of H2+O2 mixtures induced by a hot Pt surface. *Combustion and Flame* **130 (3)**, pp. 241-260.

- Horch, S., Lorensen, H.T., Helveg, S., Lægsgaard, E., Stensgaard, I., Jacobsen, K.W., Nørskov, J.K., Besenbacher, F. (1999). Enhancement of surface self-disfusion of platinum atoms by adsorbed hydrogen. *Nature* **398 (6723)**, pp. 134-136.

- Iddir, H., Komanicky, V., Öğüt, S., Hoydoo, Y., Zapol, P. (2007). Shape of platinum nanoparticles supported on SrTiO3: Experiment and theory. *Journal of Physical Chemistry C* **111 (40)**, pp. 14782-14789.

- Imbihl, R., Scheibe, A., Zeng, Y.F., Günther, S., Kraehnert, R., Kondratenko, V.A., Baerns, M., Offermans, W. K., Jansen, A. P. J., Van Santen, R.A. (2007). Catalytic ammonia oxidation on platinum: Mechanism and catalyst restructuring at high and low pressure. *Physical Chemistry Chemical Physics* **9 (27)**, pp. 3522-3540.

- Iovino, A. (2013). Studio cinetico su catalizzatori a base di perovskite per applicazioni automobilistiche. *Tesi di Laurea Magistrale in Ingegneria Chimica e dei Processi Industriali*, DII, Università di Padova.

- Kraehnert, R., Baerns, M. (2007). Morphology changes of Pt-foil catalyst induced by temperature-controlled ammonia oxidation near atmospheric pressure. *Applied Catalysis A: General* **327 (1)**, pp. 73-81.

- Ljungström, S., Kasemo, B., Rosen, A., Wahnström, T., Fridell, E. (1989). An experimental study of the kinetics of OH and H2O formation on Pt in the H2 + O2 reaction. *Surface Science* **216 (1-2)**, pp. 63-92.

- Minca, M., Penner, S., Loerting, T., Menzel, A., Bertel, E., Zucca, R., Redinger, J. (2007). Chemisorption of hydrogen on the missing-row Pt(110)-(1 × 2) surface. *Topics in Catalysis* **46 (1-2)** , pp. 161-167.

- Nilsen, O., Kjekshus, A., Fjellvåg, H. (2001). Reconstruction and loss of platinum catalyst during oxidation of ammonia. *Applied Catalysis A: General* **207 (1-2)**, pp. 43-54.

- Panster, P. (2003). Platinum Group Metals and Compounds, Section 10.3. In: *Ullmann's Encyclopedia of Industrial Chemistry* (John Wiley and Sons, Inc.).

- Park, Y.K., Fernandes, N.E., Vlachos, D.G. (1999). Effect of dilution on catalytic oxidation: Model validation through experiments and predictions of operation regimes. *Chemical Engineering Science* **54 (15-16)**, pp. 3635-3642.

- Renner, H. (2003). Platinum Group Metals and Compounds, Section 3.5. In: *Ullmann's Encyclopedia of Industrial Chemistry* (John Wiley and Sons, Inc.).

- Rinnemo, M., Deutschmann, O., Behrendt, F., Kasemo, B. (1997). Experimental and numerical investigation of the catalytic ignition of mixtures of hydrogen and oxygen on platinum. *Combustion and Flame* **111 (4)**, pp. 312-326.

- Vlachos, D.G. (1996). Homogeneous-heterogeneous oxidation reactions over platinum and inert surfaces. *Chemical Engineering Science* **51 (10)**, pp. 2429-2438.

- Vlachos, D.G., Bui, P.-A. (1996). Catalytic ignition and extinction of hydrogen: Comparison of simulations and experiments. *Surface Science* **364 (3)**, pp. L625-L630.

- Warnatz, J., Allendorf, M.D., Kee, R.J., Coltrin, M.E. (1994). A model of elementary chemistry and fluid mechanics in the combustion of hydrogen on platinum surfaces. *Combustion and Flame* **96 (4)**, pp. 393-406.

- Williams, W.R., Marks, C.M., Schmidt, L.D. (1992). Steps in the reaction H2 + O2⇌H2O on Pt: OH desorption at high temperatures. *Journal of Physical Chemistry* **96 (14)**, pp. 5922-5931.

Ringraziamenti

Dopo 9 mesi dedicati a questo lavoro, è giunto, finalmente, il momento di ringraziare tutte le persone che mi hanno aiutato finora. Innanzitutto, ringrazio il mio gruppo di ricerca a partire da **Nicola** e dal **Prof. Canu**. Il primo è sempre stato presente in ogni aspetto della mia vita nel laboratorio, cominciando dall'insegnarmi come si maneggia il platino con la pinzetta facendo finta che siano delle bacchette cinesi e finendo discutendo le teorie più variegate per interpretare i risultati. Non solo, in tutto questo tempo fatto, anche, da pranzi in Murialdo, da colazioni all'Illy e da pause caffè, è diventato anche un amico, quasi un fratello maggiore.

Non ringrazierò mai abbastanza il **Prof.** perché è stato il protagonista di tutti punti fondamentali della mia carriera universitaria non solo dal punto di vista didattico. Innanzitutto, mi ha dato la possibilità di soddisfare la mia grande curiosità di vedere le cose da un'altra prospettiva mandandomi a studiare all'estero. Inoltre, grazie a lui ho potuto condurre la mia prima ed interessantissima esperienza nel mondo della ricerca. Infine, durante il periodo di Tesi, i suoi pareri riguardo tutti i problemi che ho incontrato strada facendo sono sempre stati illuminanti e pieni di spunti di riflessione.

Il **Prof.** insieme a **Nicola** mi hanno fatto appassionare al mondo della ricerca al punto da voler continuare su questo cammino per vari anni, una scelta che fino a un anno fa non ritenevo per niente interessante, anzi quasi da *sfigati*.

Continuando a ringraziare i membri del mio gruppo, la prima persona che mi viene in mente è la Regina del laboratorio, la bella quanto intelligente **Micol**. Mi dispiace molto per **il Guio** che, per quanto cerchi di evitare di fare sia la Tesi triennale sia quella magistrale insieme a me, alla fine mi deve sempre sopportare. Un ringraziamento va anche a **Jessica, Max, Serena, Tommaso, Alberto e Ale** che hanno reso più vivace ogni momento passato in laboratorio con discorsi che spaziavano dalle teorie più avanzate in ogni campo della scienza ad argomenti molto meno impegnati. Nonostante il suo caratterino… *particolare*, ringrazio anche **Marco** anche se so che lui avrebbe preferito non essere nominato visto che deve sempre distinguersi dagli altri.

Lascio questo gruppo molto a malincuore consapevole del fatto che, per quanto mi possa trovare bene in altri ambienti, non sarà mai come il periodo che ho passato a Padova.

Desidero ringraziare anche gli amici del venerdì/sabato sera, ovvero i vari **Nick, Michele, Giovannino, Marco, Ket** e tutti gli altri con cui sono riuscito a staccare un po' la spina dopo giorni di studio/lavoro. Ricordiamoci che "*All work and no play makes Jack a dull boy*".

Dulcis in fundo, un ringraziamento va anche alla mia famiglia, a **Sergio** e **Nicola** con le loro consorti **Anna** e **Irene** ma soprattutto ai miei genitori che mi hanno sempre aiutato e dato la

possibilità di raggiungere i risultati più alti in ogni aspetto della mia vita, soprattutto durante il periodo finale della mia carriera accademica.
Ancora una volta, GRAZIE A TUTTI!!!!